EPA-460/3-76-024
October 1976

EXHAUST EMISSION AND FUEL ECONOMY CHARACTERIZATION OF A MODERN AUTOMOTIVE WANKEL ROTARY ENGINE

U.S. ENVIRONMENTAL PROTECTION AGENCY
Office of Air and Waste Management
Office of Mobile Source Air Pollution Control
Emission Control Technology Division
Ann Arbor, Michigan 48105

EPA-460/3-76-024

EXHAUST EMISSION AND FUEL ECONOMY CHARACTERIZATION OF A MODERN AUTOMOTIVE WANKEL ROTARY ENGINE

by

D.E. Cole and D.J. Patterson

University of Michigan
Ann Arbor, Michigan

Grant No. R802536

EPA Project Officer: F. Peter Hutchins

Prepared for

ENVIRONMENTAL PROTECTION AGENCY
Office of Air and Waste Management
Office of Mobile Source Air Pollution Control
Emission Control Technology Division
Ann Arbor, Michigan 48105

October 1976

This report is issued by the Environmental Protection Agency to report technical data of interest to a limited number of readers. Copies are available free of charge to Federal employees, current contractors and grantees, and nonprofit organizations - in limited quantities - from the Library Services Office (MD-35), Research Triangle Park, North Carolina 27711; or, for a fee, from the National Technical Information Service, 5285 Port Royal Road, Springfield, Virginia 22161.

This report was furnished to the Environmental Protection Agency by the University of Michigan, Ann Arbor, Michigan, in fulfillment of Grant No. R802536. The contents of this report are reproduced herein as received from the University of Michigan. The opinions, findings, and conclusions expressed are those of the author and not necessarily those of the Environmental Protection Agency. Mention of company or product names is not to be considered as an endorsement by the Environmental Protection Agency.

Publication No. EPA-460/3-76-024

FOREWORD

The concern for the preservation of our environment and dwindling petroleum resources has accelerated the search for new powerplants by the automotive industry. Numerous powerplants, including the gas turbine, Stirling, Diesel, and Wankel engines are being investigated ever so carefully to determine their potential to satisfy the many and complex criteria of modern vehicles. The University of Michigan Automotive Laboratory has been contributing to these on-going investigations for many years with a focus on:

- measurement and control of undesirable exhaust emissions
- reduction of fuel consumption
- training engineering students to better contribute to the solution of automotive problems.

During the past two years the Automotive Laboratory at the University of Michigan has directed part of its effort to the technical assessment of a modern Wankel engine which is used in the Japanese manufacturered Mazda vehicle. The following report is a culmination of this study to characterize the exhaust emission and fuel consumption performance of the 1975 Mazda 13-B rotary engine. The following objectives were addressed in this experimental program:

1. Map the fuel consumption and emission performance of both a modern rotary engine and a conventional reciprocating engine of equivalent power.
2. Compare the fuel consumption and emission performance of the selected test engines in a simulated identical vehicle.
3. Determine the effects of the principal operating variables on both emissions and fuel consumption performance of the rotary engine.
4. Identify features of key fundamental processes which could cause differences in both emission and fuel consumption performance with respect to the conventional engine.

ABSTRACT

The objective of this experimental program was to study the fuel consumption and emission characteristics of a modern automotive Wankel rotary engine, compare these with a representative reciprocating engine and form conclusions regarding economy and emission performance.

Fuel consumption and exhaust emission maps were developed for a production 1975 Mazda 13-B rotary engine both with and without thermal reactor. For comparison similar data were developed for a 3.8 liter 1975 Buick V-6 engine. Steady-state dynamometer tests were run. In addition studies were conducted on the Mazda engine to determine the influence of ignition timing and air-fuel ratio on key performance factors. Engine indicator cards and spatial distribution of hydrocarbons in the exhaust were also investigated.

The studies showed that the production Buick and Mazda engines without external emission control and as installed in a hypothetical 1975 Mazda RX-4 vehicle exhibited significant differences in fuel consumption and emission performance under steady-state operation. The fuel consumption of the Mazda was generally greater than the Buick powered vehicle with a maximum difference of 20% at 35 mph. Above 35 mph the difference diminished considerably and at 60 mph the fuel consumption results were essentially the same. Likewise the hydrocarbon emissions were found to be 6-10 times greater and the CO emissions significantly greater. The NO_x emissions were lower for the Mazda. By optimizing the mixture ratio and ignition timing, the differences in fuel consumption, CO and NO_x emissions were reduced considerably, however the hydrocarbon emissions were still 3-5 times greater for the Mazda. Without exhaust treatment the aldehyde emissions were found to be similar to reciprocating gasoline engines.

Air-fuel ratio and ignition timing variations in the Mazda influenced emissions and fuel consumption in a manner similar to that observed in typical reciprocating engines although the effect of ignition timing was less significant.

Using the spatial hydrocarbon distribution in the exhaust as an indicator, it was determined that leakage of mixture past the engine apex seals and/or incomplete flame propagation were probably the most important factors causing the high level of hydrocarbon emissions from the Mazda engine. Further evidence of seal leakage and/or excessive heat loss was obtained from an analysis of firing and motoring indicator diagram.

The Mazda engine was observed to be smooth, quiet and small for its performance capability compared to the Buick V-6. Further, the friction power was significantly lower than the Buick and increased at a lower rate with speed increase.

This report was submitted in fulfillment of Grant No. R-802536-01 by the University of Michigan, Walter E. Lay Automotive Laboratory, under the sponsorship of the U.S. Environmental Protection Agency. This report covers the period from October 1, 1974 to September 30, 1976. The experimental work was completed as of June 1, 1976.

CONTENTS

FIGURES

TABLES

ACKNOWLEDGMENTS

The authors would like to gratefully acknowledge the outstanding efforts of the following men who served as research assistants or in other ways assisted: Garry Zawacki, Joseph Weissmiller, Frank Jacobson, John White, Daniel Mehall, Anthony Brakora, Thomas Salva and Eugene Zimmerman. The excellent support of the laboratory technicians at the Walter E. Lay Automotive Laboratory at the University of Michigan is also gratefully acknowledged.

In addition we are indebted to the Toyo Kogyo Company of Japan and the Buick Motor Division of General Motors Corporation for their important contributions of test engines, technical information and other support. In particular, we would like to acknowledge the assistance provided by Mr. Iida from Toyo Kogyo who contributed his time and efforts to the initial development of the test facility.

SECTION 1

INTRODUCTION

A. BACKGROUND

During the past ten years we have witnessed ever-increasing interest in alternative powerplants for passenger automobiles. Initially a major incentive for the consideration of these different power systems was the prospect of reducing undesirable exhaust emissions. At the present time, however, we are concerned with the additional and perhaps equally important consideration of thermal efficiency. In all probability, future engines will be judged on the basis of fuel economy and emission performance considered together in addition to other important factors such as cost, driveability, manufacturability, etc.

Numerous powerplant concepts are being investigated, including both external and internal combustion engines. Of the many being considered, only one has achieved significant production status in an automobile - the Wankel, rotary combustion engine. The Toyo Kogyo Company of Japan is currently featuring this rotary engine in its Madza vehicles as is the German company NSU in the RO-80.

The rotary engine possesses numerous attractive features. Perhaps the most important advantage is its small size which promises to offer considerable packaging flexibility in a vehicle. This could enhance the auto industry's ability to design a vehicle with compact exterior dimensions while maintaining the maximum interior volume for people and luggage. The Wankel engine is substantially lighter and simpler (at least with respect to the number of parts). In addition it breathes well because of a greater length (crank degrees) of induction period and because of a relatively unrestricted flow path for the incoming mixture and exhausting products. In the one and two rotor versions, the induction system is simple which reduces problems associated with maldistribution of the air-fuel mixture. Also, the speed range of the engine is broad due to the better breathing characteristics, potentially lower mechanical friction and no limitations imposed by valve train dynamics. Further the engine appears to have a lower fuel octane requirement at a given compression ratio. An important advantage in comparison to engines with 4 or fewer cylinders is its inherent dynamic balance.

As is the case with all systems, there are areas of concern as well. The gas-sealing network in the engine requires a complex

grid which has four right angle intersections per working chamber. Effective gas sealing is very difficult and considerable development effort has been expended to resolve this problem and several groups have reported success. Lubricant must be added or injected into the working chambers with the fuel and air mixture because the apex seals slide on the rotor housing which is not lubricated otherwise. Exhaust temperatures appear to be higher than those of a conventional engine at similar operating conditions. These higher temperatures do aggravate the materials problem in the exhaust system but have a positive effect on exhaust clean-up of unburned hydrocarbons and carbon monoxide. Likewise exhaust blowdown pressures are high and exhaust silencing is difficult. Fuel economy is perhaps the most controversial aspect of the rotary engine.

A wide range of fuel consumption data has been reported. General Motors and Curtiss-Wright (1,2) have indicated that the fuel economy performance of their prototype engines is essentially equivalent to that of reciprocating engines. Conversely the Mazda engine has demonstrated somewhat inferior results compared to the reciprocating engine based on EPA data (3). In part this arises from comparing the Mazda vehicles with small 4-cylinder sub-compact cars with much inferior performance. Fuel economy improvements based on EPA tests in the 1975 and 1976 model years have been reasonably dramatic although the results are still inferior to the typical sub-compact car.

Another area of considerable uncertainty is cost. While the engine is far simpler in concept than a conventional engine, it apparently requires more sophisticated components in certain areas of the engine. Cooling, while it is apparently not a production problem, is more complex than with the conventional engine for several reasons. Part of the engine combustion chamber is always exposed to hot gases while the remaining part is in contact with the relatively cool fuel-air mixture. This gives rise to a significant temperature gradient across the engine. In addition the interior of the rotor must be cooled with either oil or fuel-air charge. Another area of uncertainty is the cold-starting performance. Some of the early production rotary engines exhibited cold starting difficulties but this has been resolved in later designs.

Perhaps the most controversial aspect of the engine next to fuel consumption is emission performance. In general, the engine is viewed as having lower NO_x emission levels than a conventional engine. Carbon monoxide emissions are essentially a function of air fuel ratio as with the conventional engine. The level of unburned hydrocarbons in the uncontrolled exhaust is generally far above that of a conventional engine. It was reported that the high level of hydrocarbon emissions from the General Motors prototype rotary engine was the major reason this engine was not brought to production in 1974.

B. OBJECTIVES

The incentive for the present investigation is the considerable uncertainty associated with both the fuel consumption and exhaust emission performance of the rotary engine. In addition only relatively little quantitative data havebeen published on the engine. Most manufacturers have been exceedingly reluctant to report engine data on preproduction engines. In order to make effective and rational decisions related to powerplants in both the public and private sectors it is imperative to have sound technical information. The objectives of this program were designed to meet this goal and are defined as follows:

1. Map the fuel consumption and emission performance of both a modern rotary engine and a conventional reciprocating engine of equivalent power.
2. Compare the fuel consumption and emission performance of the selected test engines in a simulated identical vehicle.
3. Determine the effects of the principal operating variables on both emissions and fuel consumption performance of the rotary engine.
4. Identify features of key fundamental processes which could cause differences in both emission and fuel consumption performance with respect to the conventional engine.

C. TEST PROGRAM

In the present study both the fuel consumption and emission characteristics of a modern rotary engine were measured under steady-state conditions. These data were intended to provide a more rational assessment of the potential of the rotary engine. The particular engine selected for this evaluation was a 1975 Mazda model 13-B which is used in the Mazda RX-4. To preserve a realistic perspective and a basis for comparison, a conventional spark-ignited engine, a 231 cu.in. (3786 c.c.) 1975 model Buick V-6, was tested under similar conditions. The Buick engine was evaluated without catalytic convertor whereas the Mazda rotary engine was tested both with and without its production thermal reactor.

The engines were tested over a wide range of speeds and loads simulating steady-state operation in a 3095 lb. (1404 Kg) vehicle. Data points were selected to facilitate effective mapping from road load to maximum load. Since the Mazda RX-4 uses an axle ratio of 3.9:1, whereas Buick in most of its vehicle applications generally employs a far lower ratio (approximately 2.56:1), tests were run to encompass operation with both axle ratios. The effect of axle ratio on fuel consumption with both engines could be ascertained from these data.

Emissions of carbon monoxide, carbon dioxide, unburned hydrocarbons, oxygen and the oxides of nitrogen were measured at each test point and in addition a special series of tests were conducted to determine the aldehyde emissions. This latter series of experiments were run since it was believed that the rotary engine may have had a higher level of partially oxidized hydrocarbons than found in the exhaust of a conventional engine. Aldehyde measurements were made at a relatively few representative conditions because of the tedious requirements of the wet chemical test procedure used.

In addition to the basic fuel economy and emission measurements, a parametric study was conducted on two of the most important operating variables, air-fuel ratio and ignition timing, to ascertain their influence on both emissions and fuel consumption in the rotary engine. Several representative test conditions were chosen for this parametric study. Also to gain a better understanding of key fundamental aspects of the engines, two other areas were selected for investigation:

a. Evaluation of the thermodynamic cycle during compression, combustion, and early expansion with emphasis on determining losses due to gas leakage. A quartz piezoelectric pressure transducer was used to measure the pressure data.

b. Determination of sources or processes resulting in the formation of unburned hydrocarbons. As noted earlier the most significant emission problem is the high level of unburned hydrocarbons. It has been speculated that both the high surface to volume ratio in the combustion chamber and leakage past the leading apex seal to an exhausting chamber are the major causes. Hydrocarbon source information were inferred from a spatially resolved hydrocarbon analysis of exhaust leaving the engine. Both a timed sampling and steady-state sampling technique were used.

SECTION II

OBSERVATIONS AND CONCLUSIONS

Numerous observations and conclusions can be drawn from the results of this investigation both with regard to specific exhaust emission and fuel consumption performance of the Mazda 13-B rotary engine and in comparison with the 1975 Buick V-6.

A. At wide-open throttle the magnitude and trends of BSFC, BMEP, brake torque, and BHP as a function of engine speed of the Mazda engine were generally similar to the Buick reference engine with several exceptions.

1. The BHP of the Mazda increased almost linearly with RPM and peaked above 5000 RPM.

2. The BSFC decreased with increasing RPM, whereas it increased for the Buick engine.

B. In the variable load studies of the Mazda engine the performance parameters of BSFC, BSHC, BSCO and $BSNO_x$ emissions were determined as a function of RPM.

1. The BSFC both with and without air injection was similar at a given RPM and generally decreased with increasing load.

2. The $BSNO_x$ emissions with and without air injection generally were observed to increase with load, but a sharp decrease occurred near maximum load.

3. The BSHC and CO emissions were strongly related to exhaust air injection. With the thermal reactor and air injection, BSHC and BSCO were extremely low. Where the injected air was diverted to the reactor cooling jacket these emissions increased sharply. At speeds above 4000 rpm, exhaust air injection was not used and no CO and hydrocarbon emissions reduction occurred by exhaust reactions. In the studies without air injection BSHC and CO emissions generally decreased with increasing load in the speed range from 1000-3000 rpm. Beyond this speed these emissions were reasonably constant with load variation.

C. Without thermal reactor and air injection the Mazda 13-B engine as installed in a hypothetical 1975 Mazda vehicle showed the following trends at road-load conditions.

1. Fuel economy increased as axle ratio was decreased from 3.90 to 2.56:1. Maximum fuel economy occurred between 30 and 40 miles per hour. (26 mpg with 2.56:1 axle, 23 mpg with 3.90:1 axle).

2. The BSHC emissions exhibited little variation as a function of axle ratio and speed except at the lowest road speeds. The minimum BSHC level, 6-7 g/mile, occurred near 60-70 miles per hour.

3. The BSCO emissions decreased almost linearly with increasing speed and reached a minimum level of approximately 30 grams per mile at 80 mph. Axle ratio exhibited little influence on CO emissions.

4. Brake specific NO_x emissions increased at an increasing rate with speed and peaked at 4 g/mile at 80 mph. The low axle ratio of 2.56:1 produced higher $BSNO_x$ emissions by about 20%.

D. The following observations summarize the comparison between the performance of the Buick and Mazda engines without external emission control as installed in a simulated Mazda RX-4 vehicle.

1. The Mazda engine powered vehicle exhibited nearly 20% poorer fuel economy as a maximum difference. This occurred at 35 mph. Above 35 mph the difference between the Mazda and Buick fuel economy diminished considerably and were essentially identical at 60 mph with the 3.90:1 axle ratio. Our studies indicate that the major factor causing the fuel economy deficiency of the Mazda was the rich mixture required for the effective operation of the thermal reactor. By optimizing both the ignition timing and mixture ratio, it was calculated that the fuel economy for the Mazda could be brought within 5% of the Buick powered vehicle. This result was achieved in the absence of any specific emission control requirements.

2. BSHC emissions were considerably greater, approximately 6-10 times for the Mazda. This difference appears to be a fundamental Mazda engine characteristic since optimization of the operating variables could only reduce this difference by a factor of 2.

3. The BSCO emissions were considerably greater for the Mazda. However, the difference decreased with increasing speed. The difference does not appear to be fundamental and is primarily attributable to the richer mixtures used in the Mazda.

4. The $BSNO_x$ emissions were consistently higher for the Buick than for the Mazda even though EGR was employed on the Buick. Richer mixtures and slower burning in the Mazda contributed to the difference.

E. The BSFC was consistently higher for the Mazda than the Buick V-6. At 2500 rpm, for example, the minimum BSFC was .48 for the Buick and .55 for the Mazda. The difference decreased at maximum load and at the higher speeds in the test range. The fuel economy results from the vehicle simulation which were generated from the same data showed the same trends.

F. The motoring friction horsepower and mean effective pressure increased at a significantly higher rate in the Buick engine. However the lower speed friction mean effective pressure was higher for the Mazda engine. These data offer a partial explanation for the decreasing difference in fuel economy observed with increasing speed in the vehicle simulation.

G. The exhaust temperatures at similar conditions were similar in the Mazda and Buick engines. This is primarily attributable to the fact that the Mazda was operating considerably richer than the Buick. Had they been operated with equivalent mixture ratios, the Mazda would have exhibited considerably higher exhaust temperatures.

H. The aldehyde emissions of the Mazda were generally in the range reported as typical for reciprocating engines, 30 to 200 ppm as formaldehyde. Aldehydes increased with increasing air-fuel ratio almost linearily and also increased with increasing load without the thermal reactor. When the thermal reactor and air injection were employed, the aldehydes were reduced by a factor of approximately 5.

I. Air-fuel ratio influenced the fuel consumption and emission performance of the Mazda engine in a manner essentially similar to that for reciprocating engines.

1. Brake specific fuel consumption was a minimum between .9 and 1.0 equivalence ratio (lean).

2. The BSHC emissions were minimum at approximately .9 equivalence ratio and increased by approximately a factor of 2 at an equivalence ratio of 1.4.

3. The BSCO emissions were constant at less than 25 grams per bhp hr leaner than an equivalence ratio of approximately .95 and then increased linearily with mixture enrichment.

4. The BSNO$_x$ emissions were a maximum between an equivalence ratio of .9 and 1.0. Near this maximum point, load exhibited a considerable effect on the emission level whereas at rich mixtures, in the range of 1.2-1.4 equivalence ratio, the effect of load was minimal.

J. In general the effect of ignition timing variations on fuel consumption and emissions appeared to be considerably less than expected with reciprocating engines.

1. The BSFC increased with spark retardation. For example at 2000 rpm, 26.3 bhp, the BSFC decreased from .57 to .67 with 30° retard from MBT.

2. The BSHC emissions decreased with spark retard with lean mixtures but exhibited little change when the "stock" richer mixtures were used.

3. Ignition timing did not influence BSCO emission

4. Brake specific NO_x emissions increased slightly with ignition retardation.

K. The hydrocarbon formation processes within the combustion chamber of the Mazda engine are judged to be non-homogeneous based upon studies of the exhaust gas. The exhaust from the region of the chamber nearest the apex seal was particularly high in hydrocarbons in comparison to the exhaust from the more central portion of the chamber. The variation between the maximum and minimum was approximately 3 to 1.

These data suggest that the primary sources of unburned hydrocarbons in the Mazda exhaust were from leakage of unburned fuel past the apex seal and incomplete burning in the trailing apex seal region of the chamber. The carbon monoxide emissions demonstrated little spatial variation in the exhaust gas suggesting that the mixture ratio was reasonably homogeneous in the combution chamber.

Additionally the relatively high O_2 content in the exhaust of the Mazda engine even with rich fuel-air mixtures and no air injection suggests that a significant fraction of the fuel-air mixture is exhausted without burning.

L. From the evaluation of the pressure records of the Mazda engine and by comparing them with data from the literature, several observations can be made.

1. Firing engine - The polytropic exponents for both compression and expansion were lower than data reported for reciprocating engines, suggesting that the heat transfer and/or leakage of the gases near top dead center was greater in the rotary engine.

2. Motoring engine - The motoring engine exhibited higher polytropic exponents than the firing engine. Compared to a reciprocating engine they were lower during compression and higher during expansion. Again this suggests greater leakage and heat losses in the rotary engine.

M. Qualitative Observations

The Mazda engine was remarkably smooth and quiet in the test cell, whereas the Buick V-6 was considerably "rougher", particularly at low speeds. Both engines demonstrated excellent durability and no maintenance other than normal servicing was required.

SECTION III

TEST EQUIPMENT

A. TEST ENGINES

Pertinent data for the 1975 Mazda Model 13-B rotary engine and Buick V-6 test engines are shown in Table I. The Mazda engine was furnished by the Toyo Kogyo Company of Japan and the Buick engine by the Buick Division of General Motors Corporation. The Mazda engine was evaluated both with and without its emission control system whereas the Buick was tested without a catalytic reactor but with all other emission control devices including EGR. As received, both engines were tailored to meet the 1975 emission standards of 1.5, 15 and 3 g/miles of hydrocarbons, carbon monoxide and oxides of nitrogen respectively.

Mazda Emission Control System

The Mazda 13-B engine was equipped with the standard 1975 U.S. version emission control system consisting principally of an insulated thermal reactor, Fig. 1, an air injection pump and an electronic control system. The standard Mazda vehicle emission control box was replaced with a manually operated control by which it was possible to control the air pump flow valves and spark plug firing in a manner similar to the vehicle system. The operating sequence of the air pump control valves and trailing and leading spark plugs is shown in Fig. 2. In the Mazda system both load and speed sensitive air control valves in addition to control of spark plug firing were employed. These factors together with mixture ratio were carefully tailored to ensure vehicle compliance with the 1975 Federal emission standards. The "A" air control valve is speed sensitive and in the off position directs air to the exhaust gas in the thermal reactor. When this valve is actuated (on) air is diverted to the reactor cooling jacket. In the present studies the valve was operated manually. The "C" valve is load sensitive and permits functioning of a vacuum operated air injection cut-out switch. At just "off idle" load the "C" valve is turned on. Air injection is still allowed but now when the throttle is opened, the vacuum operated air-injection "cut-out" valve stops air delivery to the exhaust and directs it to the reactor cooling jacket. Both the "C" valve and load sensitive "cut-out" valve were operated automatically in this test program. A detailed explanation of the emission control system is included in ref. 4. No EGR is used to control NO_x.

TABLE 1

TEST ENGINE SPECIFICATIONS

	Mazda Rotary	Buick V-6
Model	1975-13-B	1975 V-6
Displacement in^3 (cc)	80 (1308)	231 (3777)
	160 cid equivalent 4-cycle displacement	
Rated BHP at RPM	110 @ 6000	110 @ 4000
Rated Torque at RPM ft. lb (Nm)	117 (159) @ 3500	175 (237) @ 2000
Compression Ratio	9.2:1	8.9:1
Carburetion	Downdraft, 2-stage 4-barrel	Rochester Model 2GC
Ignition	Kettering system-2-spark plugs/housing	Delco HEI system
Ignition Timing	0°BTC leading plug, 15° ATC trailing plug, @ 500 rpm	12° BTC @ 600 rpm
Emission Control	Thermal reactor with air injection plus engine modification	Catalytic reactor, EGR, engine modifications, carb. preheat
Valve or Port Timing	Intake opens 32°ATC Intake closes 50°ABC Exhaust opens 75°BBC Exhaust closes 38°ATC	Intake opens 17°BTC Intake closes 73°ABC Exhaust opens 68°BBC Exhaust closes 29°ATC

Volume displaced by 1 rotor face in 1 rotor revolution multiplied by the number of rotors.

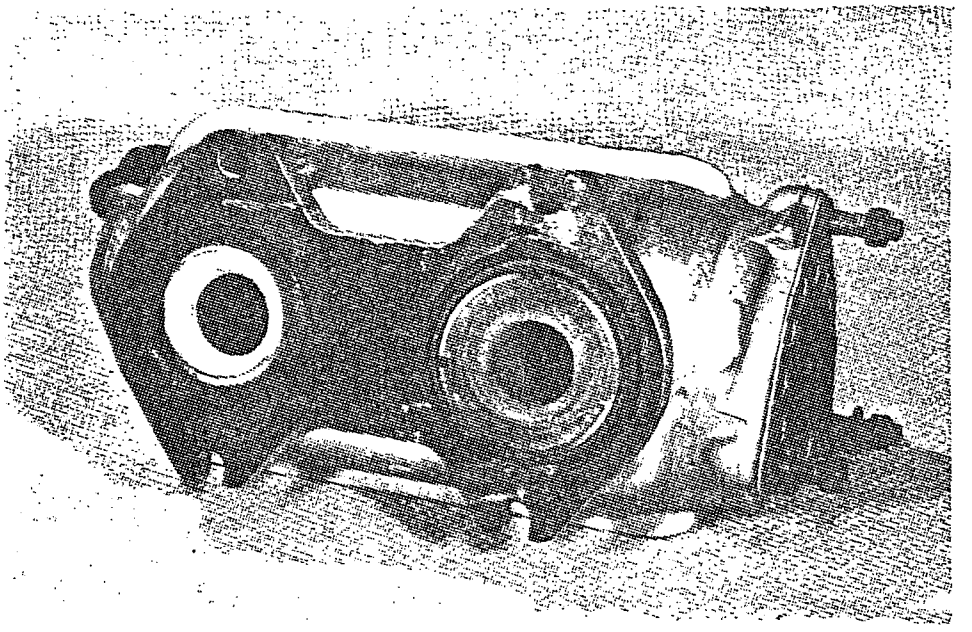

Figure 1. Insulated thermal reactor used on the Mazda 13-B engine as viewed from the engine exhaust port contact surface.

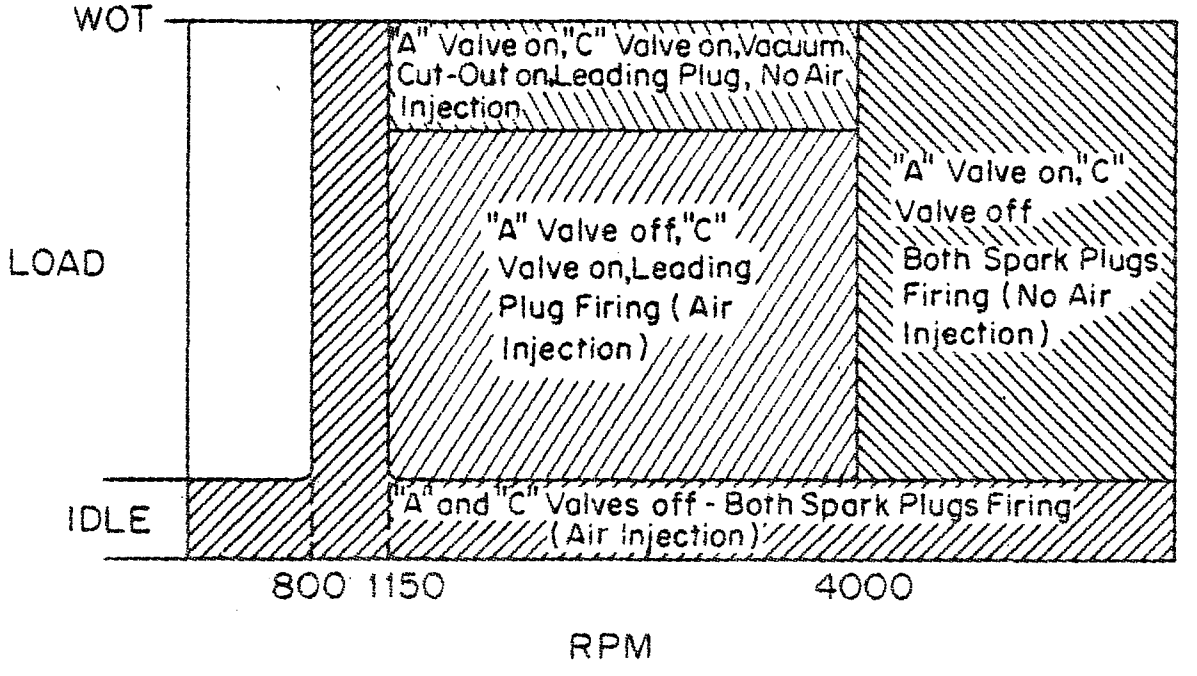

Figure 2. Schematic diagram showing operating modes of the various air injection control valves and spark plug firing of the Mazda 13-B emission control system.

B. DYNAMOMETER INSTALLATION

The Mazda 13-B and Buick V-6 engines were both installed in Room 243 at the University of Michigan Walter E. Lay Automotive Laboratory, and connected to a 200 HP Model Westinghouse electric dynamometer. Since it was necessary to test the Mazda engine at higher speeds than permitted in the dynamometer cell, this engine was connected to the dynamometer through a manual shift Mazda 4-speed transmission which was run in third gear for the higher speed tests. The installation is shown in Figs. 3 and 4. Because of a slight inefficiency of the transmission, the dynamometer load was adjusted to compensate for the additional drag in the transmission. Toyo Kogyo provided mechanical efficiency data for this correction. The Buick engine, which was connected directly to the dynamometer, is shown in Fig. 5. Both installations were performed according to established practice.

1. Engine Cooling

Water was used as a coolant in an open, tower-type cooling system. A thermostatically-controlled flow of city water was used to maintain the coolant inlet temperature in a range specified by the manufacturer.

2. Oil System

Since the Madza engine uses the lubricant to cool the rotor it was necessary to supplement the normal cooling available from the engine itself. A special cross flow water-oil heat exchanger was installed in the dynamometer cell for this purpose. The proper control of the lubricant was maintained with the engine's own internal thermistat rather than employing separate temperature controls outside of the engine. No external oil cooling was required for the Buick V-6.

3. Exhaust System

The standard laboratory exhaust system was used to remove the engine exhaust. In all tests either the standard major engine system components (thermal reactor and muffler) or a simpler system with a restriction inserted (to permit back pressure adjustment to that of the "stock" system) was used. The Mazda engine was run both with and without the thermal reactor installed. No catalytic convertor was used on the Buick.

C. INSTRUMENTATION

1. Fuel Measurement

The fuel rate was measured with a Model 1971 Testron volumetric burette associated with a timer and electronic counter. The timer was triggered by electric contacts when the fuel in the burette was displaced by electrolyte. The air flow measurements

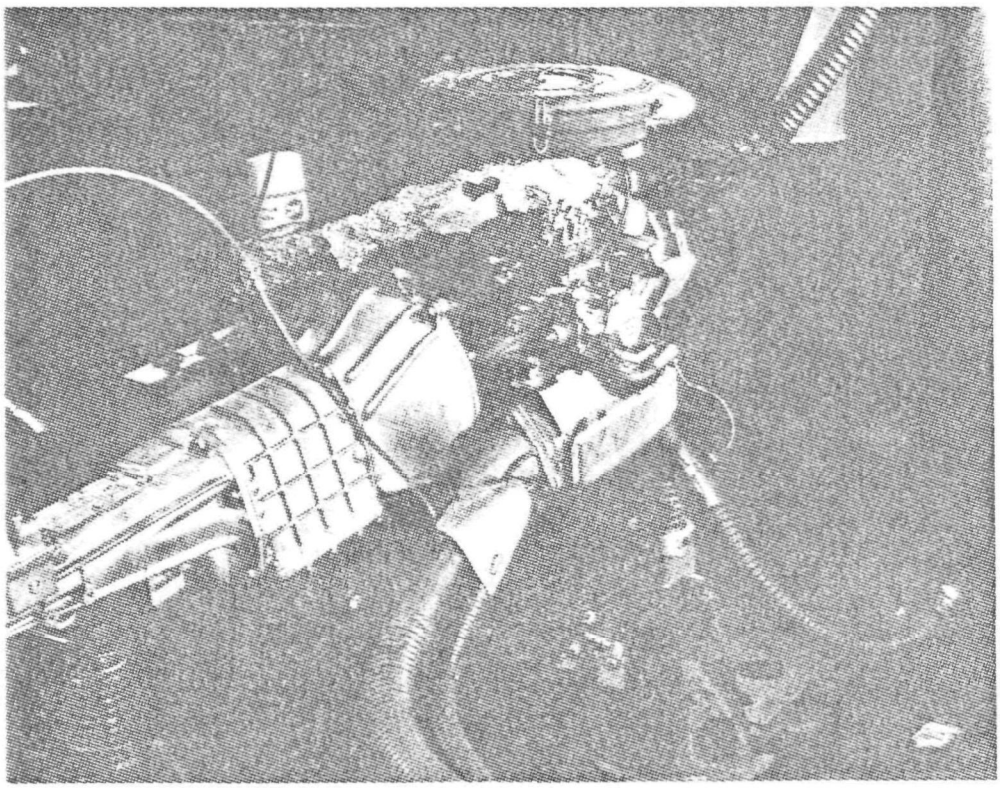

Figure 3. Rear quartering view of the Mazda 13-B engine installation.

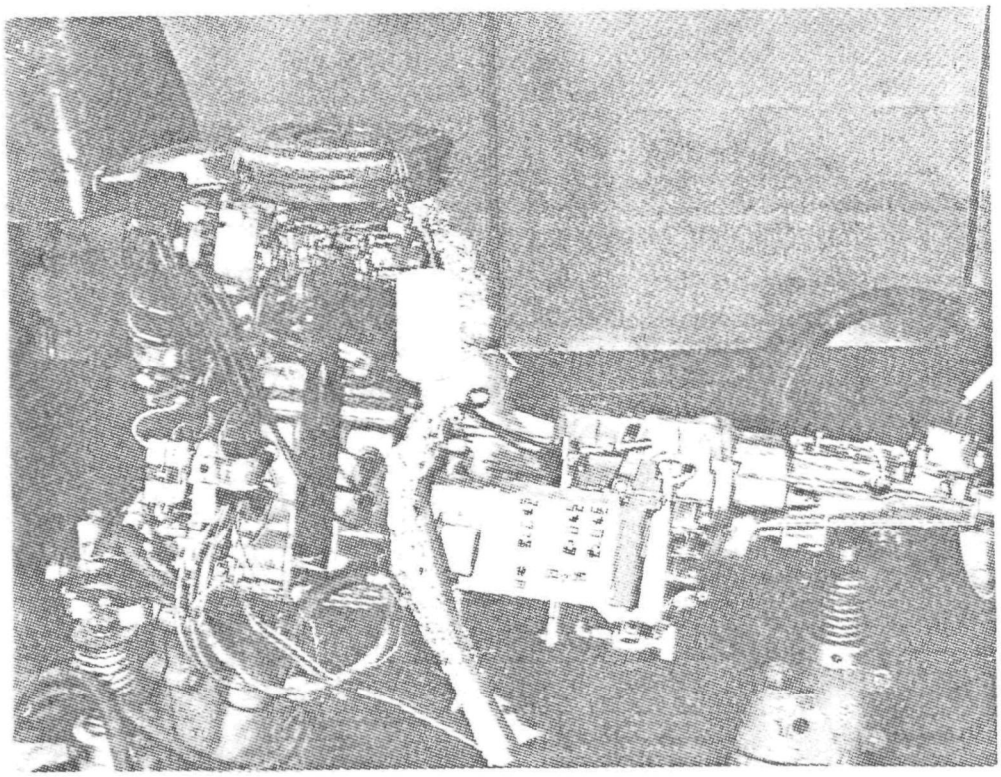

Figure 4. Side view of the Mazda 13-B engine installation.

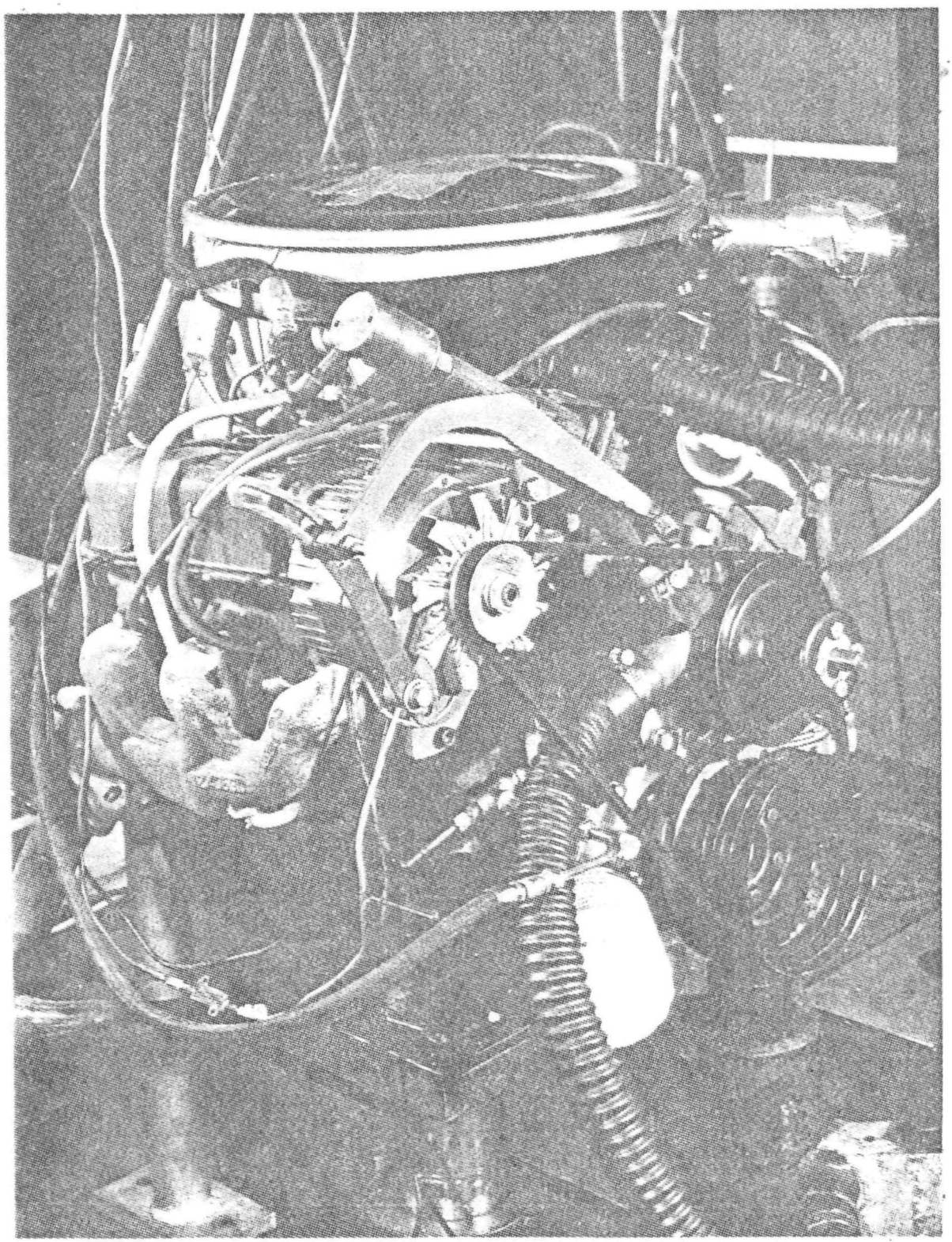

Figure 5. Front quartering view of the Buick V-6 engine installation.

were made concurrently with the fuel measurements. In this way, any abnormalities in fuel or air consumption could be detected and noted when evaluating the data. Several fuel readings were taken during each run and averaged. The run was rejected if the fuel flow varied by more than 5%.

Since the fuel volume was measured, it was necessary to determine the fuel density at the time and location of measurement. This was done before each test by measuring the API (American Petroleum Institute) number of a fresh sample of the indolene test fuel with an API hydrometer. Fuel density was corrected to the burette temperature.

2. Engine Air Measurement

Carburetor air flow was measured by a calibrated Meriam, Model 50 MC2-4SF, 400 CFM laminar flow element in conjunction with a Meriam, Model 34FB2, micromanometer, Fig. 6. To minimize flow pulsations through the laminar element, the flow meter was mounted on the inlet of a large surge tank. The surge tank was equipped with a "blowout" membrane to prevent damage to the tank and flow meter in case of "back-fire".

From the calibration curve of the flow element, the differential pressure across the flow element was converted to volumetric flow rate. In turn the flow rate was corrected for temperature, viscosity, pressure, and humidity to obtain a dry air-mass flow rate. Before and after each test, the humidity was determined from wet and dry bulb temperature readings.

3. Temperature Measurement

Because of the possible effect of temperature on engine operation and exhaust emissions (both inside of the engine and in the exhaust system), to ensure that the engines were stabilized prior to data acquisition and to permit calculation of certain performance factors, various temperature data were acquired. These included the exhaust, oil, water, fuel and ambient temperatures. All temperature measurements were made using thermocouples and various potentiometer read-out devices.

A Brown dual-range, continuous indicating potentiometer was used to read the copper-constantan (0-250°F, -18-121°C) and chromel-alumel (0-1800°F, -18-982°C) thermocouples. The temperatures at the exhaust port and at downstream sample probes were measured using bayonet-type chromel-alumel thermocouples. These thermocouples were unshielded, and therefore the actual gas temperatures were higher than those indicated because of the radiation losses from the thermocouple to the cooler exhaust pipe surfaces.

4. Exhaust Emission Measurement

a. Exhaust Gas Sampling

Water-Cooled Probes -- For all of the baseline and parametric variation tests a 1/4 in. (.64 cm) water-cooled, stainless-steel sample probe was used to collect the hot exhaust gas, Fig. 7. The water-jacketed probe was not cooled at the sample inlet but at the exterior surface of the exhaust pipe. The probe was designed to cool the exhaust sample and minimize the possibility of chemical reactions in the sample line. The "cooled" sample was then ducted, at room temperature, to the analytical instruments. While these probes could be positioned to sample anywhere across the diameter of the pipe, early tests indicated no significant concentration gradient across the diameter of the exhaust pipe downstream of the reactor in the case of the Mazda engine or in the sample section of the Buick's exhaust. As a result, the probes were adjusted to sample from the center of the exhaust stream.

Teflon tubing (1/4 in, .64 cm) was used for all sample lines involved with hydrocarbon measurement and nylon tubing (1/4 in, .64 cm) for the remainder of the sampling circuit. Previous work with exhaust sampling bags has indicated that many common tubing materials, including nylon, absorb hydrocarbons readily (5). Because the reactor output hydrocarbon concentrations were often very low and the inside of tubing comprises a relatively large surface area, Teflon tubing was used for any lines involved in hydrocarbon measurement.

To prevent water vapor and particulate contamination of the analytical system, an ice bath and particulate filter made by Gelman Instrument Company were installed in the sampling circuits ahead of the analyzers.

Uncooled Probes (Hydrocarbon Distribution Studies) -- In the steady-state sampling studies to determine spatially resolved hydrocarbon emissions in the exhaust a series of 10 sample probes located 3 in (7.6 cm) apart along a length of exhaust pipe were used, Fig. 8. The first probe was located 1.5 in (3.8 cm) from the exterior face of the exhaust port. These probes were all uncooled and employed a single inlet hole in a plane parallel to the axis of the exhaust pipe. Exhaust was sampled continuously. It was impossible to cool these probes because of cost. However, in prior studies it had been found that quenching of the sample had relatively little influence on the higher concentration emission data.

Flow from these probes was ducted to a manifold in which a series of valves enabled introduction of sample from a given probe to the main sample line. Only the exhaust from one rotor was sampled in this phase of the study. Specially contructed individual exhaust pipes of 1.5 in (3.8 cm) inside diameter were fabricated. The length of the pipe fitted with sample probes was designed to accommodate, in the sample section, at least the total mass of exhaust gas displaced by one rotor face at the highest load tested and at the temperature and pressure of the exhaust.

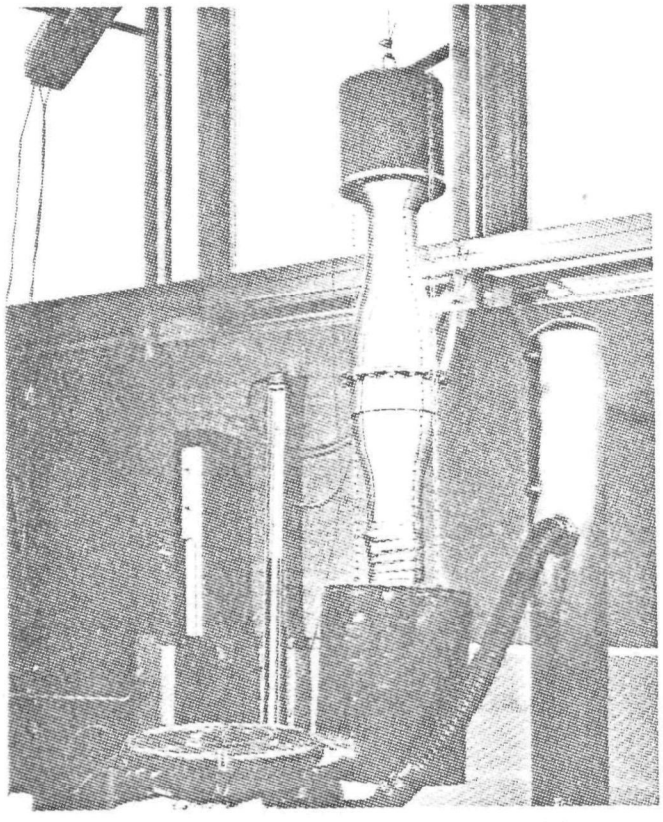

Figure 6. Merriam laminar flow meter and inlet surge chamber.

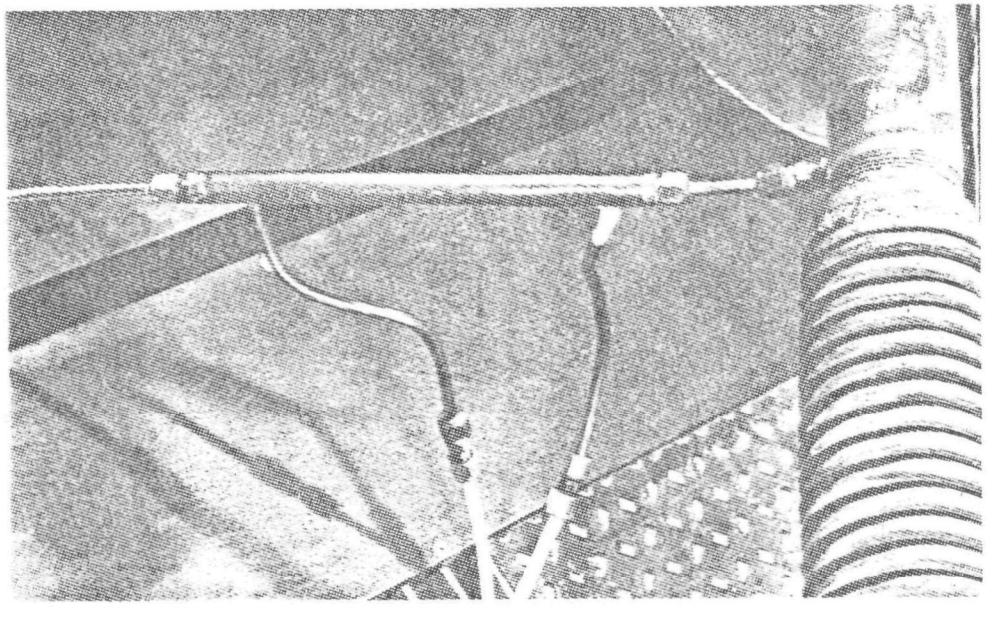

Figure 7. Water-cooled sample probe

Sampling Valve (Hydrocarbon Distribution Studies) -- The key device used in the study to determine the time resolved composition of the exhaust leaving the exhaust port was a Cox type 6 timed sampling valve, Fig. 9. The valve was located 2.5 in. (6.4 cm) from the exterior face of the drive end (toward dynamometer) exhaust port. A schematic diagram of the Cox valve is shown in Fig. 10. Basically the device consists of a 15/64 in. (.6 cm) diameter valve head with a stem which extends into and is a permeable core in an electromagnetic coil. An adjustable spring maintains the valve in contact with its seat. At a specified time in the test cycle a large capacitor is discharged through the coil and the magnetic field established attempts to eject the valve. The valve lifts approximately .012 in. (.03 cm) from its seat and during this interval the sample is obtained. Duration of valve lift was found to be less than 10 msec. Because of low valve lift and relatively short duration of opening only a small fraction of sample was extracted from the exhaust. The sample flow rate through the valve was less than .5 cfh (3.9E-.06 m^3/sec). The timed capacitor discharge was derived from a specially constructed device available at the University of Michigan Automotive Laboratory. The valve could be opened at a known and controllable crank angle position. Since the unit was designed for 4-cycle reciprocating engines, a pulse was generated and therefore the valve opened every 720 degrees of crankshaft rotation. This meant that exhaust was sampled from every other rotor chamber rather than the same one. Thus the exhaust was sampled from chamber 1,3,2,1,4,2,...i.e. every other cycle. The sample obtain- represented the integral of the exhaust from all three chambers. Therefore differences between the performance of individual chambers could not be detected.

b. Emission Analyzers

The various exhaust emission analysis techniques are summarized in Table 2.

NDIR Carbon Monoxide, Carbon Dioxide -- Carbon monoxide and carbon dioxide concentrations were measured with NDIR analyzers. This technique measures the differential absorption of infrared energy between a fixed reference gas and the exhaust sample gas. Because of the high concentration of CO in the rotary engines uncontrolled exhaust (0-10%) and even higher levels of CO_2 in all cases (0-15%), short sample cells were used. Since with lean mixture operation and/or after-exhaust treatment, concentrations of CO can be very low, it was necessary to supplement the short path Beckman instruments with a long path Horiba, Model AlA-21 CO analyzer with a range of 0-1%. Before each test, the NDIR analyzers were calibrated with dry N_2 as a zero gas and several known span gases.

FID Hydrocarbons -- A Beckman 109A unheated flame ionization detector (FID) was used to measure total hydrocarbons in the exhaust. This instrument is typical of those used by EPA and others for modal hydrocarbon measurement.

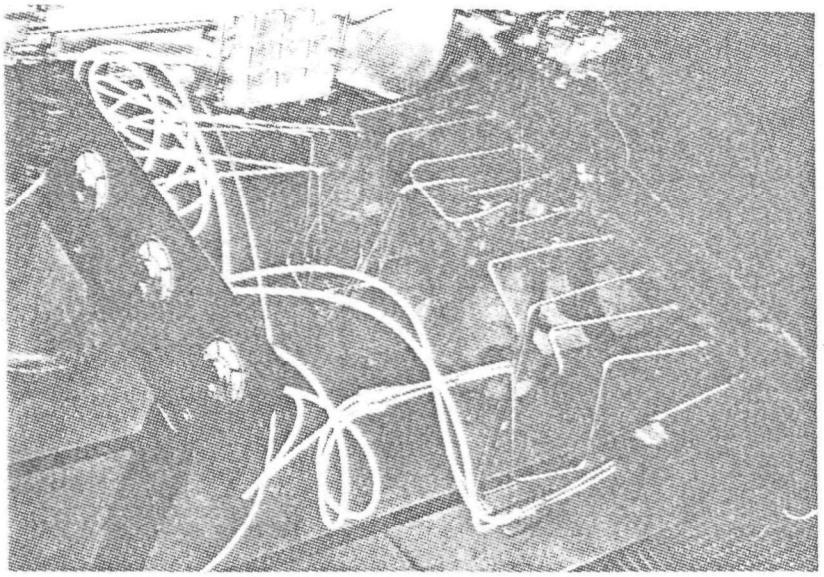

Figure 8. Manifold sampling system used in the qualitative study of hydrocarbon distribution in the exhaust gas.

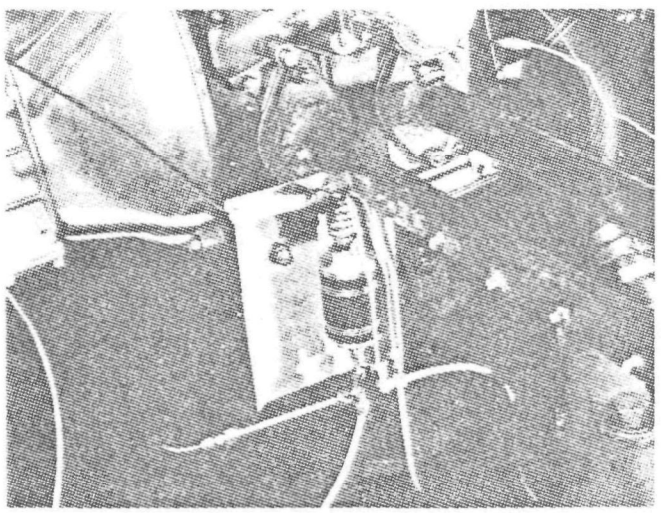

Figure 9. Cox timed sampling valve as installed in the exhaust pipe of the Mazda 13-B engine.

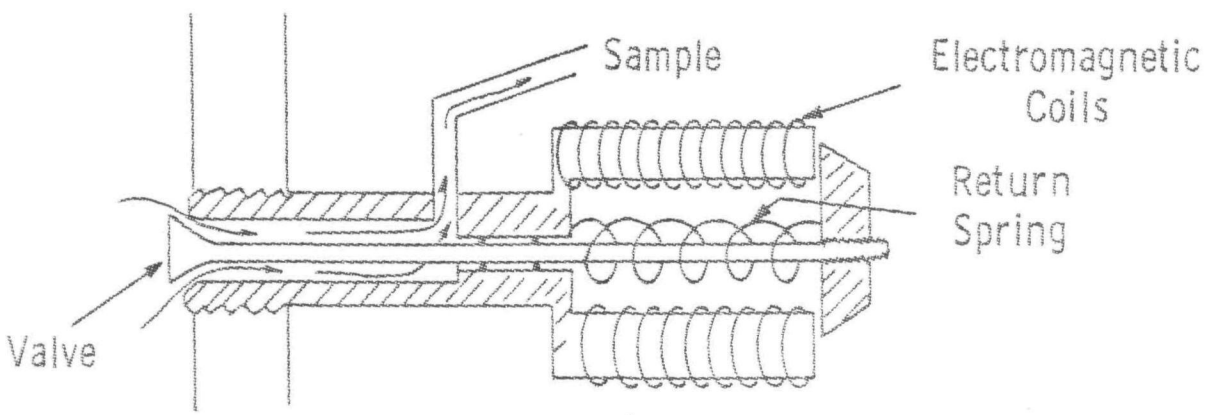

Figure 10. Schematic diagram of the Cox timed sampling valve.

TABLE 2

GAS ANALYSIS TECHNIQUES

Exhaust Specie	Technique	Manufacturer	Range
Carbon monoxide	NDIR[1]	Beckman Inst. Model 315A	0-10%
Carbon monoxide	NDIR[1]	Horiba Inst. Model A1A-21	0-1%
Carbon dioxide	NDIR[1]	Beckman Inst. Model 315A	0-15%
Nitric oxide	Chemiluminescent	Thermoelectron Inst. Model 10A	0-10,000 ppm
Hydrocarbon	FID[2]	Beckman Inst. Model 109A	0-5000+ ppm
Oxygen	Amperometric	Beckman Inst. Model 715	0-5% or 2-25%
Aldehydes	DNPH[3]	Wet chemical and Bausch & Lomb Spectronic 20 Spectrophotometer	

1. NDIR-nondispersive infrared
2. FID-flame ionization detector
3. DNPH-dinitrophenylhydrazone wet chemical method.

A separate hydrocarbon sampling circuit, complete with condensate trap, pump, and particulate filter was branched off the main sample line. Sample flow rate to the detector was mainted between 4.7 E-05-4.8 E-05 m^3/sec with the aid of a Fischer and Porter rotameter and needle type flow control valve. Since the accuracy of the FID is greatly affected by the sample bypass flow, a Fischer and Porter 7.0 SCFH, rotameter was installed in the bypass line to insure the sample flow and calibration gas flow through the burner were equal.

While the instrument was used in conventional form, the operating parameters were optimized to minimize error due to O_2 interference and to provide equal response to the various hydrocarbons in the exhaust. A mixture of 40% H_2 and 60% He was used as the FID fuel.

For the Cox timed sampling valve studies, the sample system was modified to minimize its volume to a minimum. This facilitated instrument response with the very low flow rates observed with the Cox valve.

Oxygen -- The oxygen concentration in the exhaust was measured with a Beckman Model 715 amperometric O_2 analyzer. Since the

composition of the dry exhaust gas is not altered by passage through the NDIR analyzers, the oxygen transducer was placed at the outlet of the CO_2 analyzer. Since this instrument has a linear response to oxygen concentration (actually partial pressure of O_2), it was calibrated with pure N_2 as the zero gas and atmospheric oxygen as the 21% O_2 span gas.

Several gases can cause O_2 interference, including SO_2, Cl_2, H_2S and NO. Since most of these compounds are not present in measurable concentrations, only NO could cause significant interference. However, because the NO concentrations ranged from 50-2500 ppm, its interference was also negligible.

The O_2 meter provides temperature compensation for gas temperatures between 32-110°F (0-43°C). After passing through the ice bath, the sample temperature is within this range.

Chemiluminescent NO_x -- The NO and NO_2 emissions were measured with a Thermoelectron Model 10A Chemiluminescent NO and NO_2 Analyzer. This instrument is capable to measuring either of the two nitrogen oxides or a combined concentration. All NO_x data is reported as NO. A discussion of the basic operation of this analyzer follows.

Sample is flowed to a cylinderical plug flow reactor which is maintained at a low pressure, typically five to seven torr. Simultaneously, ozone manufactured in a built-in ozonator is introduced into the reactor and well mixed with the sample in the region near the detector. A reaction between NO and O_3 occurs which produces some electronically excited NO_2 molecules. The decay to the ground state of these excited molecules emits light (photons) in the wave length region 0.6-3 u. This light is detected by a photomultiplier. The analyzer measures NO only, not NO_2. Because of the operating principle, the response is theoretically linear with NO concentration. Response is limited only by the volume of the sample lines and flow rate. By converting any exhaust NO_2 to NO, a value of total nitrogen oxides, NO_x can be attained. The conversion technique is based upon a surface reaction in which NO_2 decomposes to NO. To accomplish this, the sample gas, before entering the chemiluminescent detector, is flowed through a stainless steel tube which is resistance heated to 1200°F (649°C). This unit was periodically calibrated using appropriate span gases of NO in nitrogen.

Aldehyde Measurement - Mazda Engine -- Total exhaust aldehyde emissions were determined colorimetrically using the DNPH (dinitrophenylhydrazone) wet chemical method, (6). In this procedure, a small portion of the exhaust was bubbled through 2,4-dinitrophenylhydrazine solution. This gas volume was measured with a wet test meter. The precipitate formed was recovered, dissolved and treated with various chemicals until a color producing ion was formed. The optical density of this mixture was measured by a Bausch and Lomb Spectronic 20 Spectrometer calibrated on a formaldehyde

solution. Since the optical density is proportional to the amount of carbonyls in the sample and the principal carbonyl in the exhaust is formaldehyde, the DNPH wet chemical test is a good measurement of the aldehyde concentration in the exhaust.

The aldehyde sample was taken approximately 20 in (50.8 cm) downstream strom the thermal reactor. Heater tape wrapped around the sampling line maintained the sample temperature between 220-240°F (104-116°C) to prevent dissolution of all aldehydes in condensed water.

5. Pressure Measurement

Pressure was measured with a Kistler Model 601 piezoelectric transducer and Model 568 charge amplifier. The transducer was calibrated using a dead weight tester. It was installed in the trailing spark plug hole in place of the auxiliary spark plug. Thus during the firing sequences only the leading plug was fired. Figure 11 shows a sketch of the pressure transducer as installed in the chamber and the rotor in two positions with respect to the location of the transducer.

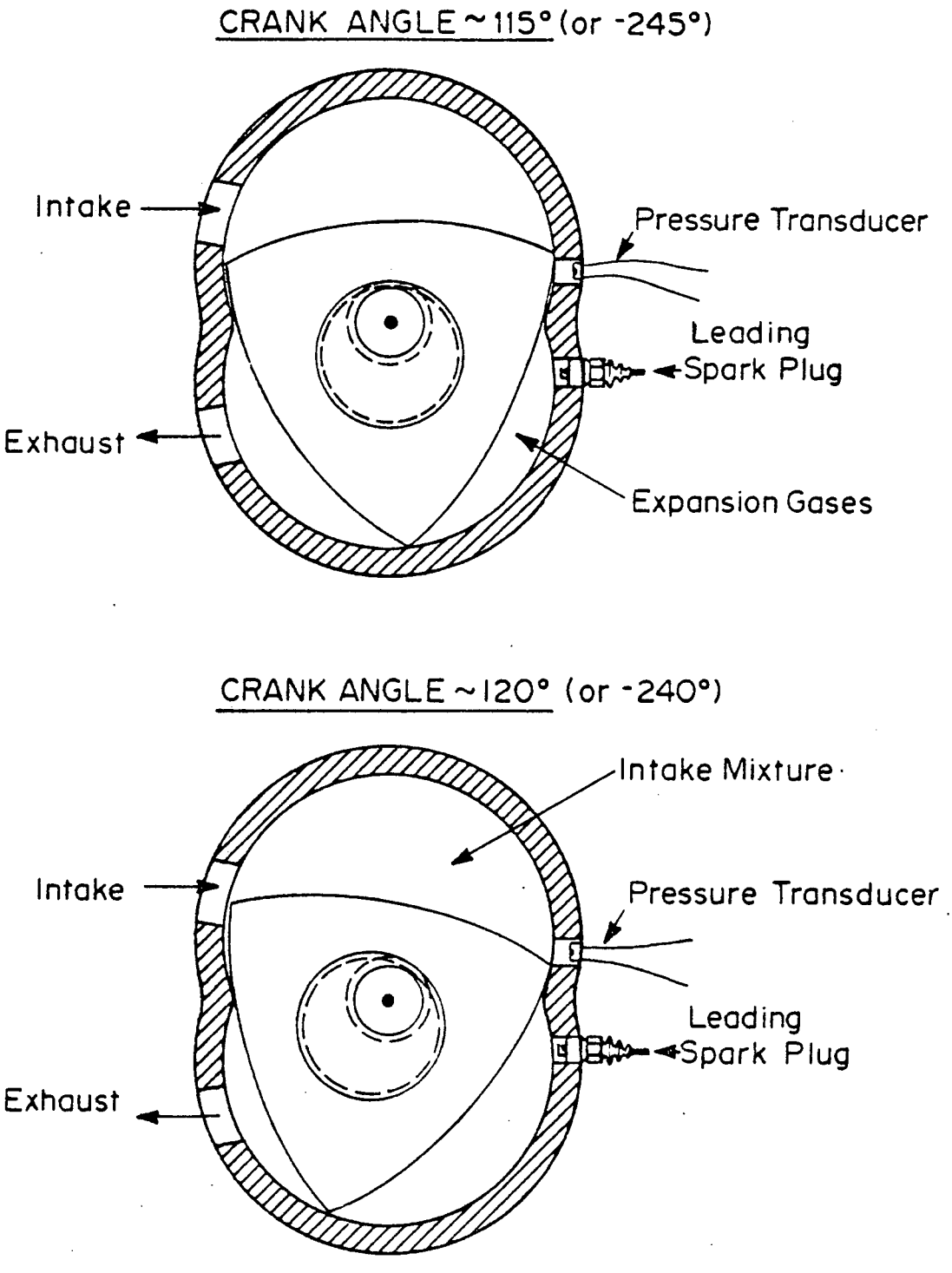

Figure 11. Schematic diagram of the pressure transducer as installed in the Mazda engine with the rotor in two different positions.

SECTION IV

TEST PROCEDURE

The testing program was divided into the following segments.

- Emission and fuel consumption map of the Mazda engine both with and without external emission control (thermal reactor).
- Emissions and fuel consumption map of the Buick V-6 engine used for comparative purposes.
- Parametric studies on the Mazda engine to determine the influence of F/A ratio and ignition timing on emissions and fuel consumption at selected test conditions.
- Evaluation of exhaust aldehyde composition at selected test conditions.
- Determination of pressure records.
- Timed sampling and manifold sampling studies to determine the sources of hydrocarbon emissions.

A. EXHAUST EMISSION AND FUEL ECONOMY MAPPING

The 1975 Mazda RX-4 vehicle was selected for definition of the engine performance requirements. Pertinent vehicle data is given in Table 3. The road load data for this vehicle, which was furnished by Toyo Kogyo, is also presented in Table 3. Two different axle ratios, 3.90:1 and 2.56:1 were used to match the engine to the vehicle. Mazda normally uses the higher ratio in the RX-4 and Buick generally employs a much lower ratio in its heavier vehicles. Both ratios were selected to span the range typically used in most vehicles.

The engines were "broken in" per each manufacturers recommendations. In addition key operating parameters were checked to ensure that they were within a range specified by the manufacturer.

The basic wide-open throttle performance of both engines was determined according to SAE procedure J245 with the exception that the stock exhaust system was used on the Mazda. Since the operator was located in the test cell the dynamometer speeds were limited to 3500 rpm maximum. However, the Mazda engine was run at a considerably higher speed, 5000 rpm, without exceeding 3500 dynamometer rpm through the use of transmission speed reduction. Since

the Mazda engine-transmission combination was used, all dynamometer loads were adjusted to compensate for transmission efficiency. Pertinent transmission data for the Mazda are also shown in Table 3.

TABLE 3

1975 MAZDA RX-4 VEHICLE SPECIFICATIONS AND ROAD LOAD DATA

Curb Weight:	2795 lb. (2168 kg)
Overall Weight:	3095 lb. (1404 kg)
Tire Size and Radius:	195/70SR13, 11.4 in (0.291 m)
Transmission Ratios and (Efficiency):	1st - 3.683 2nd - 2.263 3rd - 1.397 (.95) 4th - 1.0 (.98)

Vehicle, Speed		Engine RPM@ Axle Ratio		Horsepower
MPH	Km/hr.	3.90:1	2.56:1	HP
10	16.1	572	375	1.72
20	32.2	1144	751	3.86
30	48.3	1716	1126	6.85
40	64.4	2288	1502	11.11
50	80.5	2860	1877	17.05
60	96.5	3432	2253	25.11
70	112.6	4004	2628	35.71
80	128.7	4576	3003	49.26

All Mazda operation above 3500 rpm was in third gear. The Buick engine maximum speed was limited to 3500 rpm since it is normally used at a far lower maximum speed than the Mazda. In general sufficient numbers of points were selected to facilitate development of reasonably smooth fuel consumption and emission performance curves. A particularly large number of points were used to map NO_x data with the Buick engine which was equipped with an EGR control valve. Significant inflections of the NO_x data were observed for small load changes in the test range.

All emission and fuel consumption data were reduced and plotted with the aid of a Hewlett-packard 9830A programmable calculator-computer. Emission measurements are reported on a mass basis (grams) which necessitated the development of a program to convert concentration data to a mass base. This task was complicated when air injection was used because of exhaust dilution with the added

air. A carbon mass balance technique between the engine inlet and exhaust was used to generate a correction for the dilution factor.

B. MAZDA PARAMETER STUDIES

Fuel/Air Ratio

The fuel/air ratio was varied with the aid of a specially modified carburetor and air aspirator system furnished by Toyo Kogyo. This system enabled the pressure on the fuel in the carburetor float bowl to be varied from a partial vacuum to a positive pressure and this caused the fuel rate to be varied. Since it was expected that the effect of fuel/air ratio would follow similar trends at all speeds and loads, only three operating conditions were studied; 2000 rpm, 8.7 and 26.3 bhp, and 3000 rpm, 18.7 bhp. Two series of variable fuel/air ratio investigations were performed:

1. with standard ignition timing
2. MBT* timing

Ignition Timing

Ignition timing was varied by rotating the distributor and observing the spark advance or retard with a timing light directed at a flywheel mounted scale. This test series was conducted with both the stock carburetor mixture ratio and with a controlled air/fuel ratio of 16/1. The latter test was run with 16/1 air-fuel ratio rather than the typical reference setting of LBT (leanest air-fuel ratio for best torque) because the 16/1 ratio could be easily set, was expected to be near the point of maximum thermal efficiency, and a reasonable operating point should a catalyst be used in the future.

The ignition timing studies were also conducted at 2000 rpm, 8.7 and 26.3 bhp and 3000 rpm, 18.7 bhp.

C. ALDEHYDE EMISSIONS

Since the DNPH technique for aldehyde measurement is extremely tedious, data were acquired at selected test conditions. One series was conducted at 2000 rpm, 8.7 bhp with variable air-fuel ratio and MBT ignition timing. The other tests were run at 2000 rpm, 8.7 and 27 bhp and 3000 rpm, 18.5 bhp both with and without the thermal reactor installed. Details of the sampling procedure are presented in the earlier instrumentation section and in Refs. 6 and 7.

*MBT - minimum spark advance for best torque

D. HYDROCARBON SOURCE ANALYSIS - TIMED AND MANIFOLD SAMPLING SYSTEM

Time Resolved Sampling

This phase of the study was conducted with the Cox fast-response sampling valve. Time resolved samples of the exhaust were collected at 2000 rpm, 8.7 and 14.2 bhp, 2500 rpm, 13 and 22.4 bhp, 3000 rpm, 18.7 and 34.3 bhp from the specially constructed exhaust pipe. The time of sample acquisition was coordinated with crankshaft position which in turn was related to rotor position. All data expressed on a concentration basis.

Manifold Sampling

In this segment of the investigation data was acquired at the same conditions as in the foregoing series. It should be noted that this data was far more qualitative than that obtained with the Cox valve.

E. MAZDA ENGINE CHAMBER PRESSURE MEASUREMENT

Pressure data were acquired under both motoring and firing conditions at 2000 and 2500 rpm. The firing data were taken at part load. Motoring data were taken at both part and wide-open throttle. All data were recorded on a Tectronix dual-beam oscilloscope. These results in turn were replotted, processed and analyzed with the aid of the Hewlett-Packard Model 9830A calculator.

SECTION V

RESULTS AND DISCUSSION

A. FUEL CONSUMPTION AND EMISSION PERFORMANCE OF THE MAZDA 13-B ENGINE

1. Base Performance Data - Wide-Open Throttle

Initially a series of baseline wide-open throttle performance tests were conducted per SAE procedure J245. The corrected brake horsepower, brake mean effective pressure, brake torque, and brake specific fuel consumption are plotted as a function of RPM in Fig. 12. Generally the shapes of these curves are reasonably similar to those for reciprocating engines with the exception of the brake specific fuel consumption, BSFC. In this case, BSFC decreased significantly with increasing speed. This behavoir is probably attributable to the fact that the leakage of the fresh fuel and air mixture from a burning chamber to the exhausting chamber is essentially constant as a function of time at a given mean effective pressure. As the speed is increased, this leakage decreased as a percentage of the total mass of fuel and air provided to the engine, thereby having a lesser impact at the higher speeds than at the lower speeds. In addition, the friction horsepower increased at a lower rate than generally observed in a typical reciprocating spark-ignited engine, Refs. 8,9 and Fig. 42. The brake torque and brake mean effective pressure, BMEP, curves exhibited normal behavior although they peaked at a higher RPM than expected for a low-speed reciprocating engine. The brake horsepower, BHP, increased almost linearly with speed and attained a maximum beyond the test range. The trends evident in these wide-open throttle performance curves appear to be consistent with the excellent breathing characteristics and the lower friction horsepower at high engine speeds which are characteristic of rotary engines.

2. Fuel Consumption and Emission Performance Maps with Thermal Reactor, Air Pump and Exhaust System Installed

The BSFC map at the various test speeds is plotted as a function of BHP in Fig. 13. It should be noted that BHP was selected as the abscissa coordinate rather than BMEP for two important reasons. First, this helped to spread the data to prevent a significant "stack up" of the various curves. Secondly, with the brake horsepower information it is far easier to match the engine to the total vehicle. The BSFC curves have reasonably

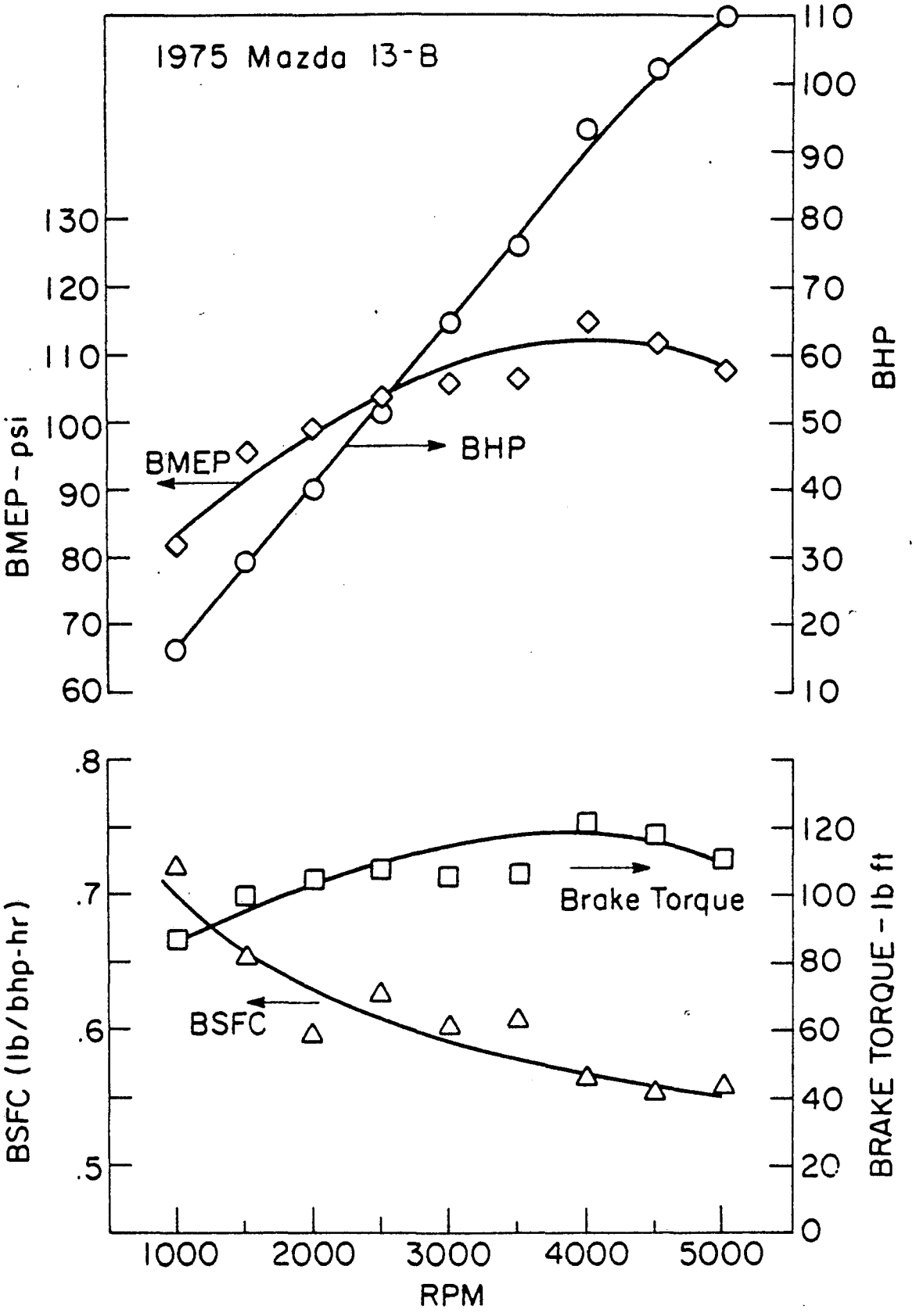

Figure 12. Wide-open throttle performance of the Mazda 13-B engine as a function of RPM.

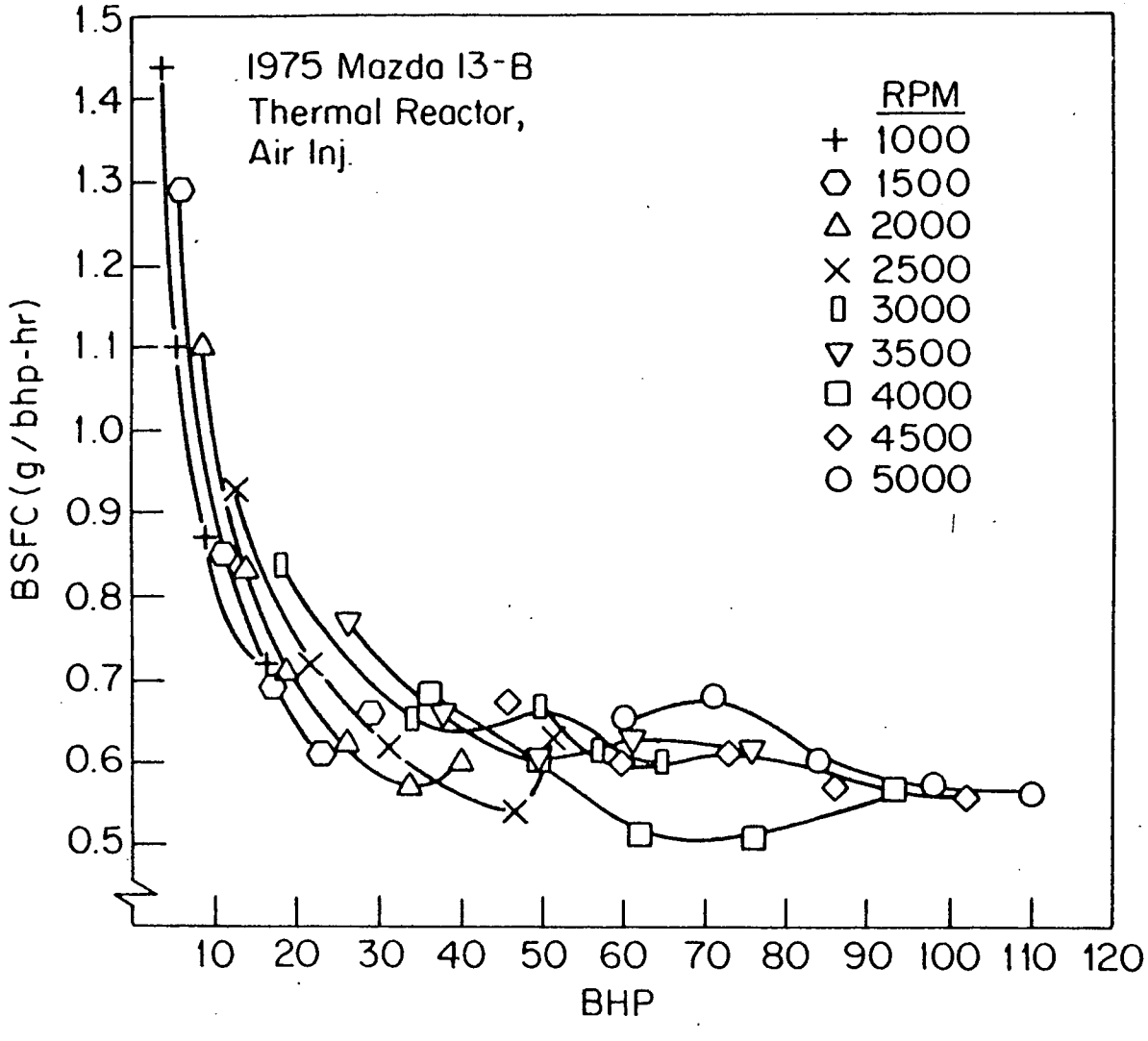

Figure 13. Brake specific fuel consumption as a function of brake horsepower, Mazda 13-B engine, with thermal reactor and air injection.

typical shapes, decreasing relatively quickly as BHP increased because friction horsepower was rapidly decreasing as a fraction of indicated power. For the lower speed runs the minimum BSFC point was attained at less than peak load which is typical of most spark-ignited engines. At moderate and high speeds, the wide-open throttle BSFC was less than at slightly lower loads which is not typical. This can be attributed to the relatively lean mixtures furnished by the Mazda carburetor at peak loads.

The exhaust emission characteristics of the Mazda 13-B engine with stock air injection with controls, and thermal reactor are plotted in Figs. 14 through 16. Specific emission rates are presented as grams of pollutant per brake horsepower hour and plotted as a function of BHP.

Figure 14 is a plot of brake specific hydrocarbon emissions, BSHC, as a function of BHP. At each speed, the lower load ranges were characterized by generally low levels of hydrocarbon emissions. As the load was increased to the point where the vacuum-operated air valve (C-valve) cut out the air injection to the reactor, the hydrocarbon emissions increased significantly. The C-valve did not operate at the 1000 rpm point but the air injection rate was not sufficient to achieve a sustaining reaction at higher loads. In addition both spark plugs were firing at 1000 rpm. For assistance in understanding the actuation of the air injection to the thermal reactor, the reader is referred to Fig. 2 in Section III. At 4500 and 5000 rpm, which are well beyond the normal driving range except for a transient acceleration or deceleration mode, the hydrocarbon emissions were relatively flat or constant at approximately 10 gram/hp-hr. At these speeds the A valve was "on" diverting the air from the exhaust ports to the reactor cooling jacket. Also both spark plugs were operating in each housing reducing the hydrocarbon input to the reactor. The tests at 4000 rpm were conducted with the A valve "off". This speed, as shown in Fig. 2, is normally the switching speed for the valve.

The brake specific carbon monoxide, BSCO, emissions are plotted in Fig. 15, and show a similar shape to the hydrocarbon data. Initially at the lower speeds and lighter loads the emission level was low followed by a rapid increase in BSCO at the higher load conditions due to elimination of the thermal reactor air injection. At 4500 and 5000 rpm the lighter load CO emissions were moderately high, approximately 50 grams/hp-hr, followed by a spike to approximately 200 grams/hp-hr. Thereafter the CO emissions were reduced rapidly to approximately 100 grams/hp-hr through the remainder of the load range. The spike was caused by a region of rich mixture at moderate load. Air was not being injected at 4500 and 5000 rpm. At 5000 rpm, for example, the air-fuel ratio was 13:1 at 71 bhp. At wide-open throttle, the production carburetor provided an air-fuel ratio of 14.5:1.

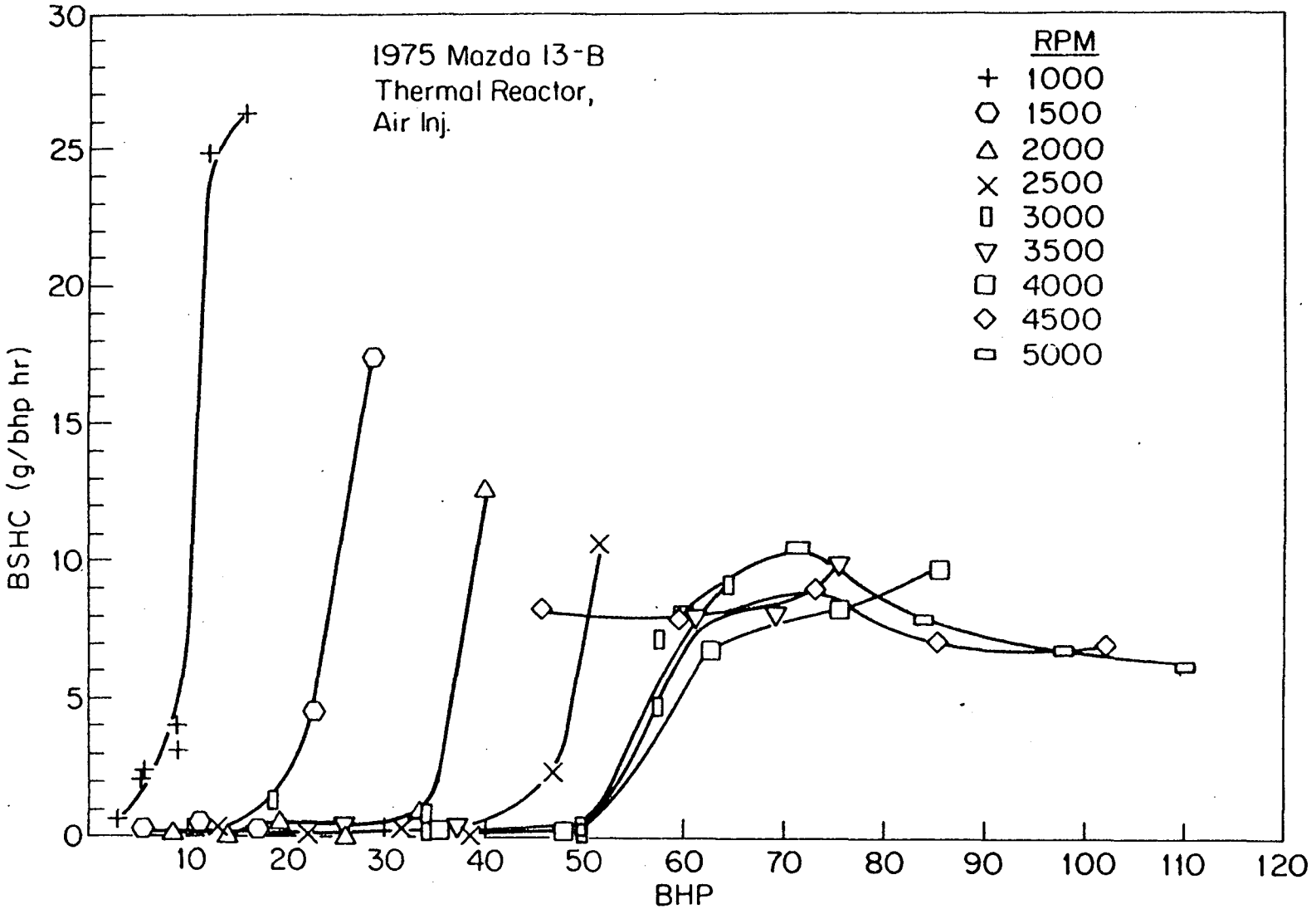

Figure 14. Brake specific hydrocarbon emissions as a function of brake horsepower, Mazda 13-B engine, with thermal reactor and air injection.

Figure 16 is a plot of the brake specific NO_x emissions, $BSNO_x$, as a function of BHP. In general the behavior was relatively erratic as is the case with most gasoline engines. At 1000 through 3500 rpm, the emissions increased to a maximum followed by a decrease at higher loads. The peak was associated with relatively lean mid-range mixture ratios. At 4500 and 5000 rpm, the NO_x emission levels followed a consistent pattern. At light loads the firing of both spark plugs caused the NO_x to be higher than light loads at the lower speeds. With increasing load NO_x increased, followed by a dip associated with the enrichment described earlier. It should be recognized that the thermal reactor has virtually no effect on the NO_x concentration. It is an oxidation device for the control of CO and unburned hydrocarbons.

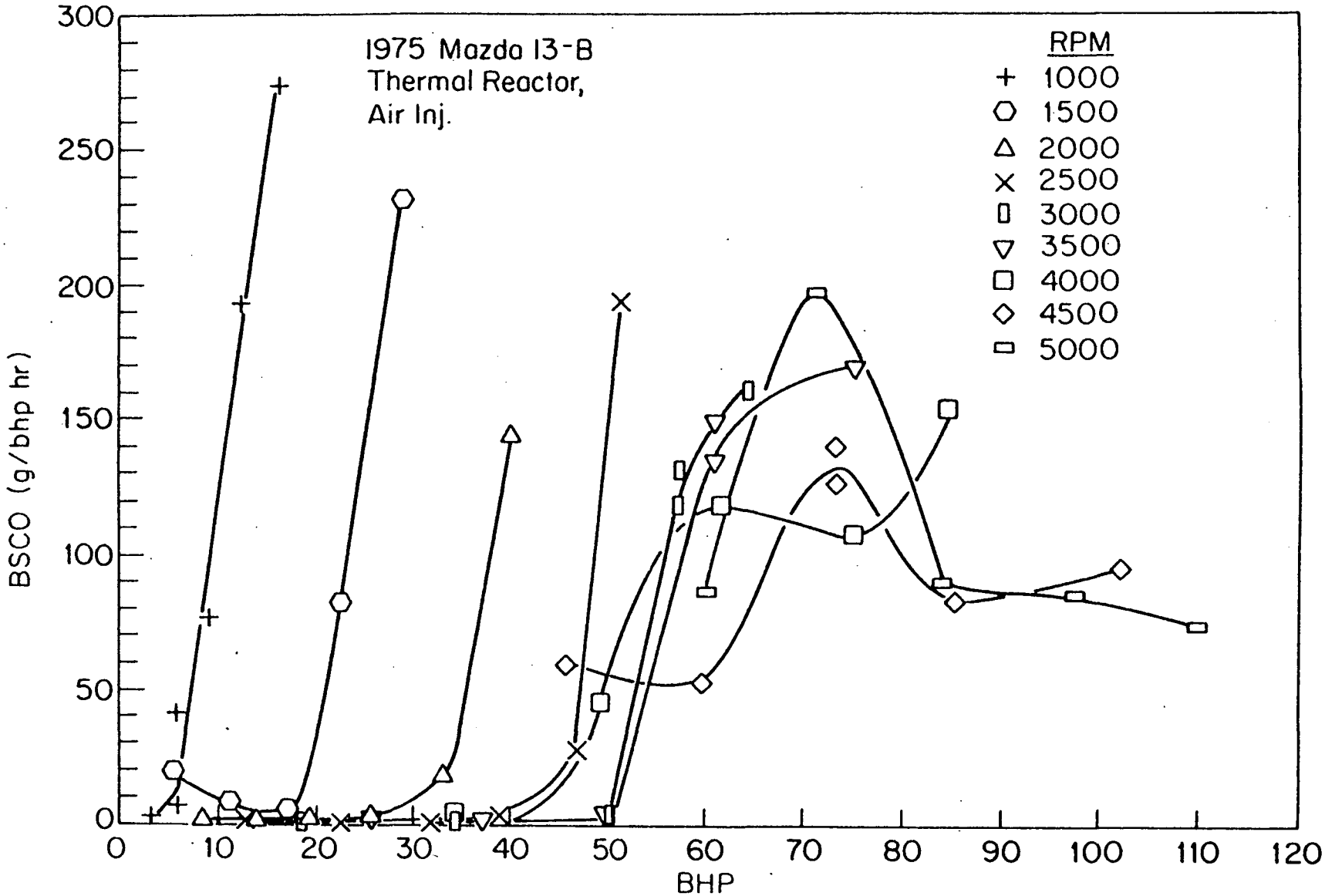

Figure 15. Brake specific carbon monoxide emissions as a function of brake horsepower, Mazda 13-B engine, with thermal reactor and air injection.

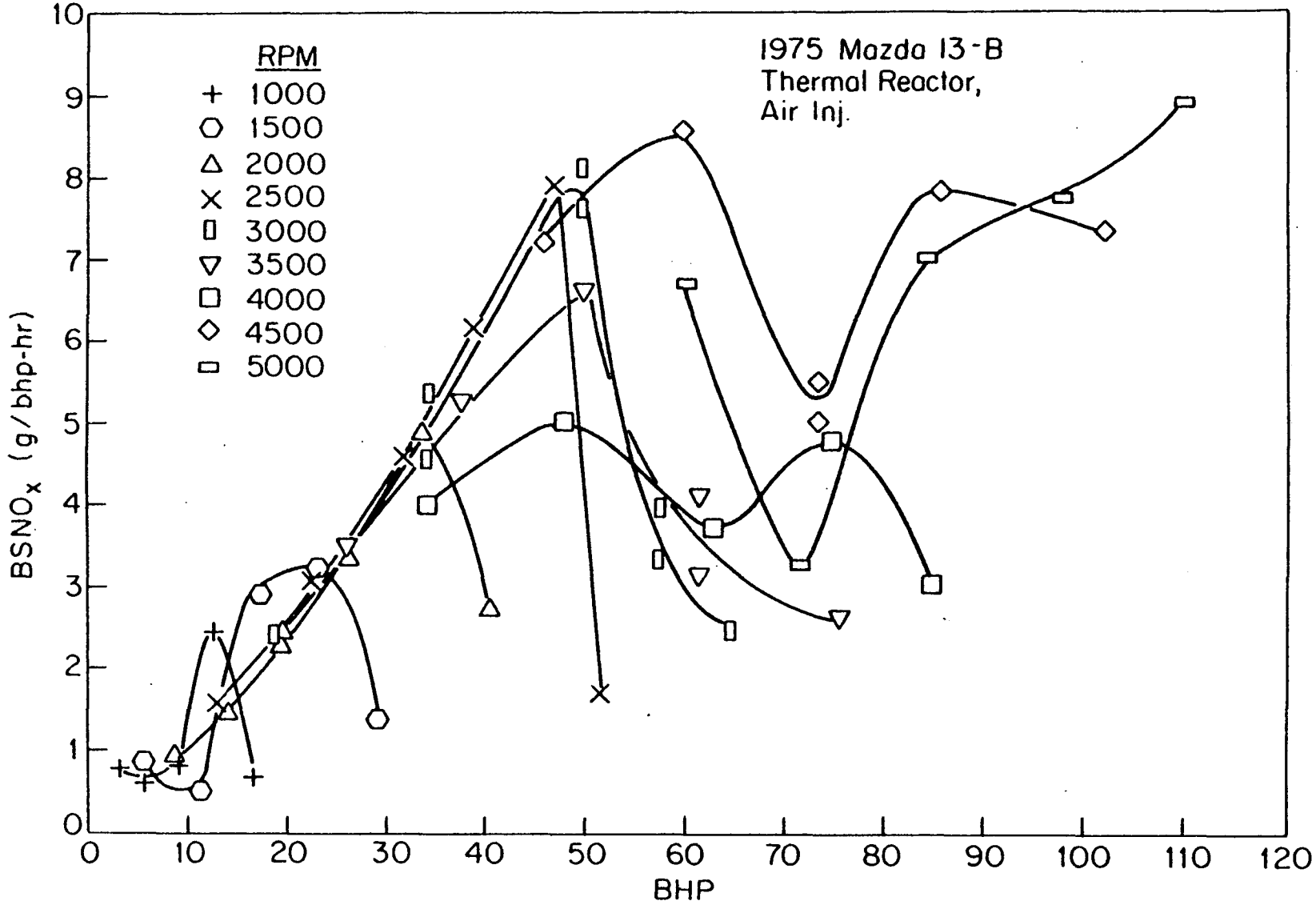

Figure 16. Brake specific nitrogen oxide emissions as a function of brake horsepower, Mazda 13-B engine, with thermal reactor and air injection.

3. Exhaust Emission and Fuel Consumption Performance Without Reactor Air Injection

In this series of tests the air injection was cut off to the thermal reactor and used totally as a coolant in the jacket around the reactor. The BSFC performance of the engine with and without the air injection was essentially the same, as would be expected, therefore these data are not re-plotted.

The hydrocarbon emissions are shown in Fig. 17. At 1000 and 1500 rpm the data were erratic. At moderate loads the emission level increased rapidly to a maximum and then exhibited a moderate decrease at the highest loads tested. The variation appeared to be consistent with variations in the engine air-fuel ratio. No explanation is apparent for the disproportionally low minimum at the light loads since the NO_x emissions were also relatively low. Hydrocarbon performance may have been influenced by a leak through the air control valve to the thermal reactor at these points. The remainder of the hydrocarbon data followed a reasonably consistent pattern. As speed and load were increased, the specific hydrocarbon emission level trended downward. The 4500 rpm point exhibited a slight variation from this behavior with a moderate peaking of the data in the mid-load range. The hydrocarbon results are closely related to air-fuel ratio and significantly to speed and load. As noted earlier at a given mean effective pressure the leakage rate of unburned fuel from the combustion to exhausting chamber is thought to be essentially constant in mass time per unit. With increasing mixture flow the leakage contribution to the total decreased on a fractional basis. The trend of the data strongly supports the view that leakage past the apex seal is a predominent factor in the formation of exhaust hydrocarbon emissions. In addition, at the higher loads at a given speed a more favorable condition exists for the after or thermal reaction of the unburned fuel and air-mixture in the exhaust. Of course this assumes that sufficient O_2 is present.

The O_2 content of the exhaust provides an indication of leakage and/or misfire. Figure 18 is a plot of exhaust O_2 concentration as a function of BHP at several representative engine speeds. With the rich mixtures normally used in the Mazda engine, one would expect the O_2 content of the exhaust to be low if combustion is reasonably complete. The significant O_2 content present is a strong indication that a substantial fraction of the mixture has not burned and either reflects leakage to the exhausting chamber, incomplete flame propagation or unburned mixture trapped and then released from the chamber crevices. It is our belief that the leakage factor is the most important of the three. Unfortunately, it is not possible to separate the influence of the various hypothesized sources with conventional emission sampling and analysis techniques. Gas chromotographic studies could provide considerable insight as to the source however.

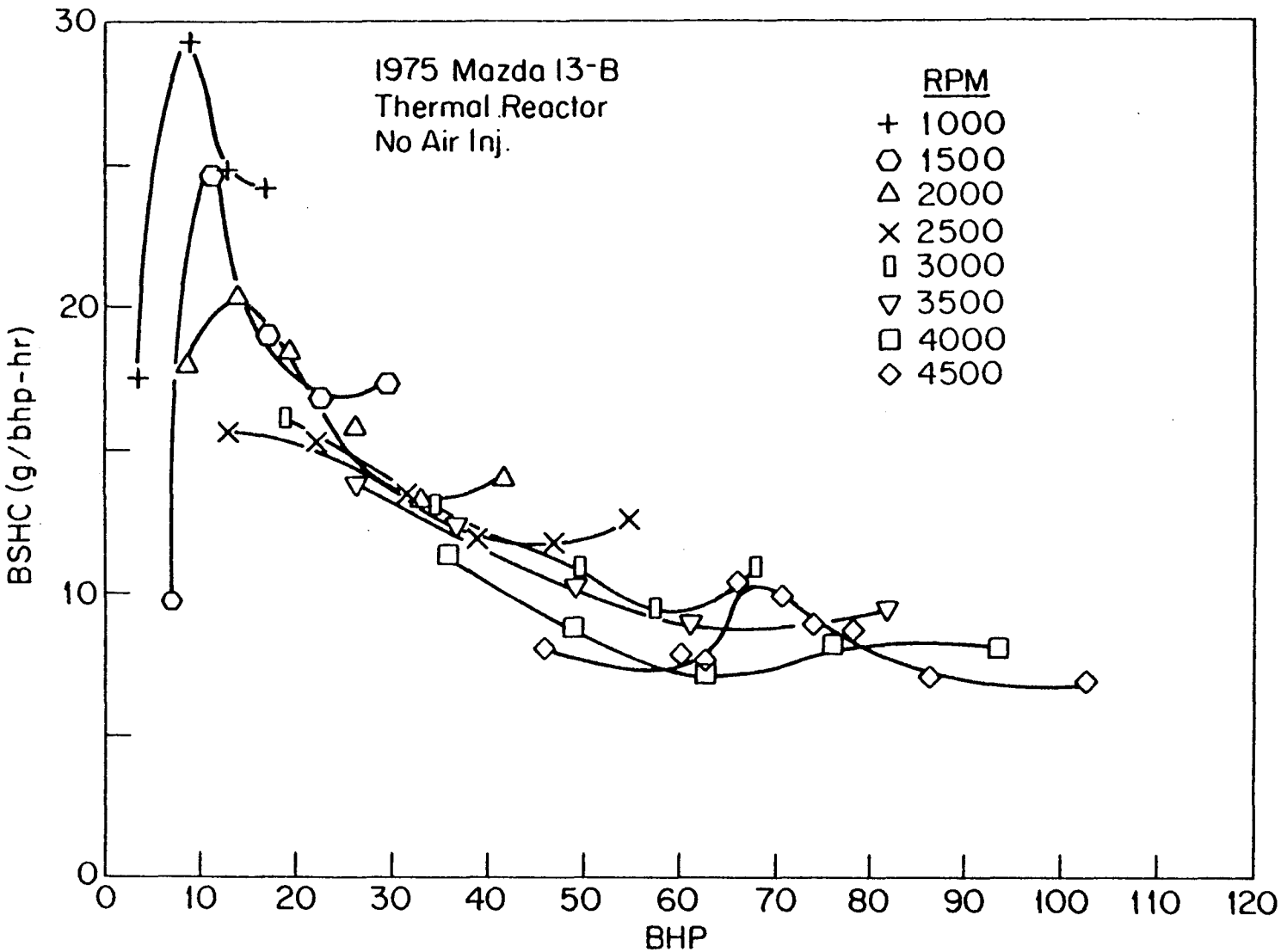

Figure 17. Brake specific hydrocarbon emissions as a function of brake horsepower, Mazda 13-B engine, with thermal reactor but without air injection.

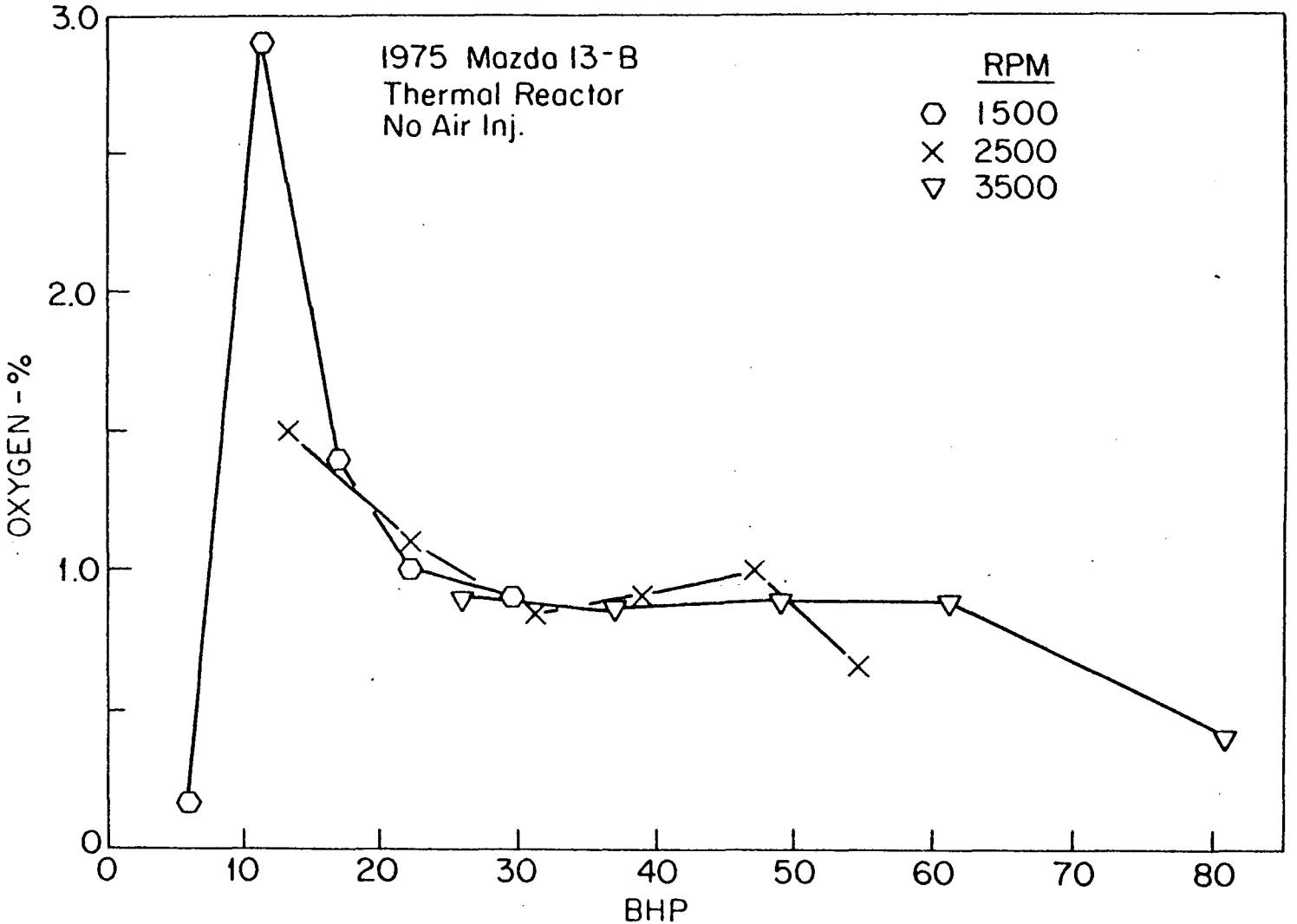

Figure 18. Exhaust oxygen concentration as a function of brake horsepower, Mazda 13-B engine, with thermal reactor but without air injection.

The BSCO emission data are shown in Fig. 19. In general the data follow a similar pattern to that of the hydrocarbon emissions. The light load data at 1000 and 1500 rpm was relatively low, again perhaps caused by slight air leakage to the thermal reactor. The remainder of the data appear to be consistent with the trend in mixture ratio.

For comparative purposes, plots of air-fuel ratio as a function of BHP are shown in Fig. 20, at several representative speeds. The performance of the Mazda carburetor is reasonably typical of conventional engine carburetors, although the mid-range mixture ratios are considerably richer than normally used. The thermal reactor required careful tailoring and generally rich mixtures to operate effectively.

Figure 21 is a plot of the BS NO_x as a function of BHP and shows that the NO_x emissions with or without air injection were similar. Certainly this was expected since the major operating variables were the same. The variation exhibited seems consistent with our experience with other engine data in which variations in atmospheric conditions, mixture ratio, and spark timing from test to test, could readily cause the observed differences.

4. Exhaust Emission and Fuel Consumption Performance Without Thermal Reactor and No Exhaust Port Air Injection

In this series of tests the thermal reactor was replaced with a conventional exhaust manifold. The air-injection air pump was operated but no air was injected into the exhaust stream. The data from this test series have been used in the comparison with the Buick 231 CID V-6 engine. As anticipated, fuel consumption and emission results are similar to the previously discussed tests with thermal reactor but without air injection. Several minor anomolies were observed which may have been related to changes in carburetion, thermal oxidation in the engine and/or exhaust system, and effects due to day-day variations in atmospheric conditions.

The BSFC curve is shown in Fig. 22. In general the data shows that the specific fuel consumption decreased with increasing load and speed which was the case for the engine operating with the thermal reactor with and without the air injection. The only differences of significance were the disappearance of the slight peaks observed in the earlier data at 3000 and 3500 rpm in the mid-load ranges. This reduction in the mid-load range can be attributed to a slightly leaner mixture relative to the prior data. At 4000 rpm the BSFC curve is of similar shape but the moderate load data is slightly higher than observed in Fig. 13.

The BSHC emission performance of the engine as a function of BHP is shown in Fig. 23. These curves are almost identical to the data with the thermal reactor and no air injection. In the study

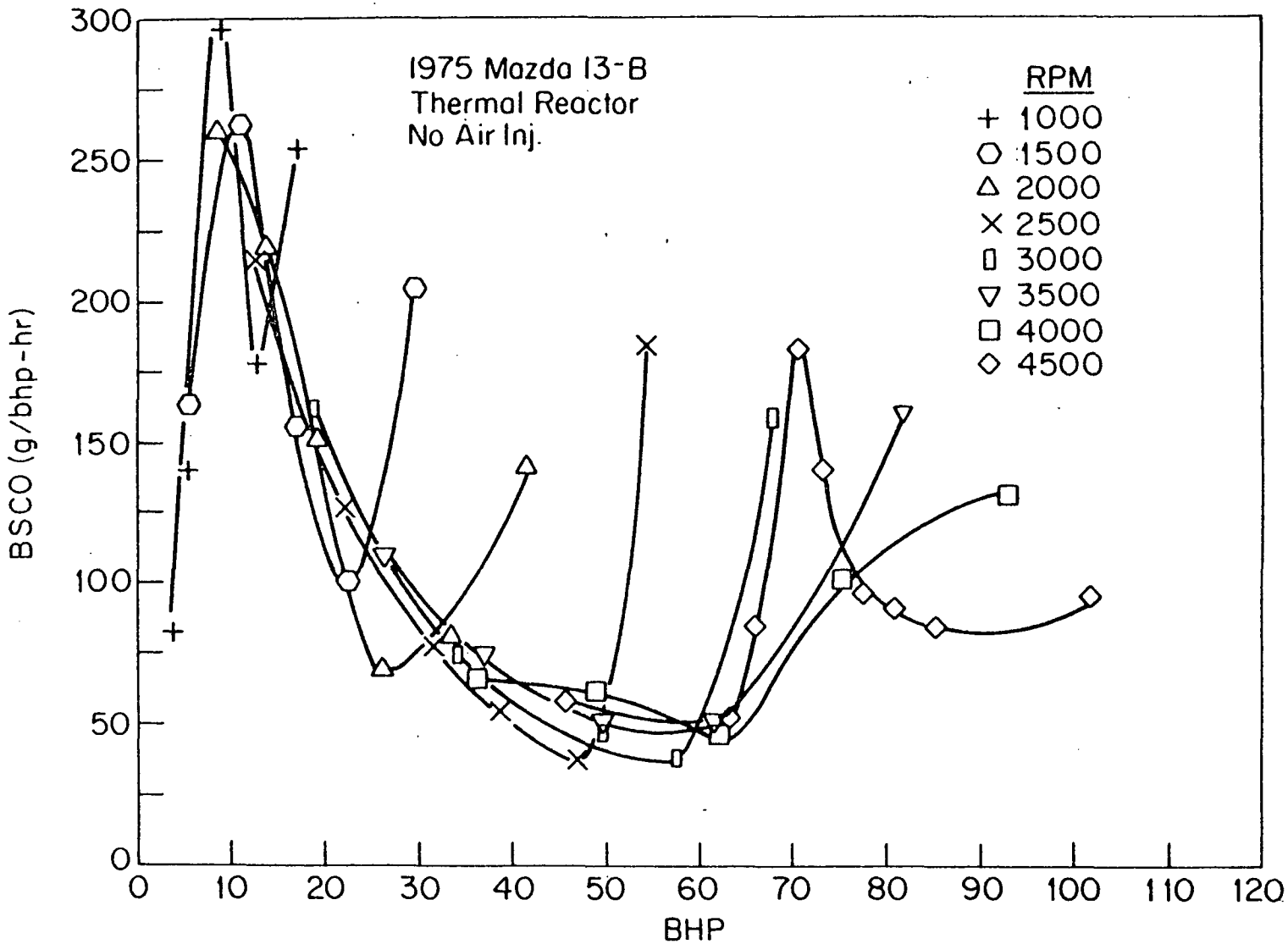

Figure 19. Brake specific carbon monoxide emissions as a function of brake horsepower, Mazda 13-B engine, with thermal reactor but without air injection.

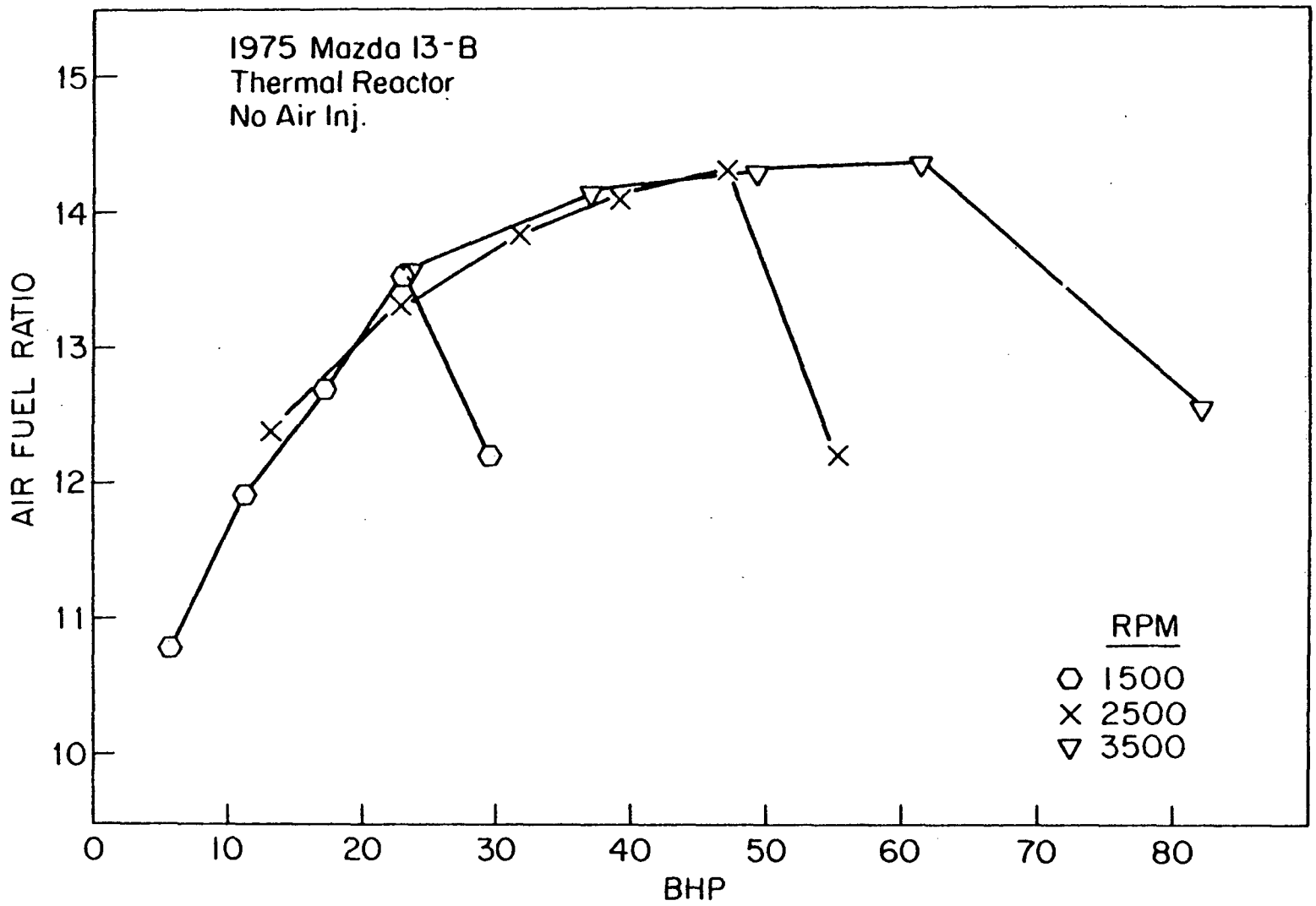

Figure 20. Air-fuel ratio as a function of brake horsepower at selected test conditions, Mazda 13-B engine, with thermal reactor, but without air injection.

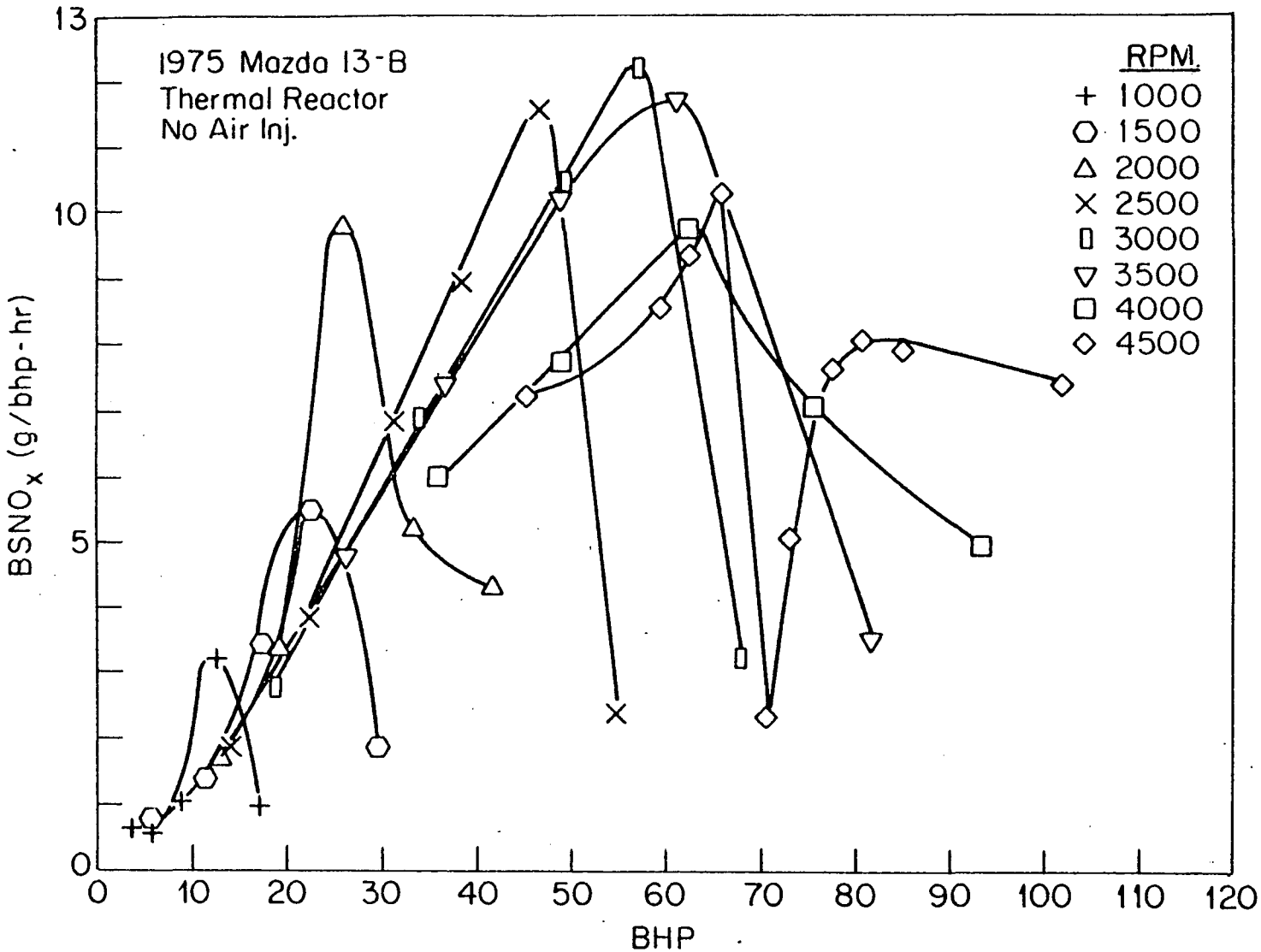

Figure 21. Brake specific nitrogen oxide emissions as a function of brake horsepower, Mazda 13-B engine, with thermal reactor but without air injection.

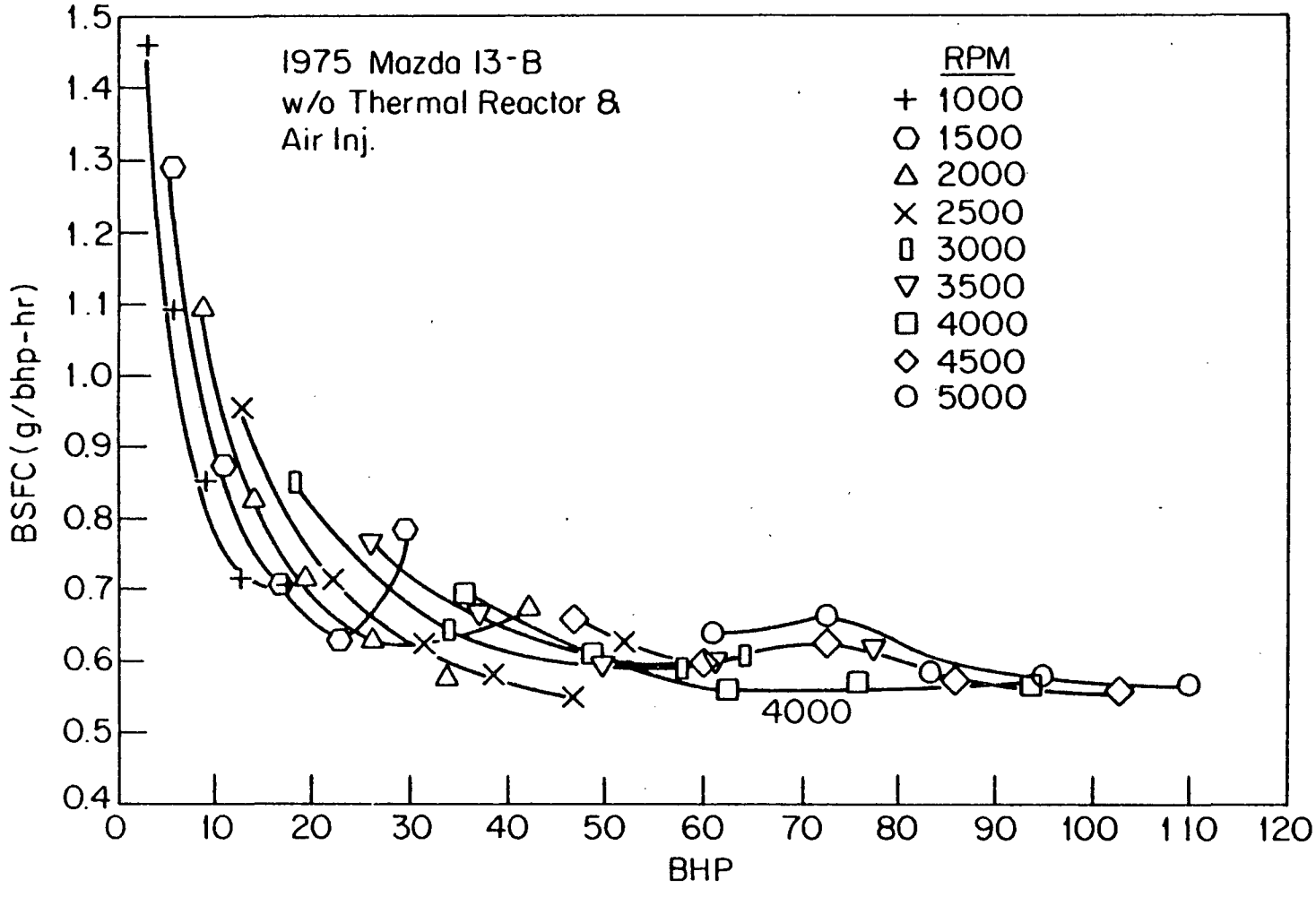

Figure 22. Brake specific fuel consumption as a function of brake horsepower, Mazda 13-B engine, without thermal reactor and air injection.

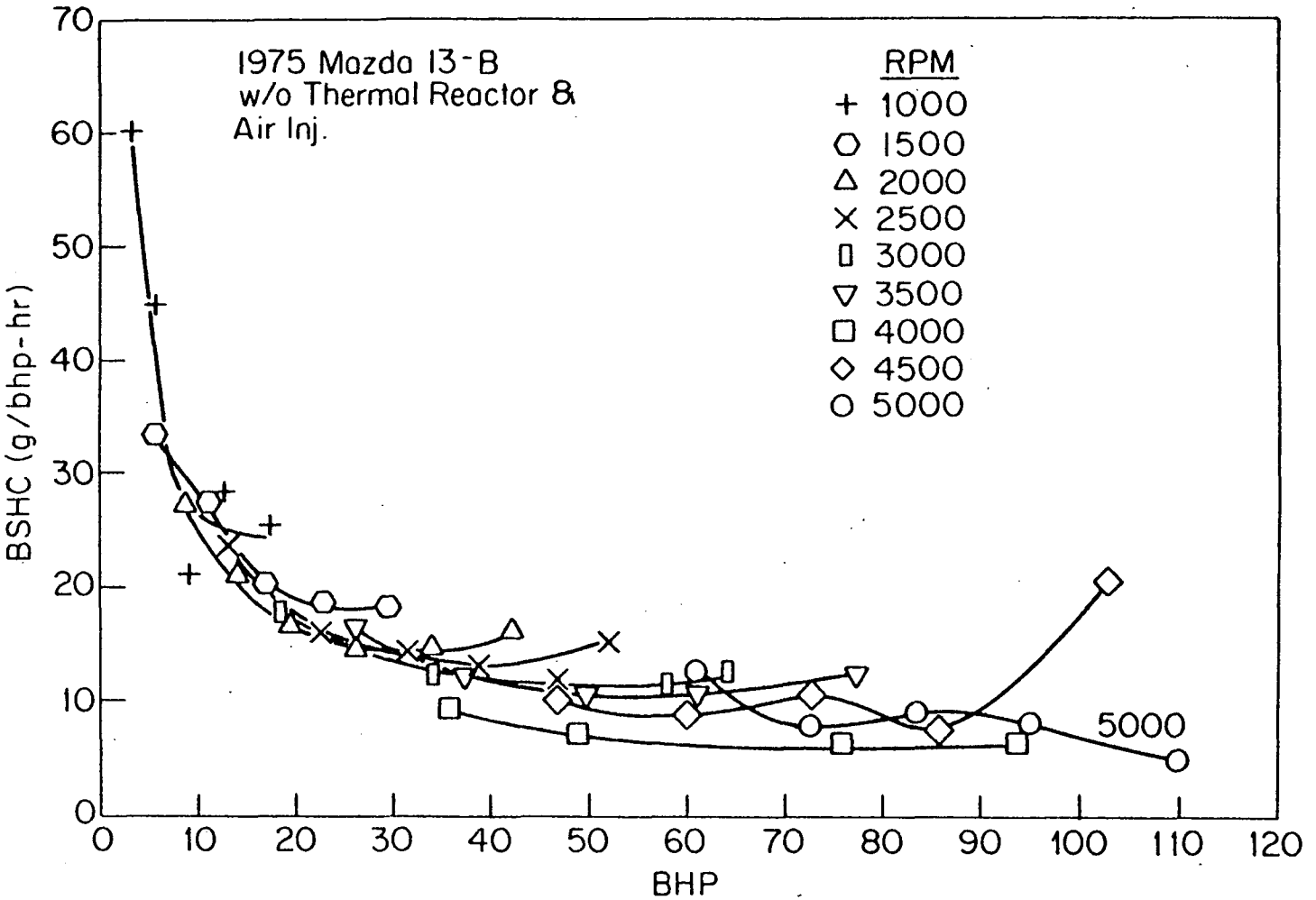

Figure 23. Brake specific hydrocarbon emissions as a function of brake horsepower, Mazda 13-B engine, without thermal reactor and air injection.

with the thermal reactor the light load hydrocarbon emissions at 1000 rpm were low and followed no distinct trend. As noted this was believed to be due to leakage of air past the air control valve. Hydrocarbon emissions generally decreased with increasing speed and load. An exception to this trend was observed at the highest load setting at most test speeds because of mixture enrichment. Another anomally compared to the data for the engine with thermal reactor and no air injection is the substantially higher hydrocarbon emissions at 4500 rpm maximum load. The mixture ratio was essentially the same as that observed in the prior test series. Therefore the increase was probably due to a slight misfire. Considering the reasonable scatter expected in engine emission data, it appears that the results are remarkedly repeatable.

The BSCO emissions are shown in Fig. 24. The anomalies observed for the hydrocarbon emissions at the highest loads at both 1000 and 500 rpm are present. Again this can be attributed to a slight inadvertent air injection in the studies with the thermal reactor. The general trend shows clearly the predominant influence of mixture ratio on CO emissions. Again the data is reasonably consistent with the results shown earlier.

The brake specific NO_x emissions are shown in Fig. 25. The trend of the data is consistent with the measurements obtained from the engine with thermal reactor and both with and without air injection. However, significant variations in the vertical position of most of the curves with respect to earlier data were present. At 1000 rpm, the light-load emissions are less than 1 gram/bhp-hr followed by a rapid increase to a maximum at approximately 5.5 which in turn is followed by a rapid decrease to less than 1 at maximum load. The peak is considerably higher than observed earlier. At 1500 rpm the shape and magnitude of emissions are similar. At 2000-3500 rpm the shape is consistent, showing that $BSNO_x$ is a maximum in the mid-load range. The peak emissions were consistently lower than those observed in the study with the thermal reactor. The 4000 rpm data is similar in shape to the lower RPM results, and similar in magnitude to the earlier data. At 4500 RPM the curve is characterized by two peaks at light and moderate load, and the curve is generally lower than observed with the thermal reactor. At 5000 rpm the characteristic shape is similar to the 4500 rpm results. The trends at a given speed were consistent with variations in air-fuel ratio and appear to be influenced by ignition timing as well. In this engine the timing is set in a relatively narrow band which suggests that at both higher speeds and lighter loads the effective timing may be retarded from the MBT setting, whereas MBT is approximated more closely at lower speeds and at heavier loads. The effect of ignition timing on all emissions will be discussed in a later section. The shifts in magnitude of brake specific NO_x emissions from data observed earlier is in most cases signficant. This can be attributed to several factors. Normally the repeatability of NO_x emissions is

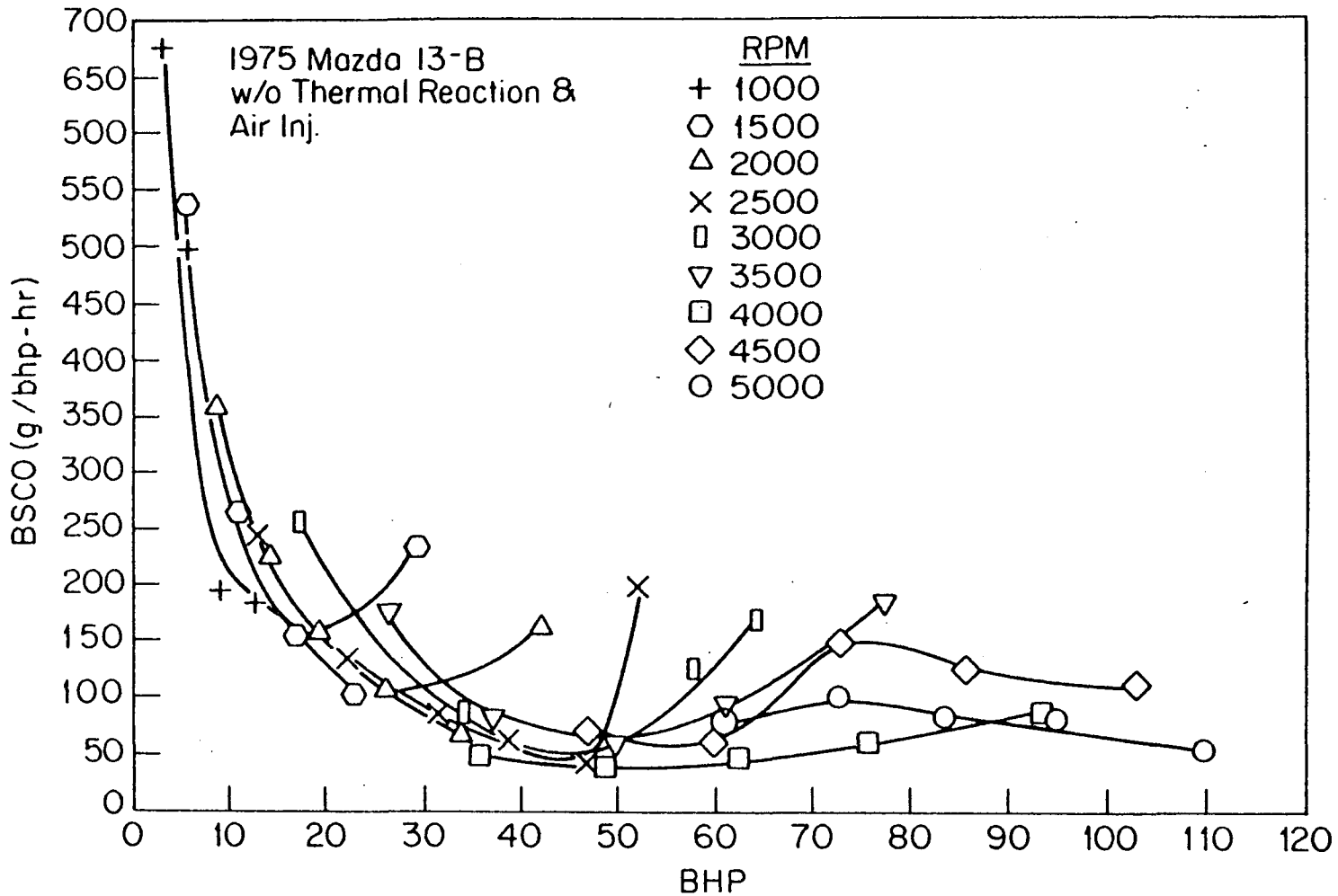

Figure 24. Brake specific carbon monoxide emissions as a function of brake horsepower, Mazda 13-B engine, without thermal reactor and air injection.

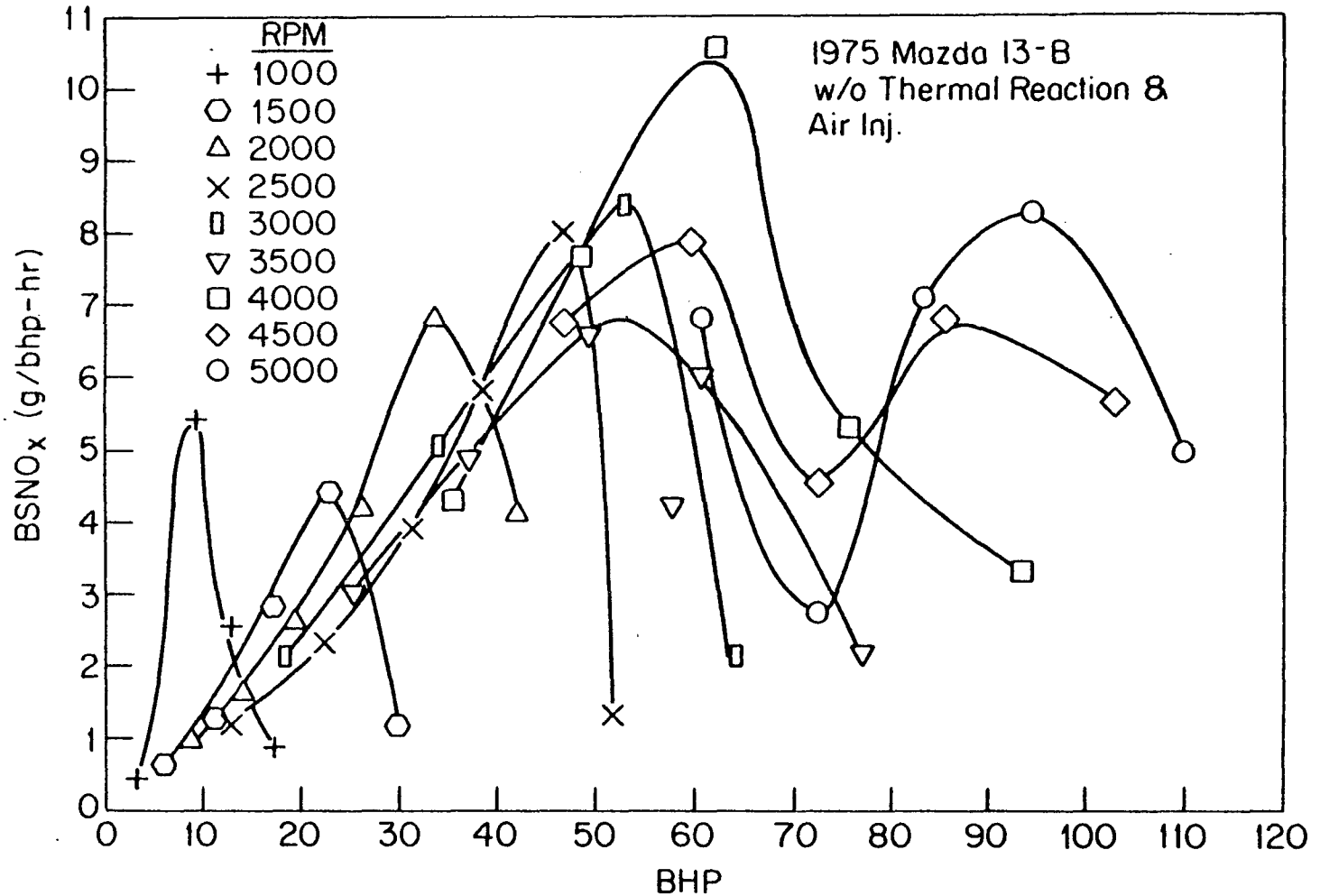

Figure 25. Brake specific nitrogen oxides emissions as a function of brake horsepower, Mazda 13-B engine, without thermal reactor and air injection.

not good because NO_x is extremely sensitive to small variations in operating parameters. For example, a variation in air-fuel ratio of as much as 1/2 ratio was observed between the test with thermal reactor to the present test. In addition, changes in atmospheric conditions such as inlet temperature, and humidity appear to have a reasonably significant effect. Another potential factor causing the deviation is related to the basic characteristics of the data. The NO_x emissions tend to rise quickly with increasing load followed by a rapid decrease. A slight shift in the load setting could cause a considerable variation in magnitude of NO_x emissions. For example, at 1000 rpm if the mid-range load had been set slightly lower than in the test, the magnitude of the NO_x peak could have been attenuated significantly.

5. Fuel Consumption and Emission Performance of the Mazda 13-B Engine without Thermal Reactor in a Simulated Mazda RX-4 Vehicle

To provide a more graphic basis for comparison, the fuel consumption and emission performance of the rotary engine as installed in the simulated Mazda RX-4 vehicle were determined under road load conditions. These data are plotted in Fig. 26 through 29 as a function of vehicle speed. Two axle ratios, 2.56 and 3.9:1, were selected as the final drive ratio. These data in no way reflect the type of performance that could be expected on the EPA emission cycle, rather they reflect the projected performance of this engine in a simulated vehicle at a series of steady-state test conditions.

The fuel economy in miles per gallon is plotted in Fig. 26. The shape of the curves and their relative position are similar to those expected for reciprocating engine powered vehicles. The use of the higher axle ratio results in a considerably lower fuel economy, approximately 3 miles per gallon, across the range of the test. With the lower axle ratio the engine is operating at a higher load factor and lower RPM for a given vehicle speed. At the higher load factor the engine thermal efficiency is significantly greater because of the reduced throttling losses, less exhaust residual dilution and other more minor factors. In addition, the lower RPM results in less engine friction (higher mechanical efficiency). The shapes of these curves are similar. The fuel economy is relatively constant through the mid-range, suggesting that at the lower speeds the engine efficiency is increasing at approximately the same rate as the road load horsepower requirement as vehicle speed increases. At the higher speeds the road load horsepower, which contains an important term proportional to velocity cubed (aerodynamic resistance), increases rapidly and becomes the dominant factor resulting in a significant reduction in fuel economy.

The hydrocarbon emissions in grams per mile are plotted as a function of miles per hour in Fig. 27. There is no significant difference exhibited with the two axle ratios. The level of emissions would be considered high by comparison with typical reciprocating engines. The trend of the data suggests that mass hydrocarbon emissions decrease with speed. This characteristic can

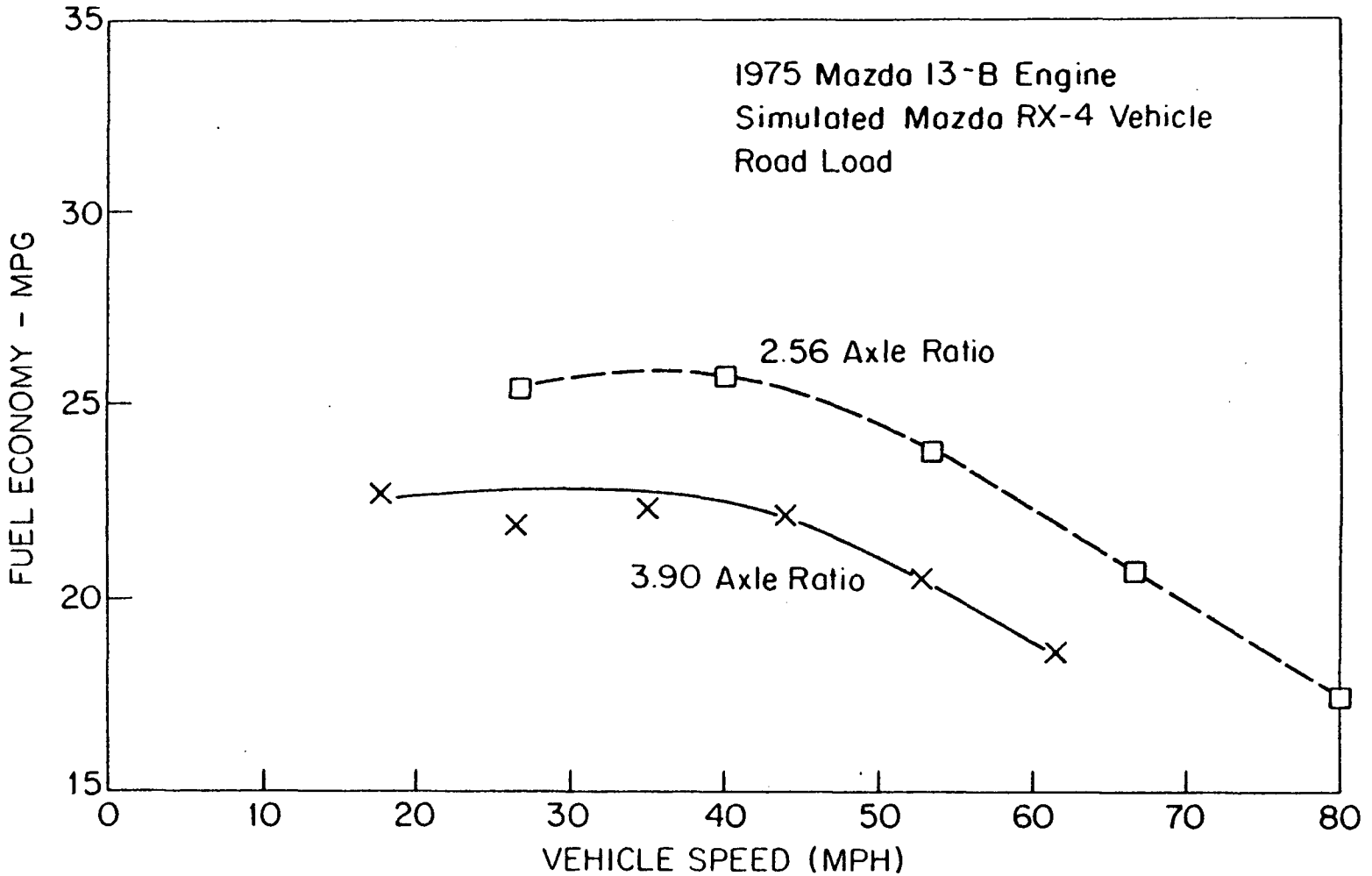

Figure 26. Fuel economy as a function of vehicle speed of the Mazda 13-B engine installed in a simulated Mazda RX-4 vehicle, road load, 2.56 and 3.90:1 axle ratios.

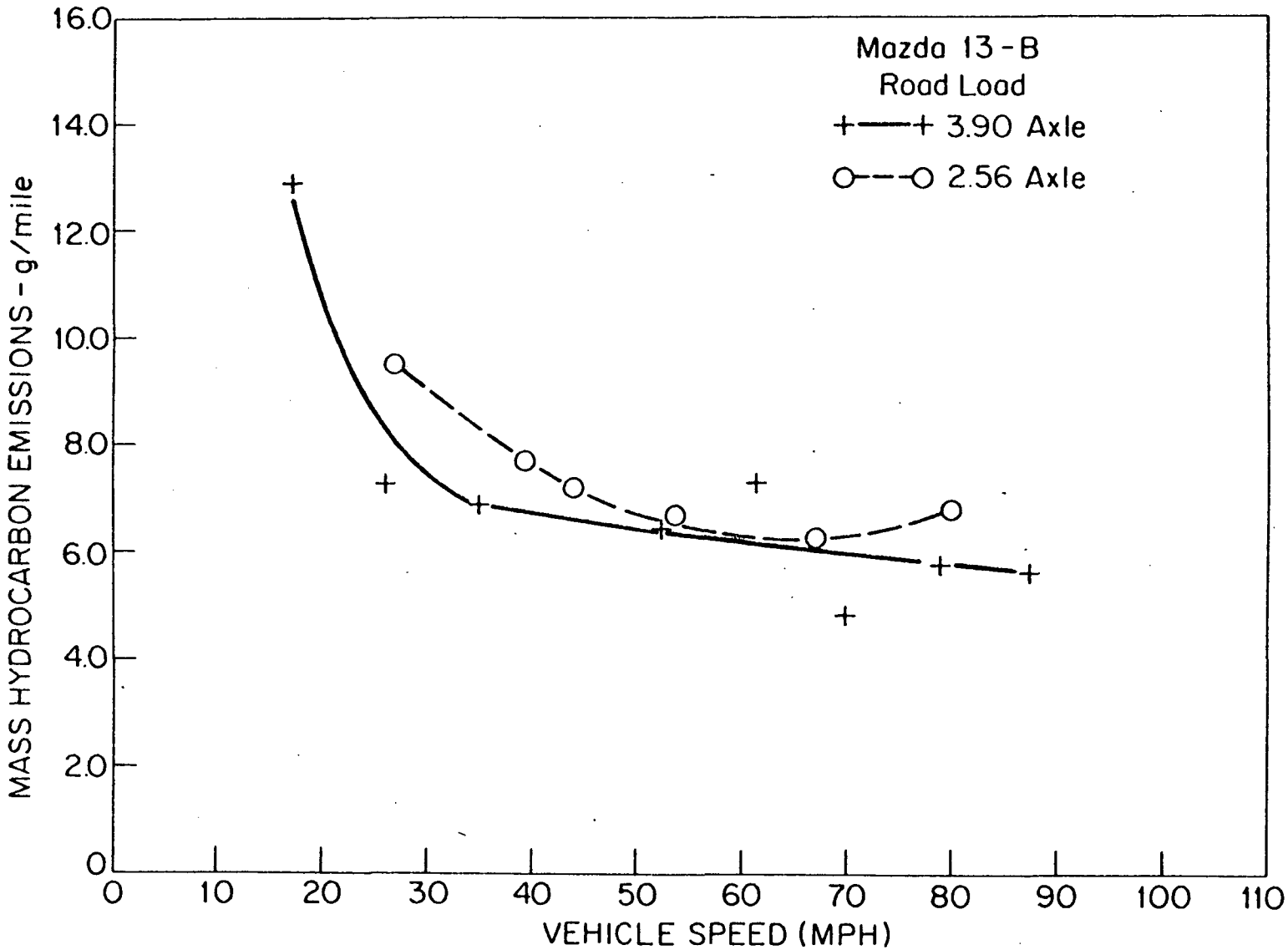

Figure 27. Mass hydrocarbon emissions as a function of vehicle speed of the Mazda 13-B engine installed in a simulated Mazda RX-4 vehicle, road load, 3.90 and 2.56:1 axle ratios.

probably be attributed to a significant decrease in the percentage of mixture that is leaked to the exhausting chamber volume with an increase in engine air flow. An additional factor causing this decrease is leaning of the air-fuel ratio in the mid-operating range.

The mass emission rate of CO is shown in Fig. 28. Here also little difference is evident between the two axle ratios. The data trends downward significantly with increasing vehicle speed although with the 3.90:1 axle mass emission rate increased near maximum speed. The similarity of the two curves is indicative of the fact that the carburetted air-fuel ratio used with the two axle ratios is essentially the same.

Figure 29 shows the mass emission level of NO_x as a function of vehicle speed. Clearly the level of NO_x emissions increases with increasing speed because of a significant increase in engine load factor. The 2.56 axle ratio exhibits a greater mass NO_x emission rate than the 3.90 axle because it also causes the engine to operate at a greater load factor than with the higher axle ratio. The curve shapes for the NO_x data are reasonably typical of that for reciprocating gasoline engines installed in vehicles.

B. FUEL CONSUMPTION AND EMISSION PERFORMANCE OF THE BUICK 231 cu. in. V-6 ENGINE, NO EXTERNAL EMISSION CONTROL

The Buick 231 cu. in. V-6 engine was tested to obtain a piston engine comparison to the Madza 13-B rotary engine. The engine was tested without emission control to facilitate comparison to the rotary engine without emission control. The Buick engine is representative of a modern medium-sized reciprocating engine, utilizing a relatively efficient open combustion chamber, and has demonstrated attractive EPA fuel economy performance in vehicle installations. In addition, it is evident that with the increasing concern for energy conservation as well as reduction of emissions, there will be a general scaling down in the displacement of American automotive engines. The V-6 promises to be a very important configuration in American passenger cars during the next ten year period.

1. Base Performance Data - Wide Open Throttle

Initially the Buick engine was tested per SAE procedure J245 to determine its wide-open throttle performance characteristics. The engine was not tested with the standard exhaust system, but with an exhaust restriction installed to provide the back pressure of a production system. The WOT performance data are plotted in Fig. 30. The BHP, BMEP, and brake torque data are all corrected per SAE procedure to standard conditions. The torque and mean effective pressure curves are relatively flat with a maximum occurring between 2000 and 2500 rpm. The BHP increases at a decreasing rate beyond 2500 rpm which is typical. The engine was not tested to the BHP peak because this region is not generally important in

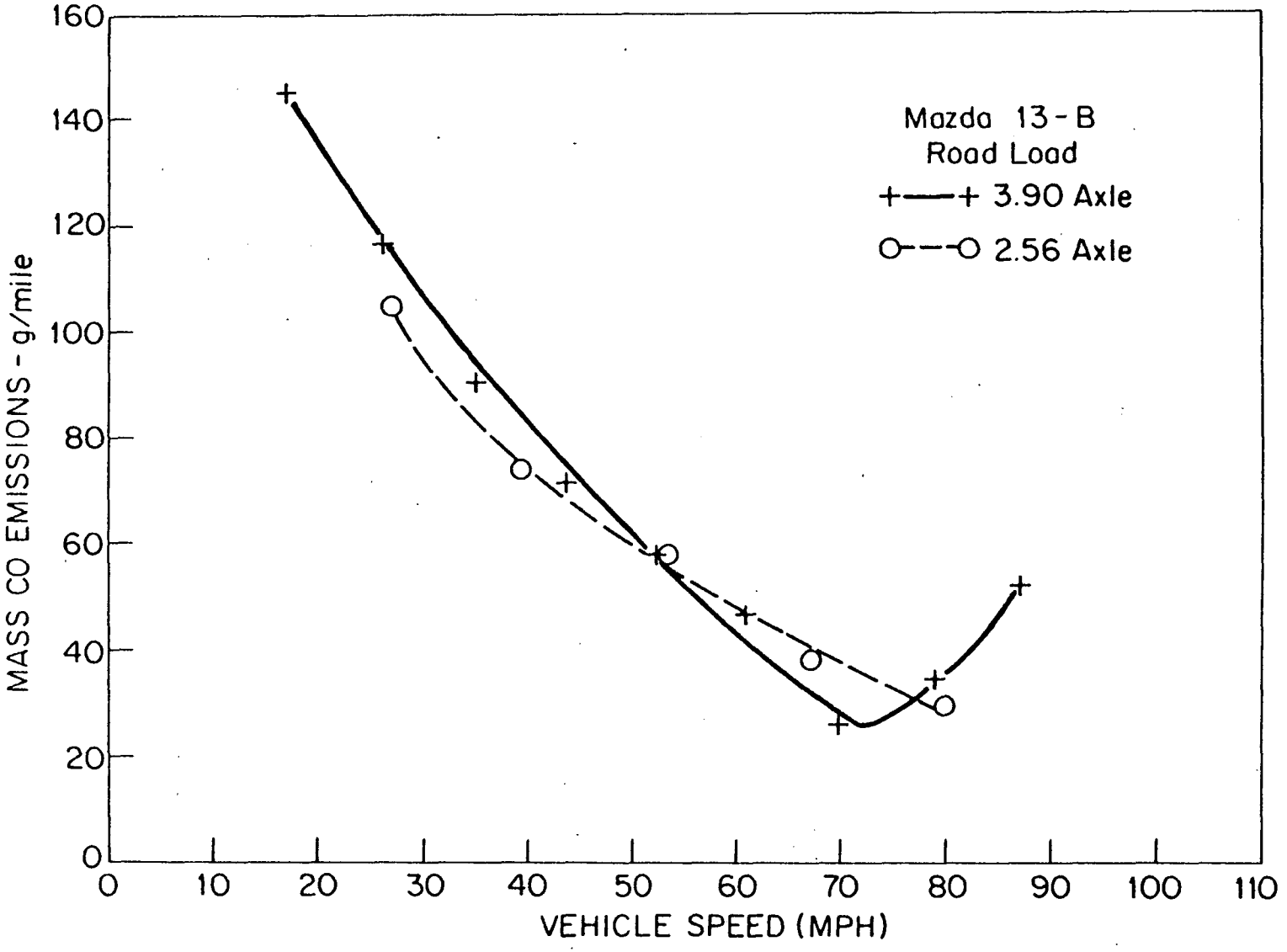

Figure 28. Mass carbon monoxide emissions as a function of vehicle speed for the Mazda 13-B engine installed in a simulated Mazda RX-4 vehicle, road load, 3.90 and 2.56:1 axle ratios.

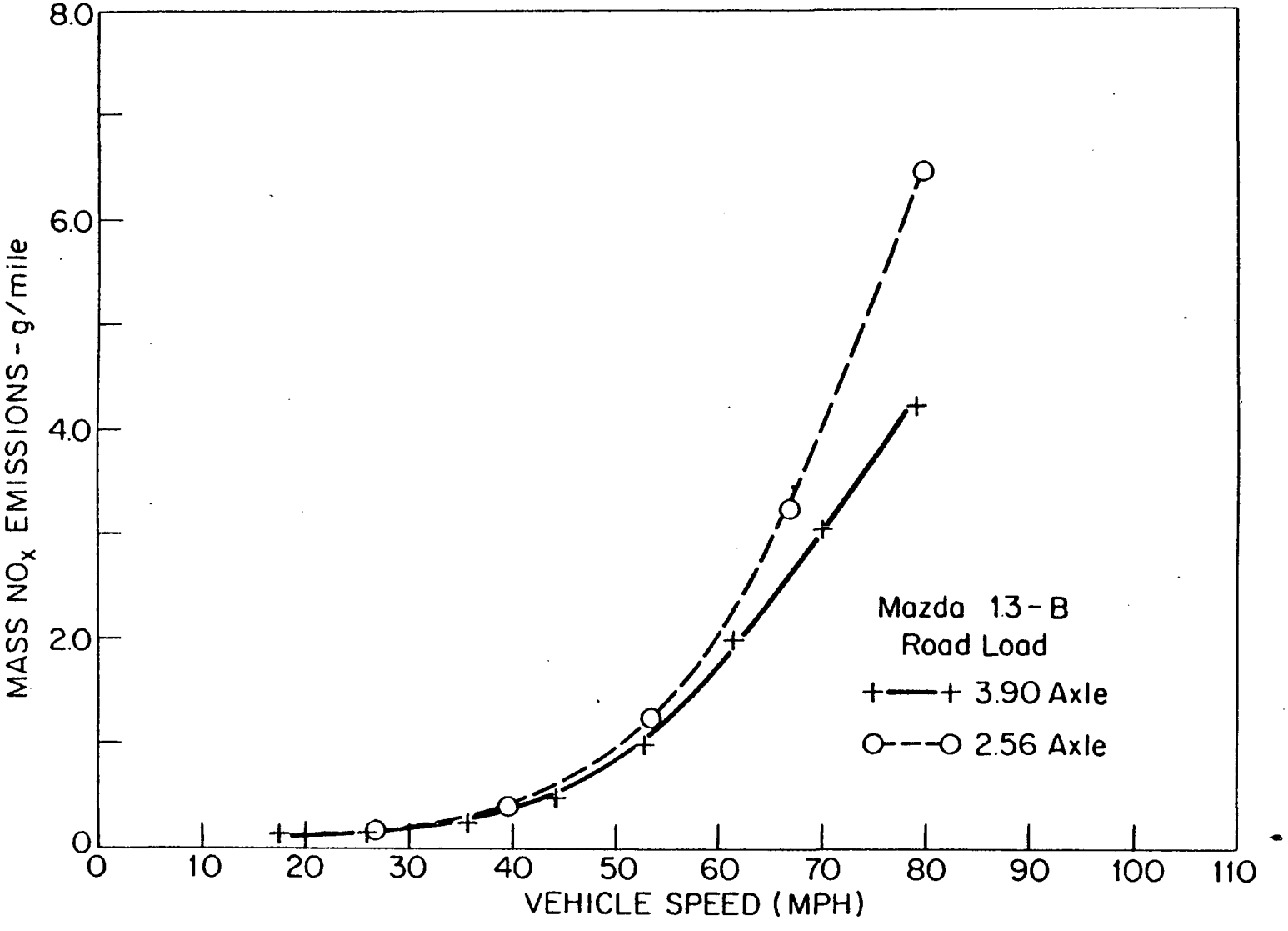

Figure 29. Mass nitrogen oxide emissions as a function of vehicle speed for the Mazda 13-B engine installed in a simulated Mazda RX-4 vehicle, road load, 3.90 and 2.56:1 axle ratios.

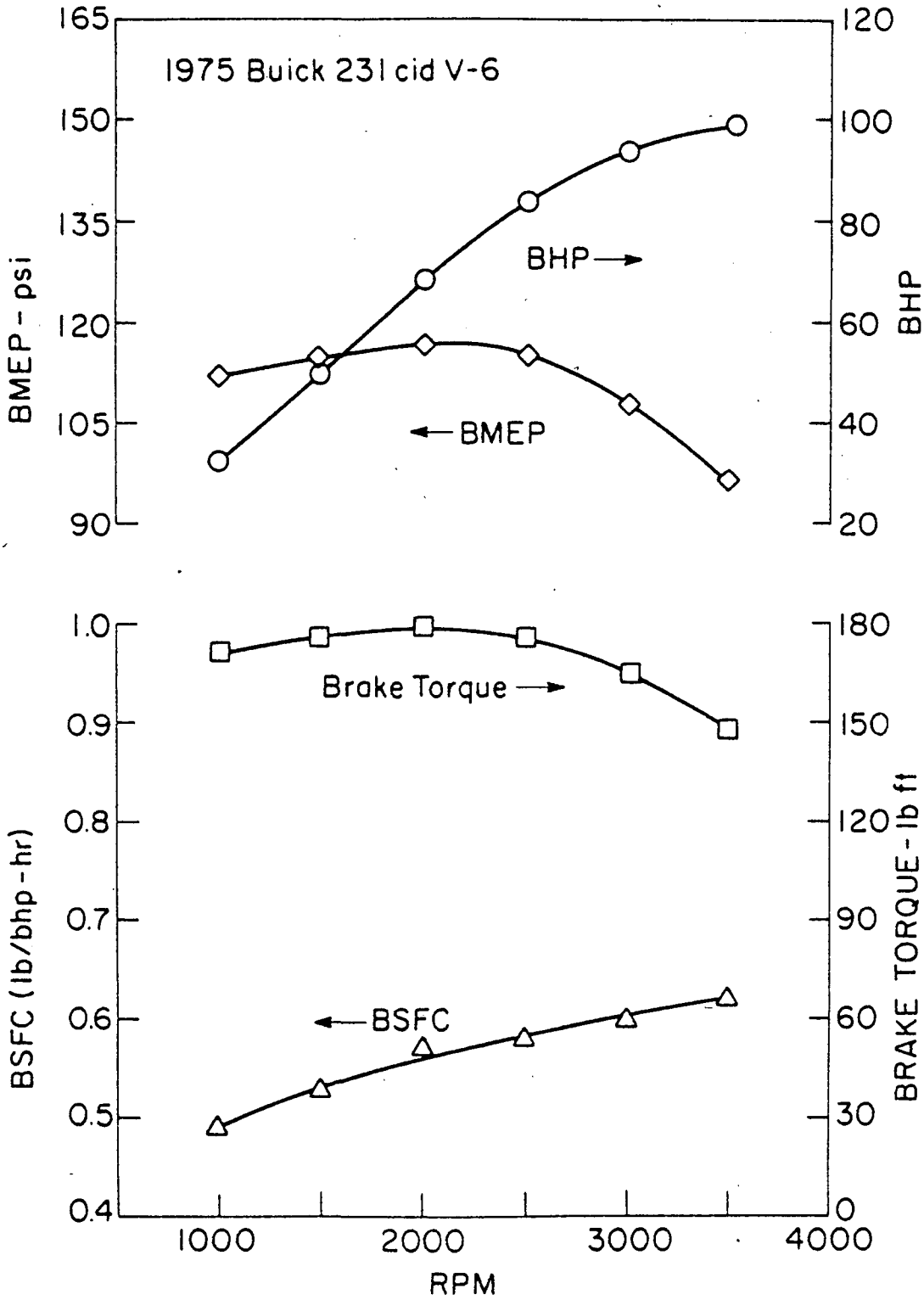

Figure 30. Wide-open throttle performance of the 1975 Buick V-6 engine as a function of RPM.

the typical driving cycle and because of safety consideration in the laboratory. The specific fuel consumption increased almost linearily with RPM. This increase is associated primarily with the nearly cubic increase in friction horsepower with increasing engine speed.

2. Fuel Consumption and Exhaust Emission Maps of the Buick V-6 Engine with EGR and without Catalyst

Figure 31 is a plot of the BSFC as a function of BHP in the range from 1000 to 3500 rpm in 500 rpm increments. These data are perceived to be typical of modern reciprocating engine behavior also. Specific fuel consumption was high at low-load factors because friction horsepower is a significant fraction of indicated horsepower. At moderate loads BSFC was reduced to approximately 0.5 lb/hp-hr. and then increased sharply at wide-open throttle because of mixture enrichment. This enrichment was particularly large at high loads since the part-load mixtures were generally leaner than stoichiometric in most of the operating ranges. Generally the curves were much smoother than those of the Mazda.

Brake specific hydrocarbon emissions are shown in Fig. 32. All the data were reasonably consistent. At the lowest speeds, 1000-2000 rpm, and light loads, residual dilution and perhaps reduced combustion efficiency caused a reasonably high level of hydrocarbon emissions. Idle mixture enrichment and spark retard were also factors in these higher hydrocarbon mass emissions. As the load was increased, BSHC emissions were reduced since BHP was increasing at a greater rate than air flow. At and near wide-open throttle where mixture enrichment was used for maximum power and internal engine cooling the BSHC emissions increased sharply.

The BSCO emissions shown in Fig. 33 are typical of reciprocating engines in which reasonably lean mixtures are used through most of the driving range. At high loads mixture enrichment caused a dramatic increase in CO level.

The BSNO_x emissions are shown in Fig. 34 as a function of BHP. These data proved to be very complex and difficult to acquire because of the rapid change in NO_x emissions with load change at each speed due to EGR valve action. Consequently, a large number of data points were used to generate the precise shape of these curves. In general, the NO_x emissions increased with increasing loads. However, they were attenuated as the exhaust gas recirculation was increased. Near maximum load NO_x levels were reduced sharply because of mixture enrichment. The irregularity in these curves is reasonably typical of modern engines equipped with vacu-modulated EGR, and suggest the potential of better EGR control schemes. Ignition timing is an additional factor affecting NO_x levels. However, it was believed that the Buick timing was programmed to follow closely the MBT settings except at very light

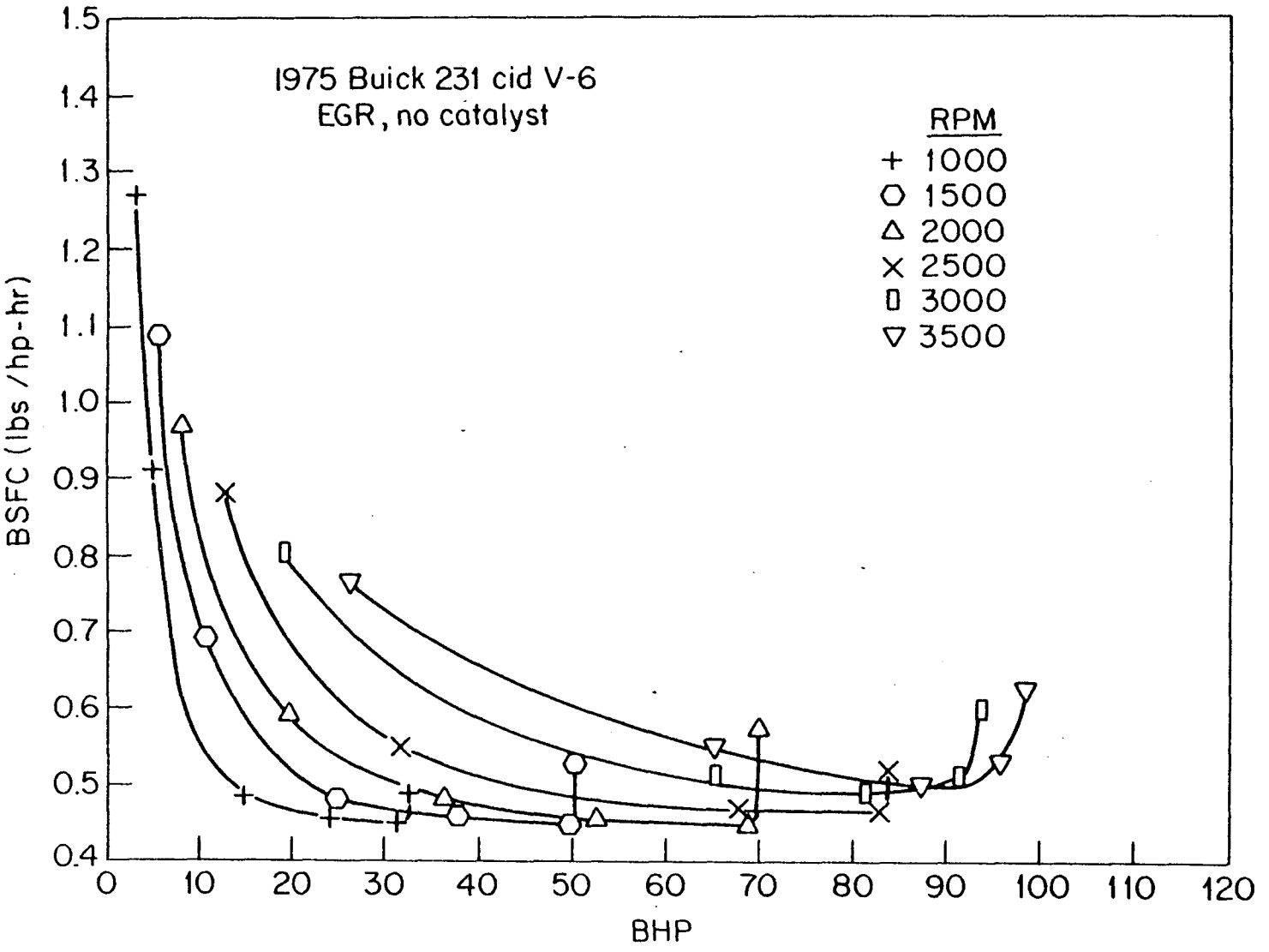

Figure 31. Brake specific fuel consumption as a function of brake horsepower, 1975 Buick V-6 with EGR and no catalyst.

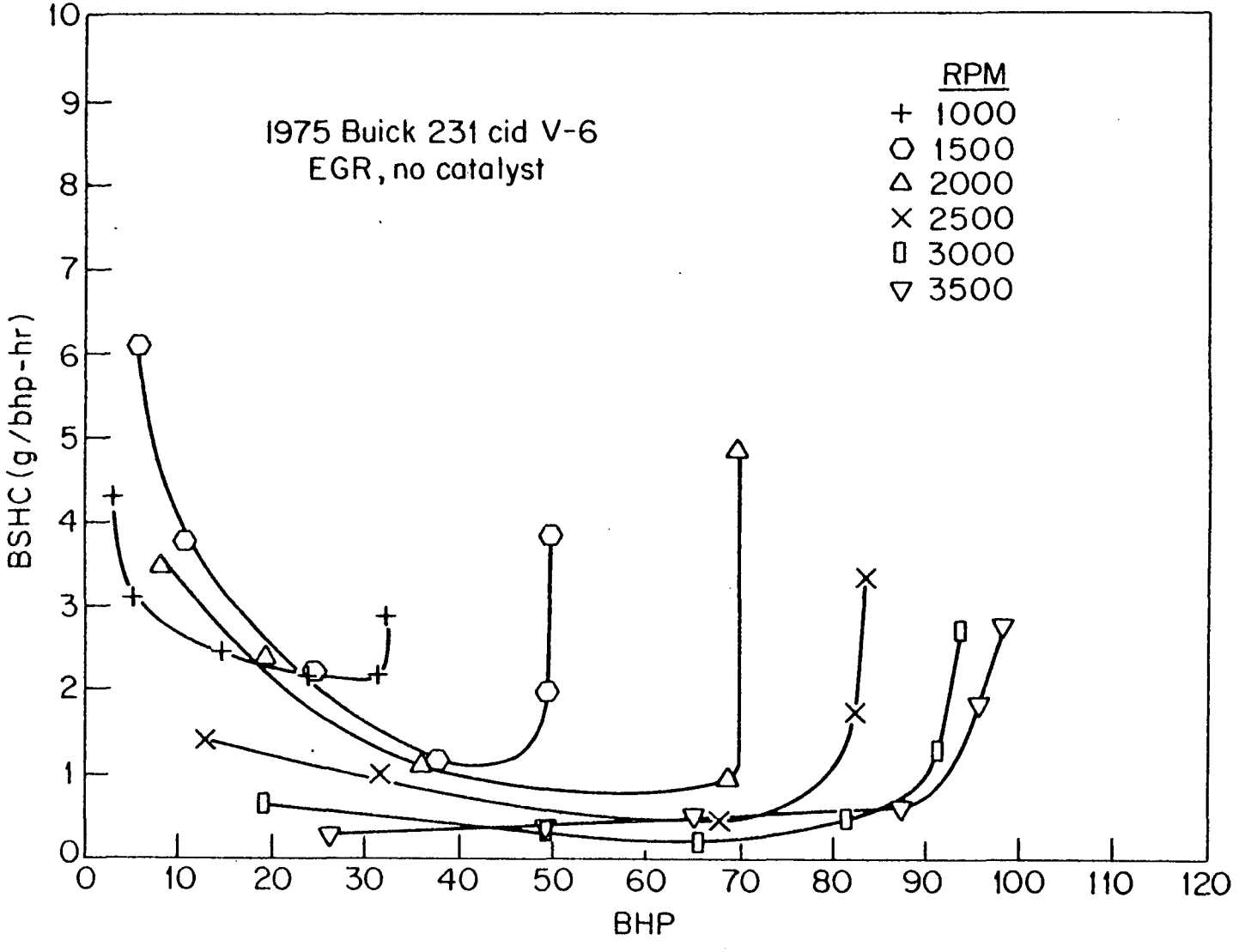

Figure 32. Brake specific hydrocarbon emissions as a function of brake horsepower, 1975 Buick V-6 with EGR and no catalyst.

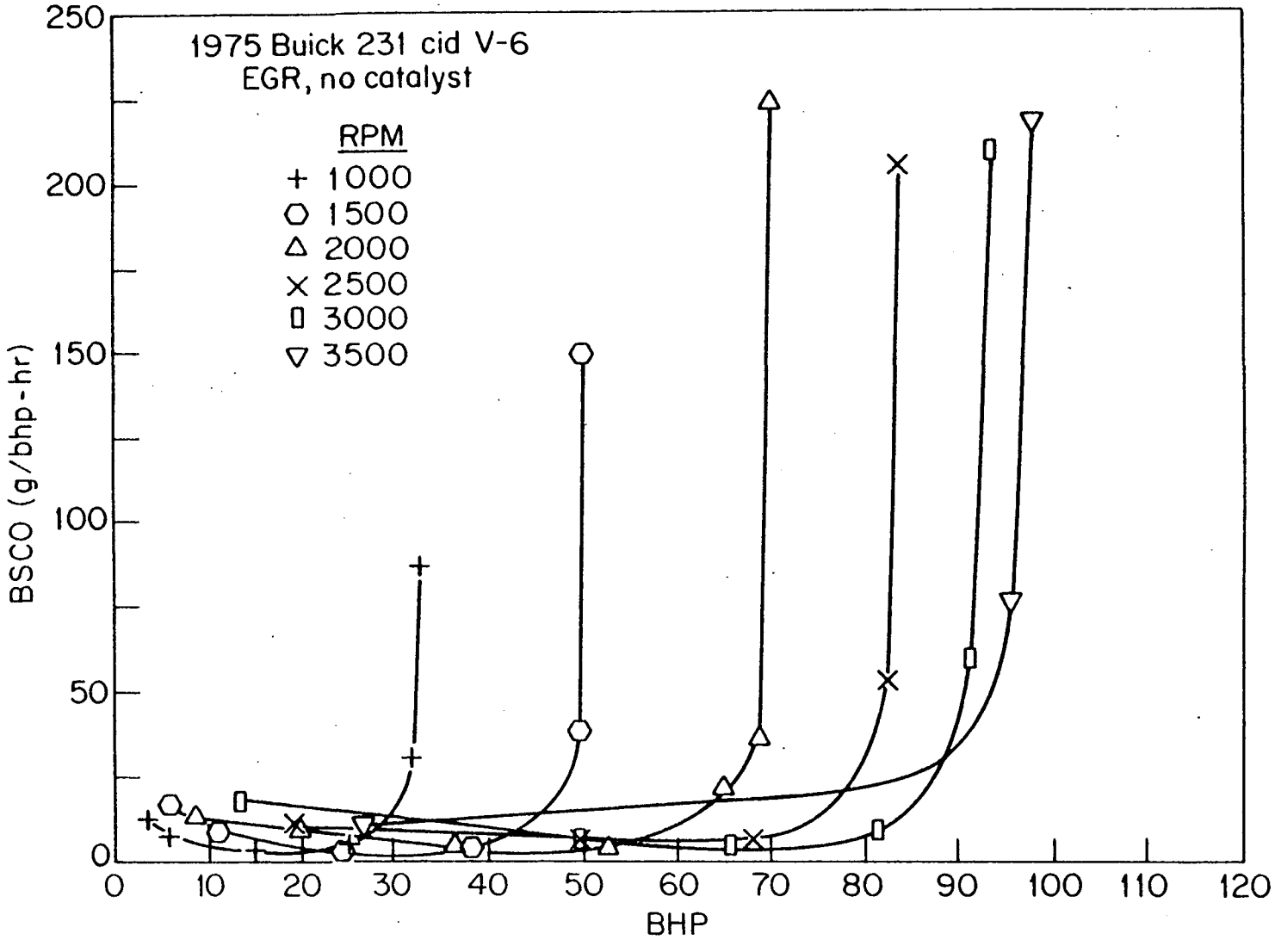

Figure 33. Brake specific carbon monoxide emissions as a function of brake horsepower, 1975 Buick V-6 with EGR and no catalyst.

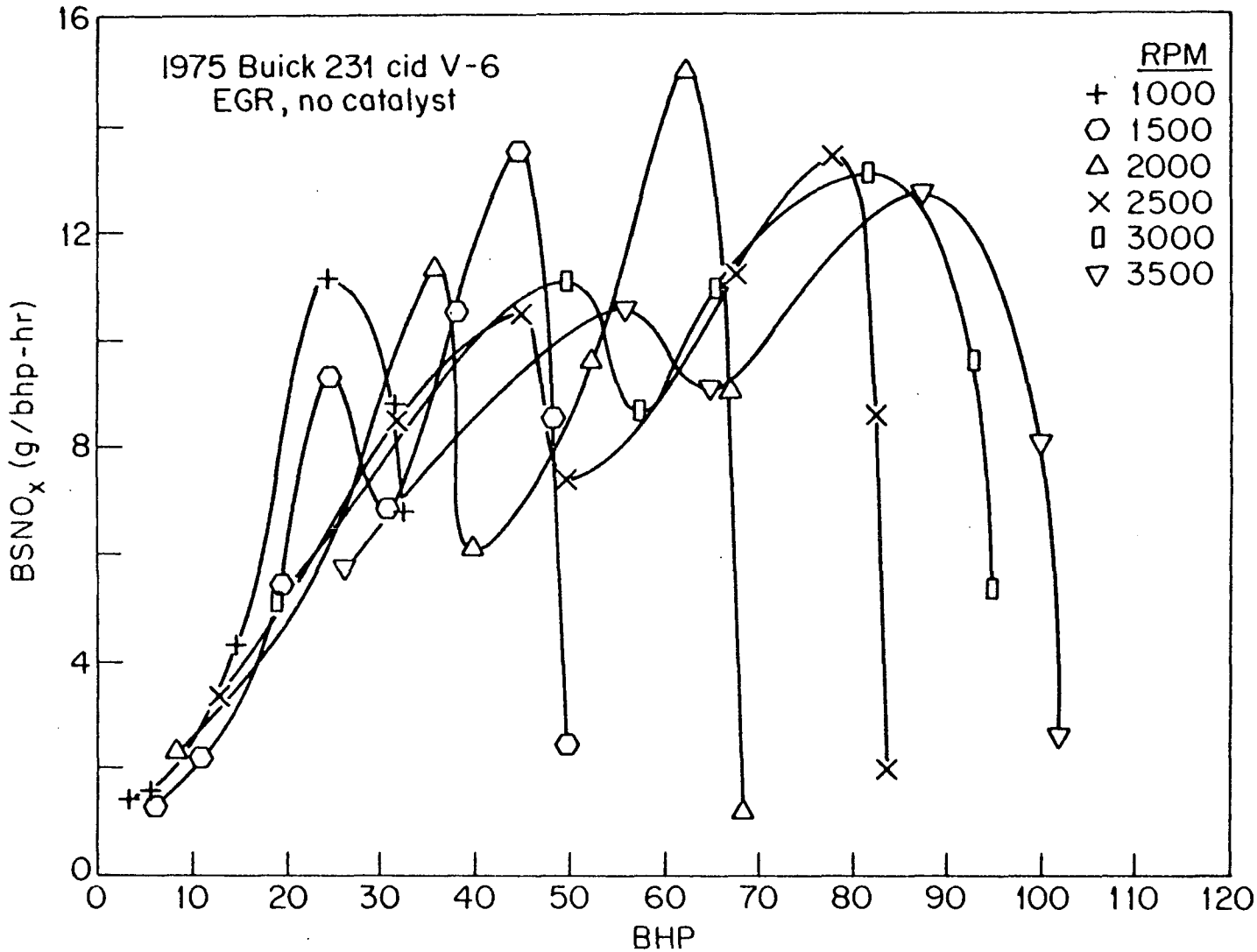

Figure 34. Brake specific nitrogen oxide emissions as a function of brake horsepower, 1975 Buick V-6 with EGR and no catalyst.

loads where significant retardation was used.

Figure 35 shows a plot of air-fuel ratio as a function of horsepower at 1750 and 3000 rpm. The mixture is relatively close to stoichiometric at low loads leaner than stoichiometric at moderate loads and is enriched considerably at the higher load operating conditions.

Using the emission maps, the Buick engine was installed in a hypothetical vehicle, Mazda RX-4, with two different axle ratios, 2.56 and 3.9:1 to assess the simulated steady-state mass rate of emissions. The various emissions in grams/mile are plotted as a function of vehicle speed at road load conditions in Fig. 36. The CO emissions increase moderately with increasing speed and then are reduced. The CO emissions for the higher axle ratio are greater than for the lower 2.56:1 axle ratio. The hydrocarbon emissions are reasonably similar in shape to the CO curves. However, above 35 mph the high axle ratio exhibits a lower hydrocarbon emission level than with the lower axle ratio. Axle ratio has apparently little effect on the NO_x emissions which increased at an increasing rate with speed.

C. FUEL CONSUMPTION AND EXHAUST EMISSION COMPARISON BETWEEN MAZDA 13-B AND BUICK V-6 ENGINES

The fuel consumption and exhaust emission performance of the test engines are plotted as a function of vehicle speed as installed in the simulated Mazda RX-4 automobile in Figs. 37 through 40. Figure 37 is a plot of fuel economy in miles per gallon as a function of speed for both engines with two different axle ratios. With the 2.56 axle ratio the Mazda engine exhibits a maximum of approximately 20% lower fuel economy and this occurs at 35 mph. With the 3.90:1 axle ratio the maximum difference is approximately 15% which also occurs at 35 mph. As vehicle speed is increased beyond 35 mph, the difference in fuel consumption between the two vehicles decreases considerably. This can be attributed primarily to the significantly lower friction at high speeds with the Mazda engine. It must be recognized that a large part of the observed difference is associated with the type of emission control technique selected for the engines. The Mazda is operating with far richer fuel-air ratios than those for best thermal efficiency whereas the Buick V-6 is operating very close to its peak efficiency air-fuel ratio. The Mazda carburetor is calibrated rich because the thermal reactor used in the present Mazda design requires a rich mixture to develop a self-sustaining oxidizing reaction for control of the unburned hydrocarbons and CO. Another important consideration relates to the vehicle package itself. In this particular vehicle simulation, the weight was the same for both the rotary and V-6 engines. The weight of an actual vehicle with a rotary engine would be less and thus the vehicle could be made smaller and lighter for a given interior package volume especially if secondary weight savings were made. These factors suggest that

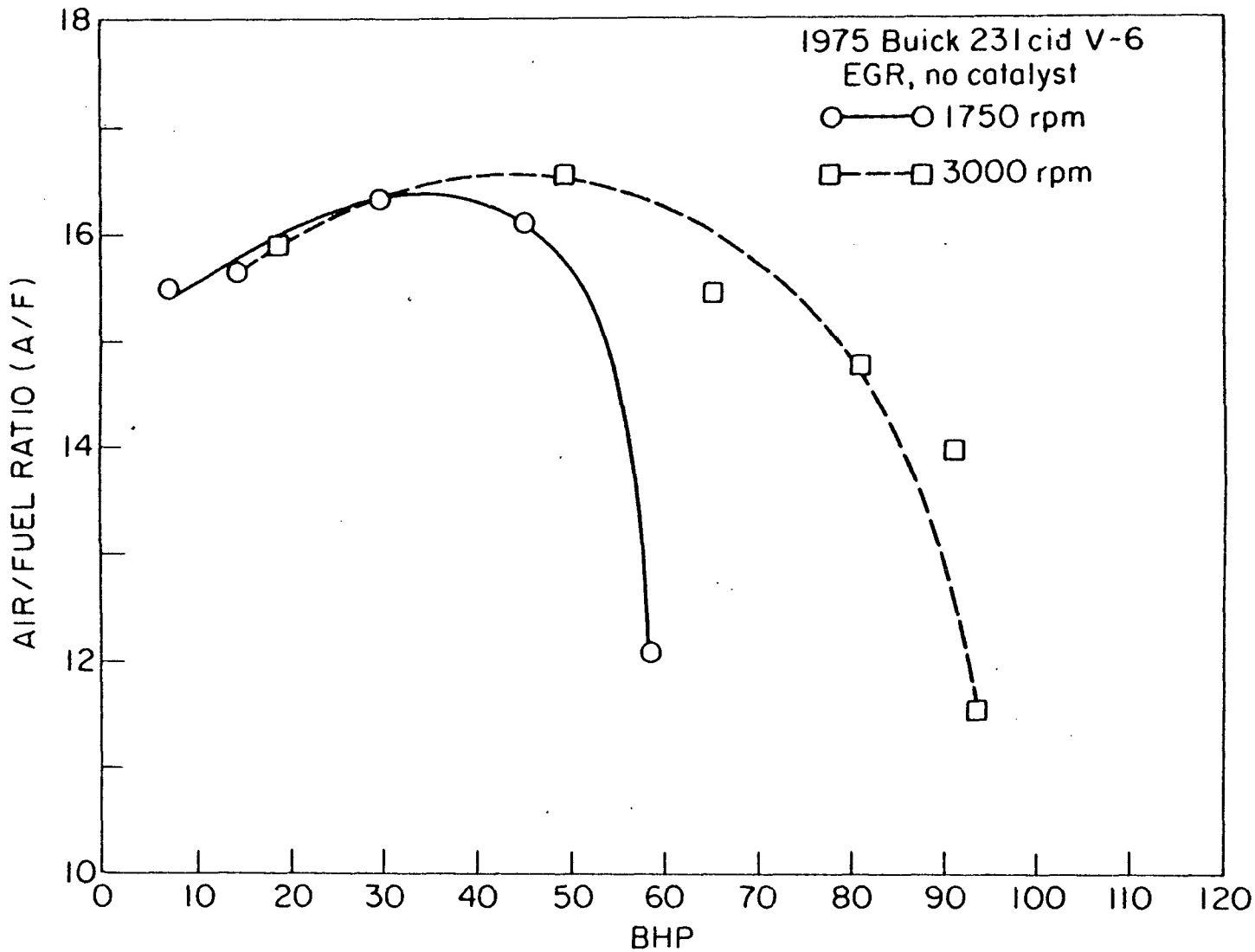

Figure 35. Air-fuel ratio as a function of brake horsepower for the 1975 Buick V-6 engine.

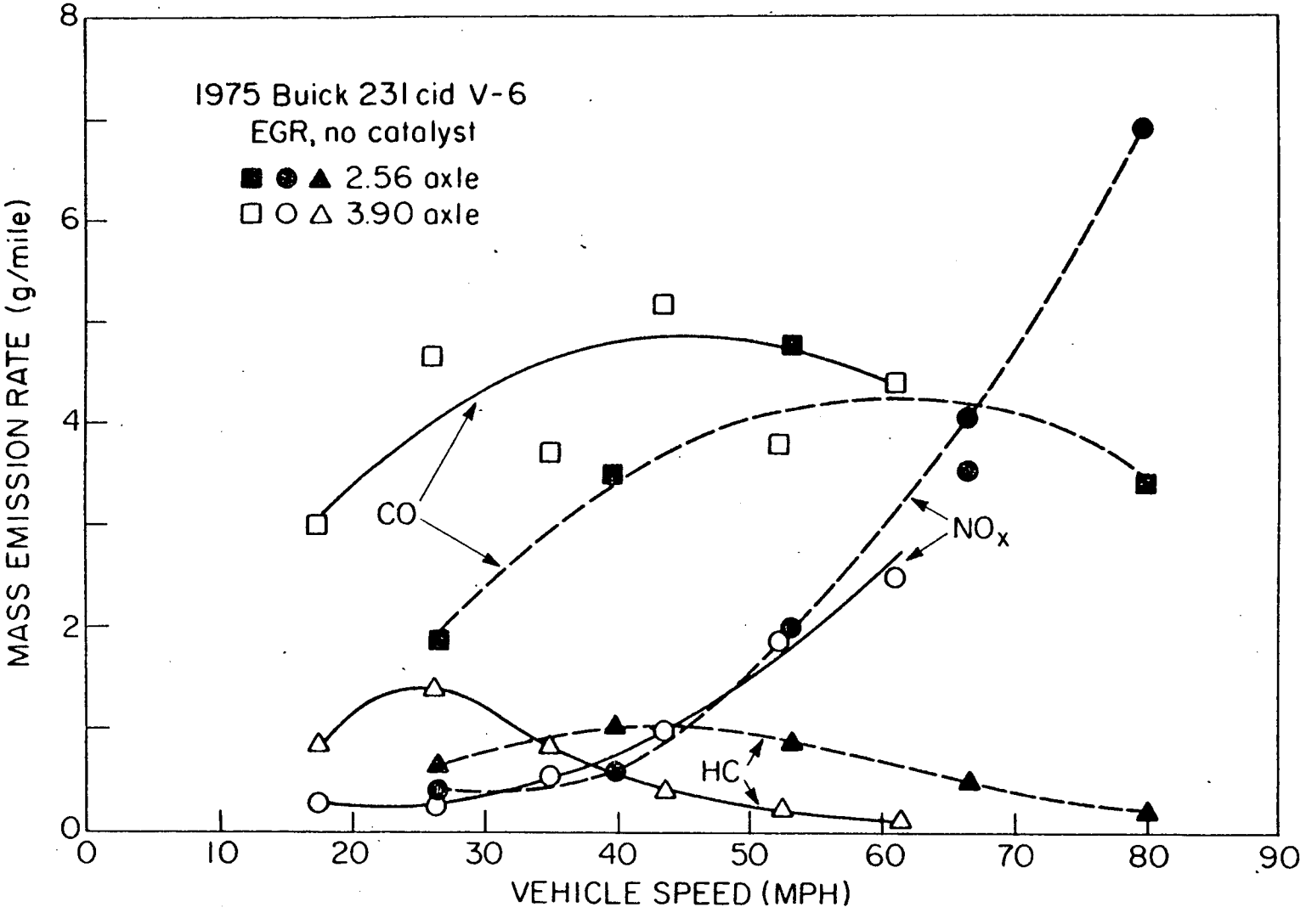

Figure 36. Mass emission rate of hydrocarbons, carbon monoxide, and nitrogen oxides as a function of vehicle speed, Buick V-6 engine installed in a simulated Mazda RX-4 vehicle, road load, 2.56 and 3.90:1 axle ratios.

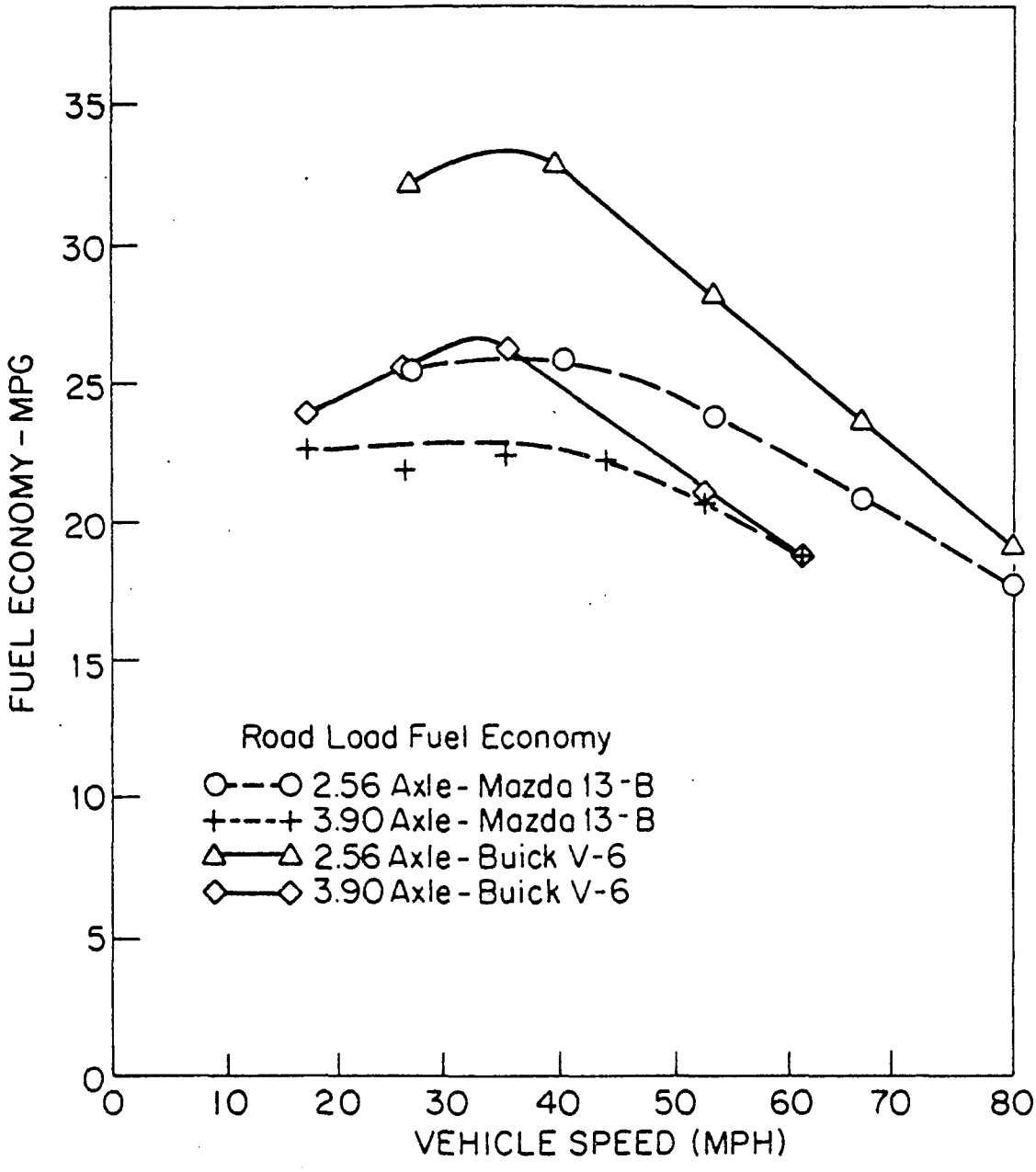

Figure 37. Road load fuel economy as a function of vehicle speed- a comparison between the Mazda 13-B and Buick V-6 engines installed in a simulated Mazda RX-4 vehicle.

the deviation in fuel economy performance would be reduced with optimization of both operating parameters and vehicle package.

The hydrocarbon emissions in grams per mile are plotted for both vehicles in Fig. 38. In this figure a major deficiency of the present Mazda engine design is clearly demonstrated. The hydrocarbon emissions of the Mazda are approximately eight times those of the Buick powered vehicle. The major factors causing this major difference are:

.Significantly richer air-fuel ratio employed by the Mazda

.Major loss of unburned mixture either due to leakage or poor combustion

The compact combustion chamber of the Buick has a minimum quench area and its open design promotes efficient flame propagation throughout the total volume. In addition, the engine is well sealed from the ambient with the poppet type exhaust valves and multi-ring gas sealing around the pistons.

Figure 39 shows the CO emissions in grams per mile as a function of vehicle speed. The difference in CO emissions between engines is also dramatic although it is not of the same magnitude as the hydrocarbon emissions. The deviation between engines expressed in this figure is primarily associated with the far richer mixture ratio employed in the Mazda. At an equal fuel-air ratio the mass CO emissions would be essentially the same. On the other hand the hydrocarbon emissions while also related to air-fuel ratio are in addition associated with fundamental processes not closely related to operating variables but rather to basic design characteristics.

The mass emission rate of NO_x as a function of vehicle speed for the two engines is shown in Fig. 40. In this case the emission performance relationship between the two engines has reversed and the Buick exhibits a higher level of NO_x emissions than the Mazda. This greater level in the Buick is in part due to the leaner mixtures employed although it must be recognized that the Buick V-6 was equipped with EGR whereas the Mazda engine was not. The fact that the data for this comparison were taken from both engines without their normal exhaust after-treatment devices is of little consequence since neither the thermal reactor or presently used designs of catalytic reactors affect NO_x emissions.

Representative brake specific fuel consumption data from the Mazda 13-B and Buick V-6 engines are plotted as a function of BHP in Fig. 41 at selected engine speeds. As is true of the miles per gallon plot the Buick exhibits considerably better fuel consumption. The brake specific fuel consumption is approximately 20% lower throughout most of the test range although there are regions where it is similar particularly at high engine speeds and near maximum load at all speeds. It should be observed that if the Mazda engine had been operated with as lean carburetion as the Buick engine, the difference in BSFC and for that matter MPG

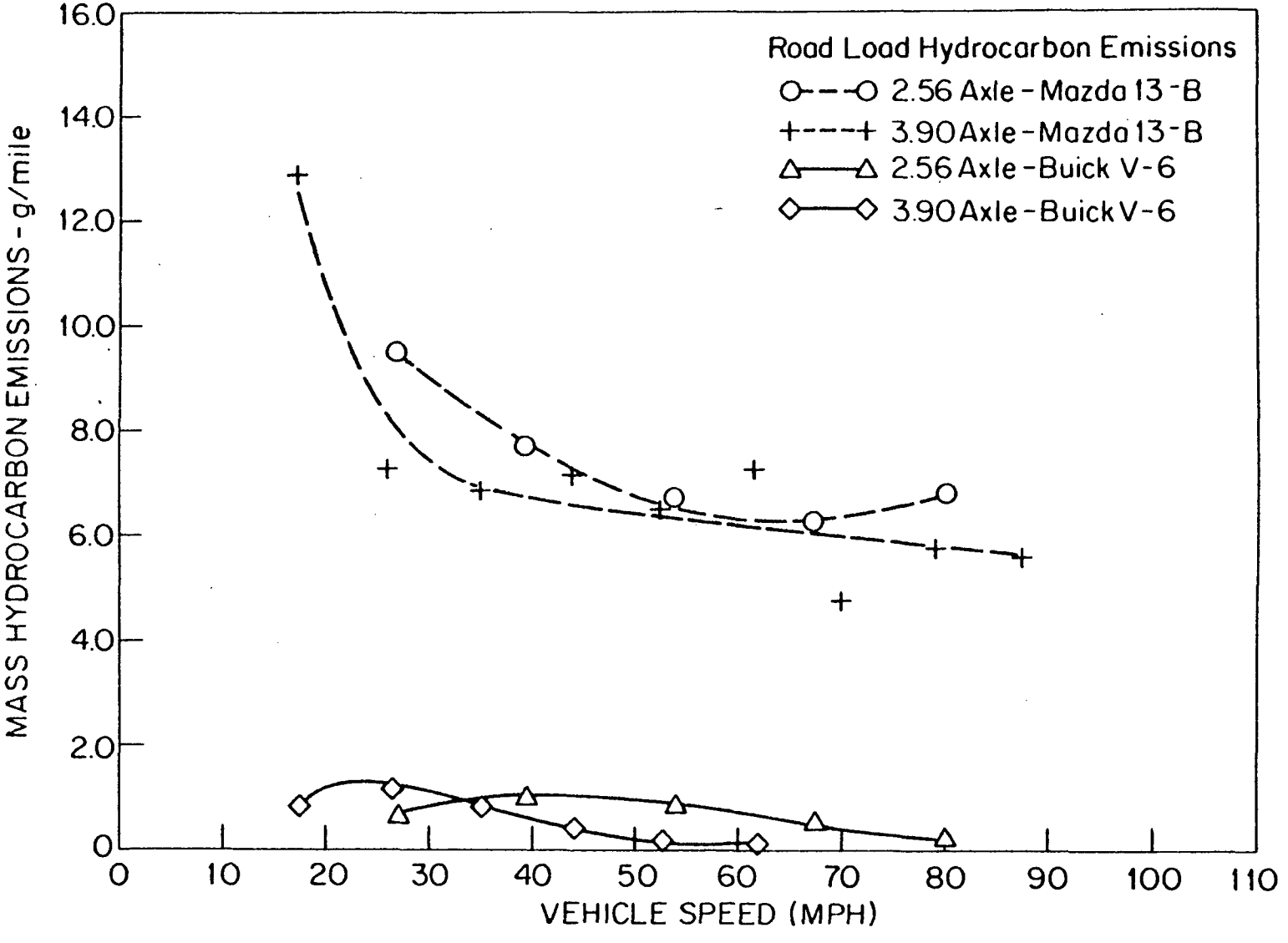

Figure 38. Road load hydrocarbon emissions as a function of vehicle speed - a comparison between the Mazda 13-B and Buick V-6 engines installed in a simulated Mazda RX-4 vehicle.

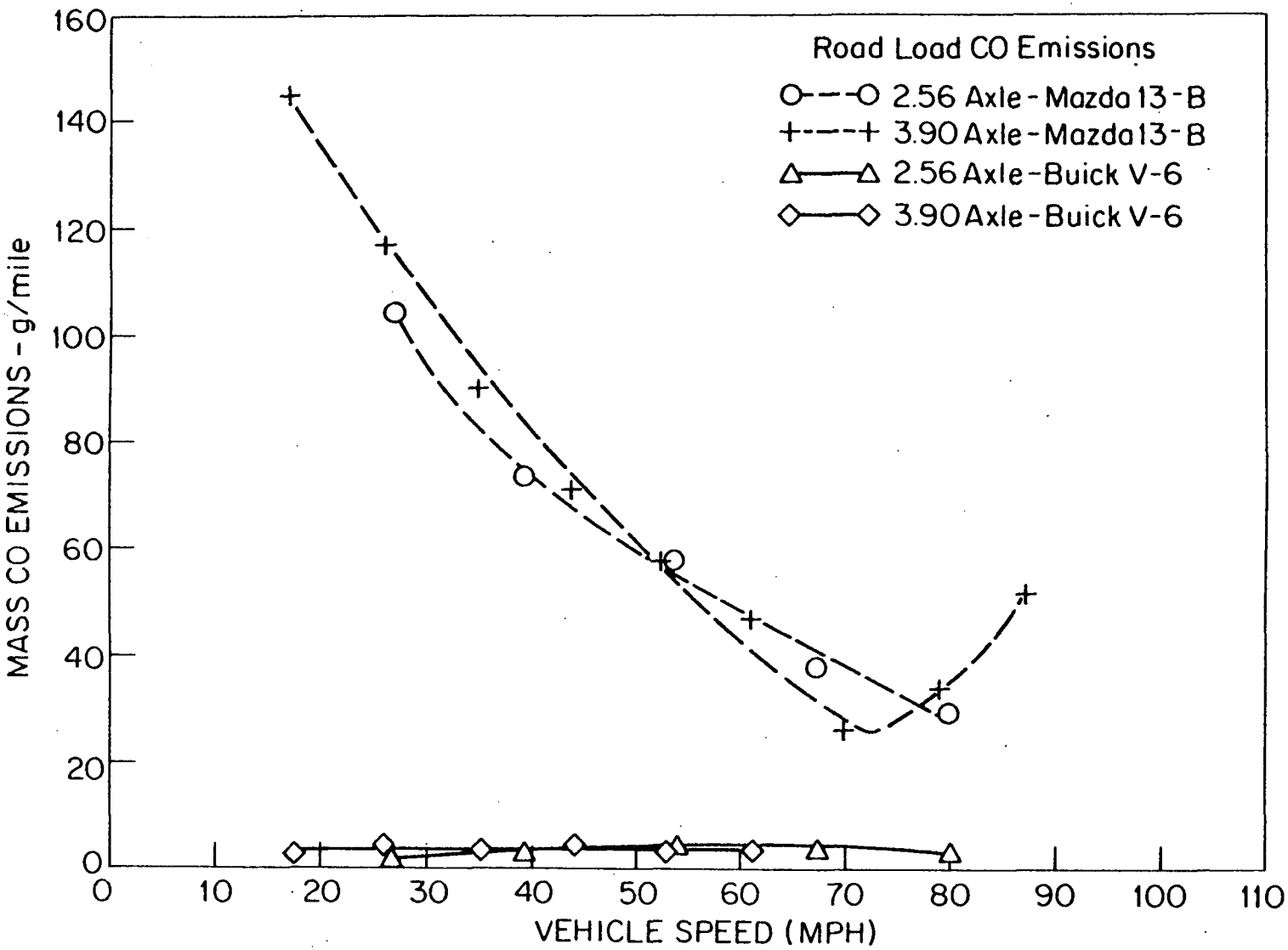

Figure 39. Road load carbon monoxide emissions as a function of vehicle speed - a comparison between the Mazda 13-B and Buick V-6 engines installed in a simulated Mazda RX-4 vehicle.

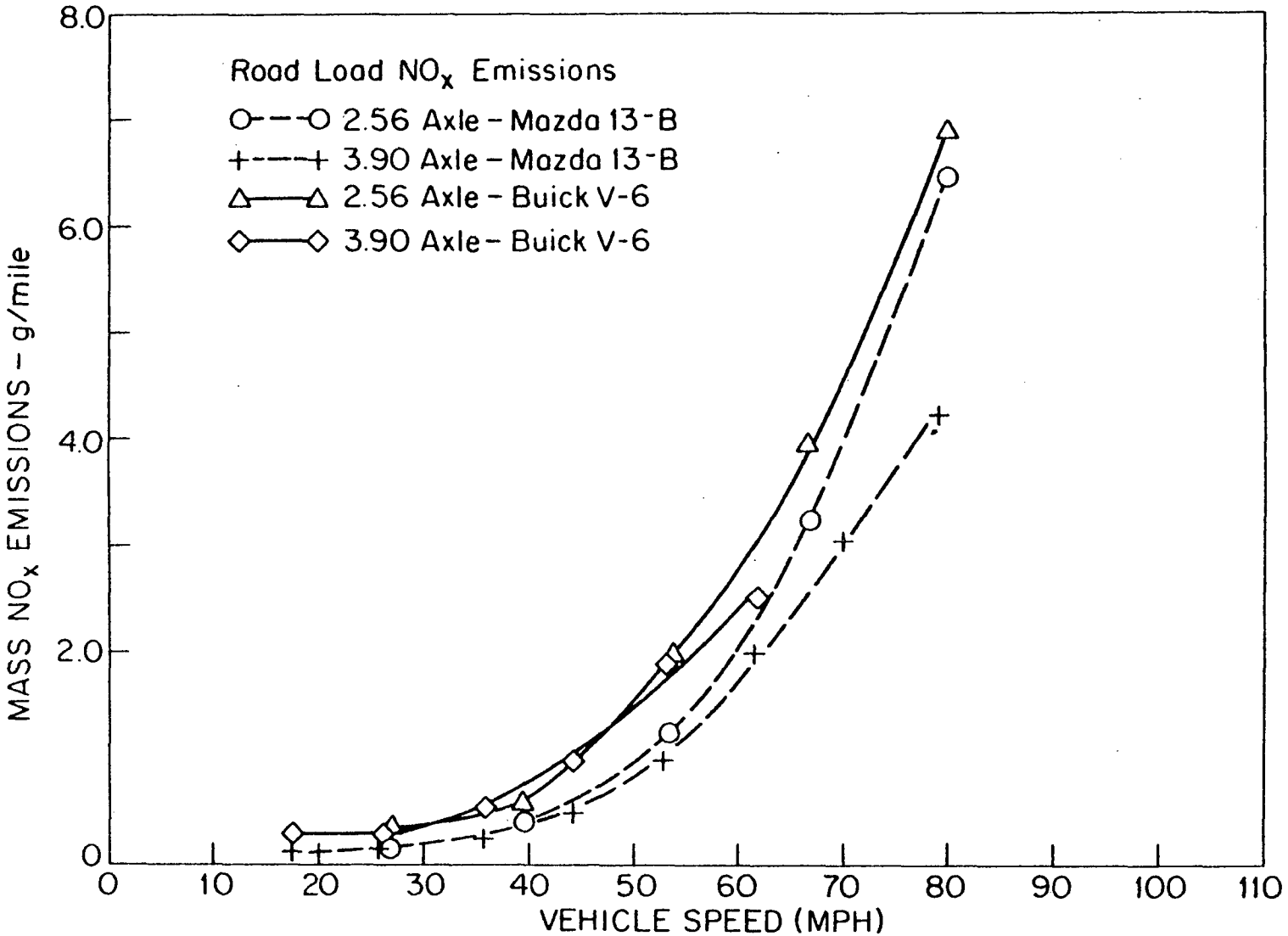

Figure 40 - Road load nitrogen oxide emissions as a function of vehicle speed - a comparison between the Mazda 13-B and Buick V-6 engines installed in a simulated Mazda RX-4 vehicle.

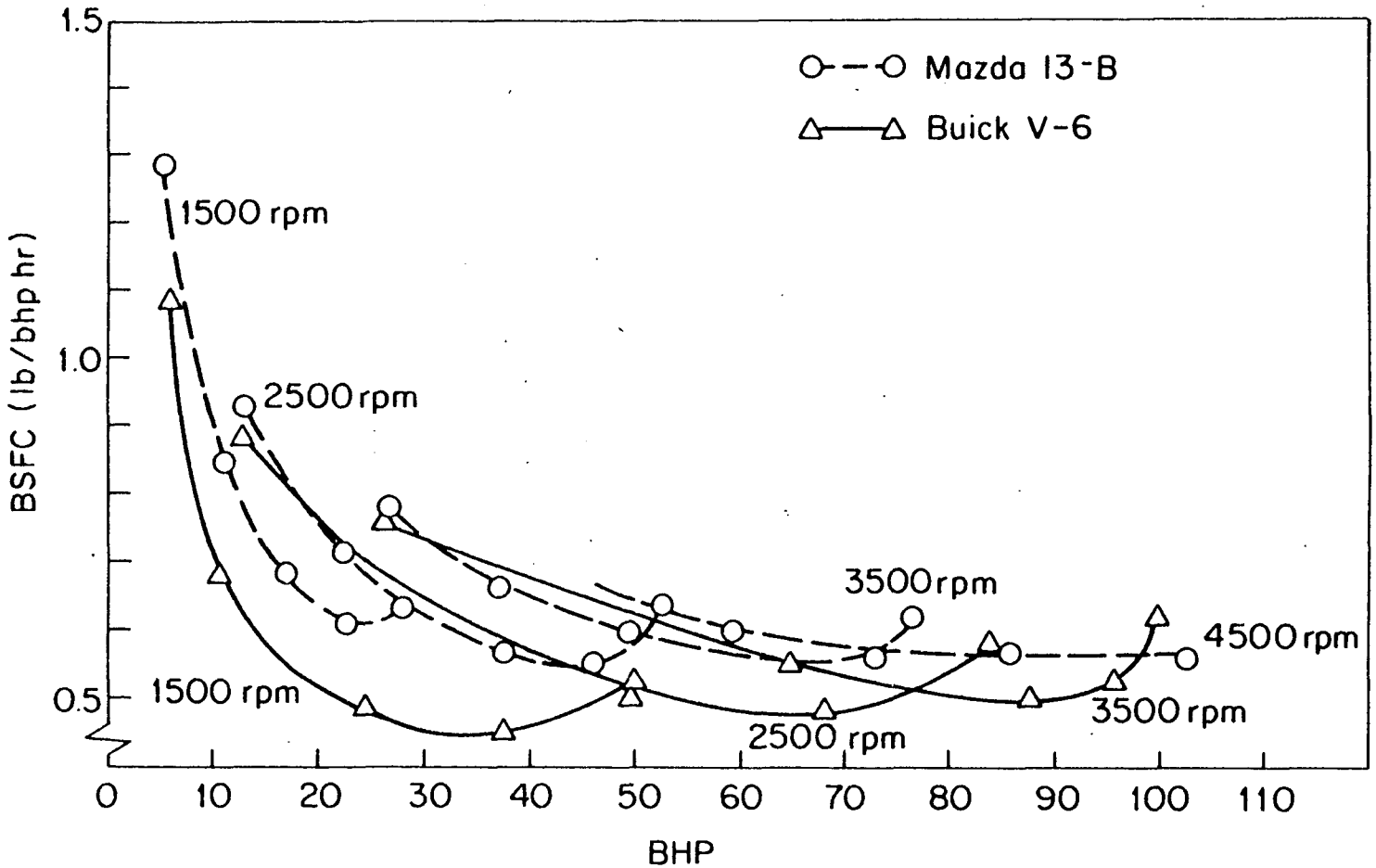

Figure 41. Brake specific fuel consumption comparison between the Mazda 13-B and Buick V-6 engines as a function of brake horsepower at selected operating conditions.

would have been considerably reduced. For example, consider operation at 2000 rpm. In the Buick engine with the development of 20 hp, the air-fuel ratio was 15.2:1 and in the Mazda engine at approximately the same load, the measured air-fuel ratio was 13.5:1. If the mixture ratio had been optimized for thermal efficiency in the Mazda, the BSFC could have been reduced from approximately 0.63 to 0.56, a 13% improvement. Thus air-fuel ratio optimization alone could bring the Buick V-6 and Mazda engine performance considerably closer together. Unfortunately, as noted before, the rich mixtures used in the Mazda are required because of the selection of the thermal reactor emission control device. If, in addition, to air-fuel ratio optimization the spark had been advanced closer to its optimum (MBT) as was the apparent case for the Buick V-6, the fuel consumption differences would have been even less. Thus it can be concluded that while one observes a significant deficiency of the rotary engine in comparison to the reciprocating engine, this defficiency is not totally associated with fundamental factors but rather because it has not been optimized with respect to operating parameters because of the choice of the thermal reactor as a control system. This consideration is particularly important when estimating the long-term potential of the rotary engine.

One of the most interesting comparisons between the Mazda 13-B and Buick V-6 engines is evident in the plot of friction horsepower and friction mean effective pressure as a function of engine speed in Fig. 42. These data were all taken at wide-open throttle in a motoring engine per accepted procedure. The friction horsepower curves show that the rotary possesses a significant advantage over the V-6 under these conditions. This advantage is attenuated somewhat in the plot of friction mean effective pressure which rates the friction performance on a per unit displacement basis. In any event the rotary appears to have a favorable relationship to the reciprocating engine at higher speeds and of significance is the fact that the rate of increase in both the FMEP and FHP is considerably lower for the rotary engine. It must be remembered that when one views the brake thermal efficiency of the total engine this reflects both the efficiencies of the various thermal processes (indicated thermal efficiency) and, in addition, the mechanical efficiency of the mechanism. Thus while the combustion chamber surface to volume ratio of the rotary is not as well suited to attaining an ultimate indicated thermal efficiency, it does possess attractive mechanical efficiency which can at least partially compensate for indicated performance deficiencies. Further, these data lend credence to the argument that the rotary engine is well suited to high-speed operation. It must be remembered, however, that the data presented here as is the case with most reported friction data was obtained from a motoring engine. Thus it is a measurement under an unrealistic operating condition. For example, in the rotary engine, the gas pressure behind the sealing grid, which assists contact of the seals with various engine surfaces, is considerably lower than in the firing engine. The same effect is present in the reciprocating engine to a

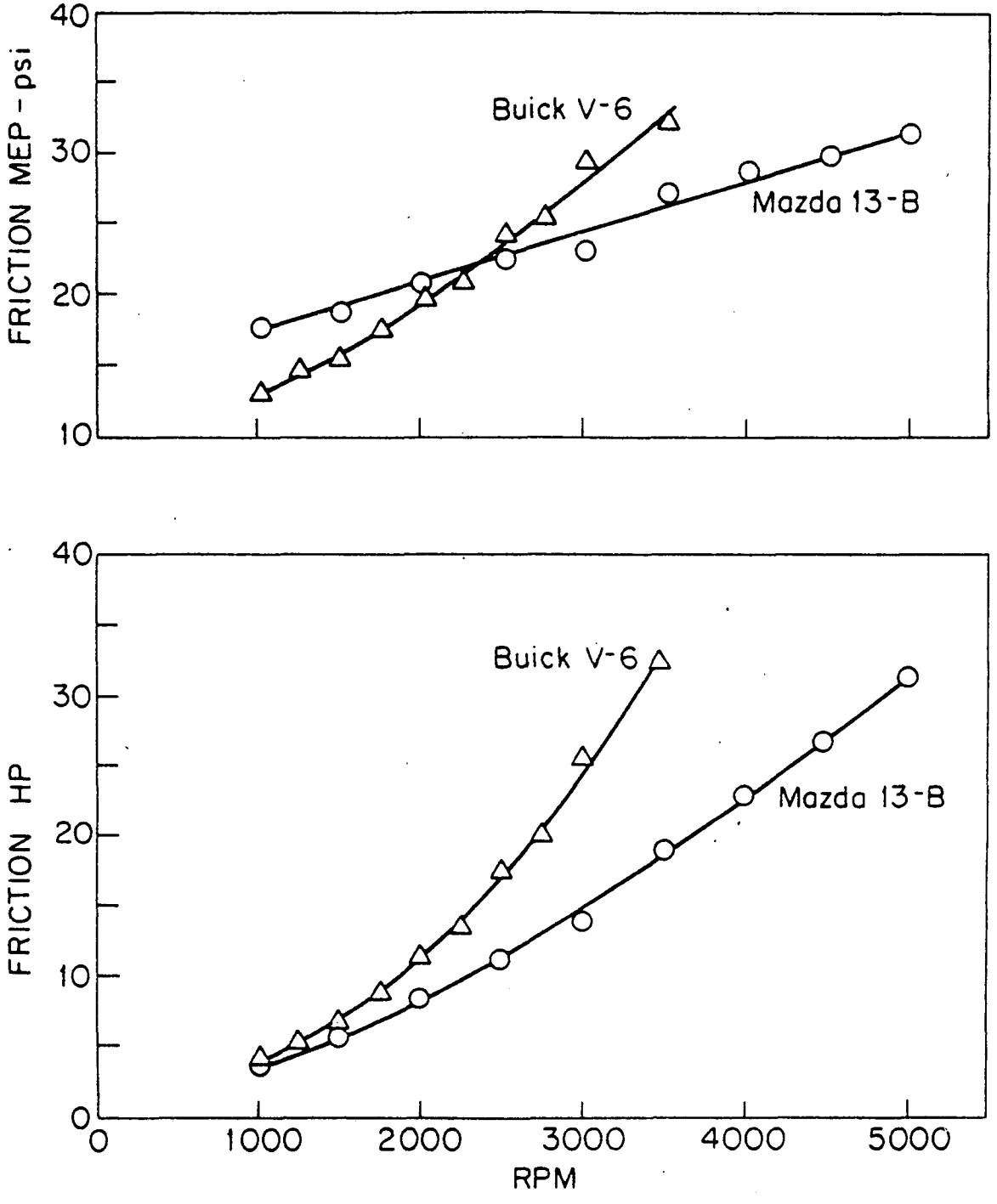

Figure 42. Motoring friction mean effective pressure and friction horsepower as a function of RPM for the Mazda 13-B and Buick V-6 engines.

degree. It is only possible to infer the relative friction performance from this data rather than to say that is is a true measure of firing engine friction.

Another interesting aspect of the Mazda performance in comparison with the Buick is the relationship between their respective exhaust gas temperatures. While this comparison is relatively qualitative because of the nature of exhaust temperature measurement (limited radiation shielding and variation in sensor location with respect to the engine exhaust port) it is useful for assessing the potential for "clean-up" due to thermal reaction in the exhaust. Exhaust temperature is plotted at selected speeds as a function of brake horsepower in Fig. 43. In general these results showed that the exhaust temperature of the Mazda is similar to the Buick engine. Exhaust temperature data in the literature, Ref. 10 , suggests that the Mazda exhaust temperature should be considerably higher at a given speed and load than the reciprocating engine. This behavior may be true here as well if the engines had been compared at an equivalent set of operating conditions. But, as noted earlier, the Mazda engine is operating with a considerably richer mixtures resulting in a significant reduction in exhaust temperature over most of the operating range. It must be noted however that temperature is only one factor governing the ability to oxidize the exhaust gas. This is particularly true with a thermal reactor. Mazda believes a sacrifice in exhaust temperature is more than offset by enrichment of the mixture.

D. ALDEHYDE EMISSIONS FROM THE UNCONTROLLED AND EMISSION CONTROLLED MAZDA MODEL 13-B ENGINE

Aldehydes, particularly formaldhyde and acrolein have been shown to be important constituents in spark-ignited engine exhaust, (6,7,11). They are apparently direct contributors to problems associated with photochemical smog and exhaust odor.

Aldehydes which are an intermediate product of hydrocarbon combustion are generally associated with low temperature combustion reactions. Wall-quenching or quenching by excessive exhaust dilution are possible ways in which partially oxidized hydrocarbon molecules may arise. In addition low temperature reactions may occur during expansion, blowdown, and exhaust which may either decrease or increase the aldehydes emissions.

Little published data exists on aldehyde emissions from internal combustion engines. This is in part because of the complexity of making such measurements rapidly. The wet chemical techniques used are complex and time consuming.

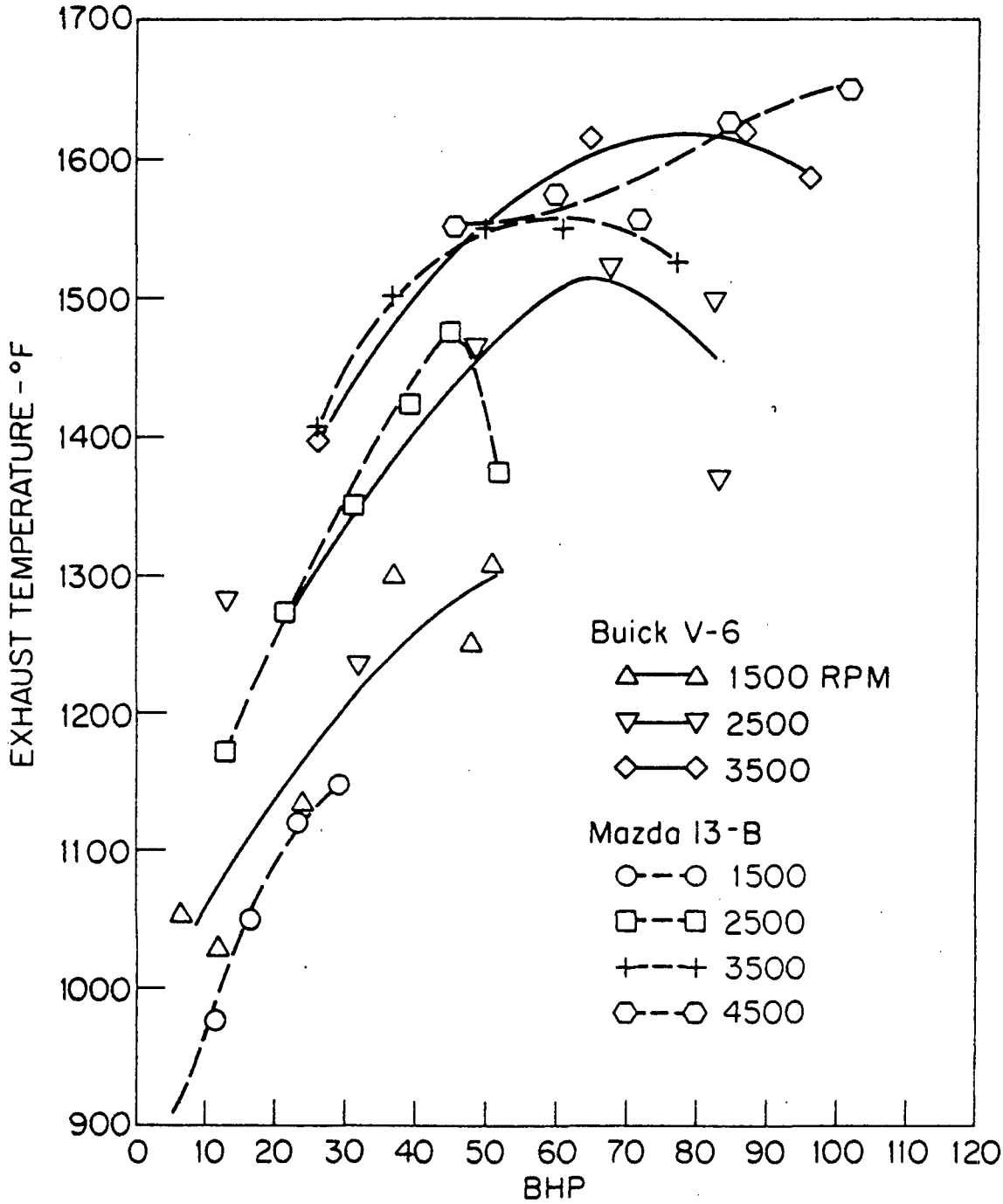

Figure 43. Exhaust gas temperature as a function of brake horsepower at selected conditions, Mazda 13-B and Buick V-6 engines.

Several series of experiments were conducted on the Mazda engine to determine the aldehyde concentration using the DNPH method. In the first series the aldehydes were determined at 2000 rpm, 8.7 bhp for the uncontrolled engine at several air-fuel ratios. These data are plotted in Fig. 44. The aldehyde concentration was observed to increase almost linearly with air-fuel ratio. This trend is generally consistent with behavior exhibited by spark-ignited reciprocating engines. Clearly in the rich mixture operating region, typically used in the Mazda engine for effective operation of thermal reactor, the aldehydes are substantially lower than with operation at lean mixture ratios.

A second series of tests was conducted with and without the thermal reactor at stock engine operating conditions. The test points selected were 2000 rpm, 8.7 bhp and 26.3 bhp and 3000 rpm, 18.6 bhp. Figure 45 shows clearly that the thermal reactor effectively reduces the aldehyde concentration by a factor of more than 4. The reactor is particularly effective at higher speeds and higher loads. The effect of load is shown in the data and illustrates that the aldehydes tend to increase with load, although additional factors in this relationship would be changes in mixture ratio and ignition timing.

For comparative purposes typical aldehyde data for a 350 cid (5735 cc) spark ignited reciprocating engine are presented in Table 4. Note that the data were not obtained from the Buick reference engine nor at similar operating conditions to the Mazda. Therefore only a highly qualitative comparison is justified.

TABLE 4

ALDEHYDE EMISSIONS FROM A 350 cid (5735 cc) AUTOMOTIVE ENGINE AT 1200 RPM, 30 BHP (Ref. 11)

Air-Fuel Ratio	Aldehydes - ppm CH_2O
12	120
14	130
16	170
18	200

The trends of aldehyde emissions as a function of air-fuel ratio are similar for both engines.

E. INFLUENCE OF AIR-FUEL RATIO ON SPECIFIC FUEL CONSUMPTION AND EMISSIONS - MAZDA 13-B ENGINE

Three representative test conditions were selected for the parametric study of air-fuel ratio. These were 2000 rpm, 8.7, and 26.3 bhp and 3000 rpm, 18.7 bhp. Two series of tests were

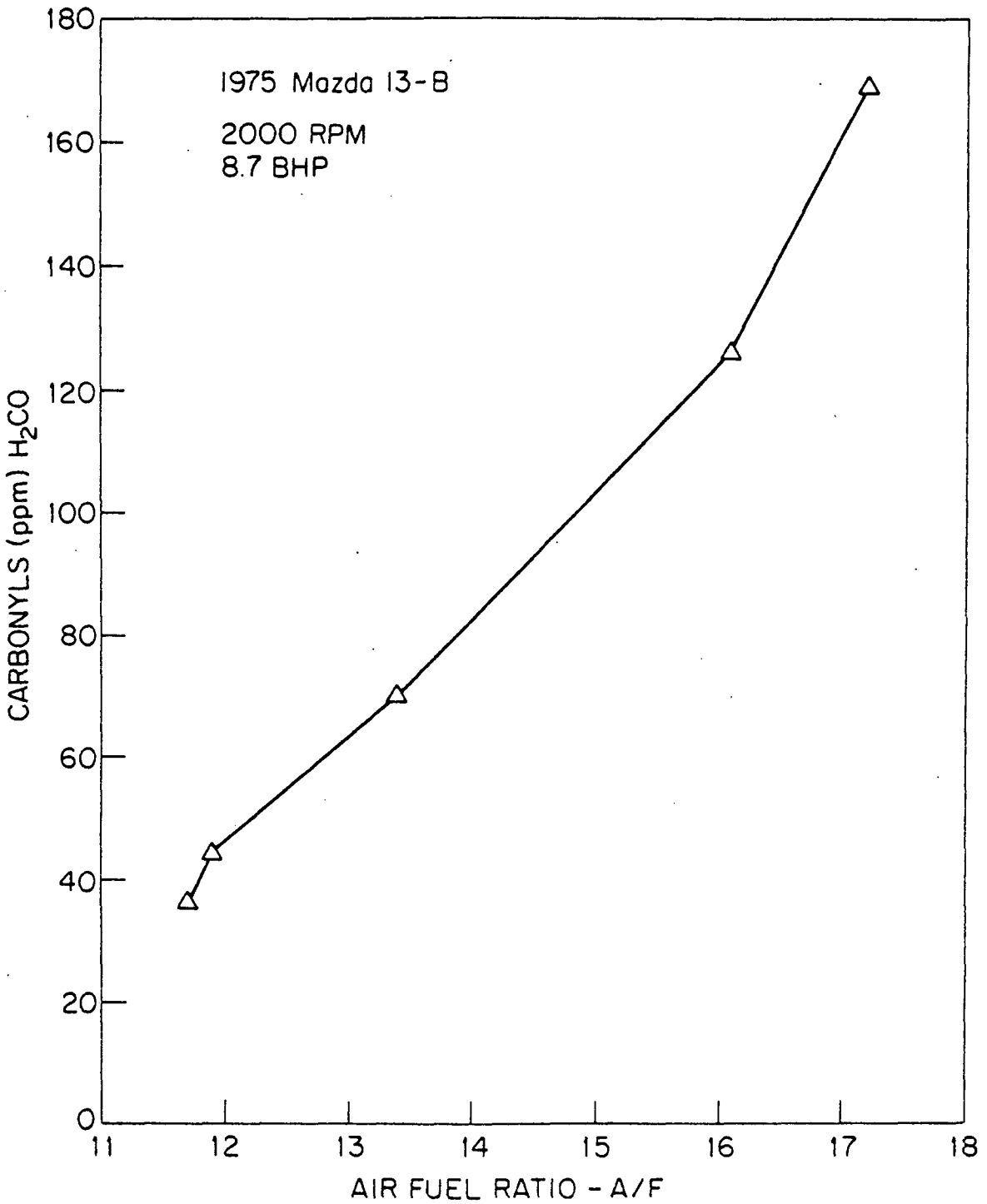

Figure 44. Aldehyde emissions as a function of air-fuel ratio, the Mazda 13-B engine at 2000 rpm, 8.7 brake horsepower.

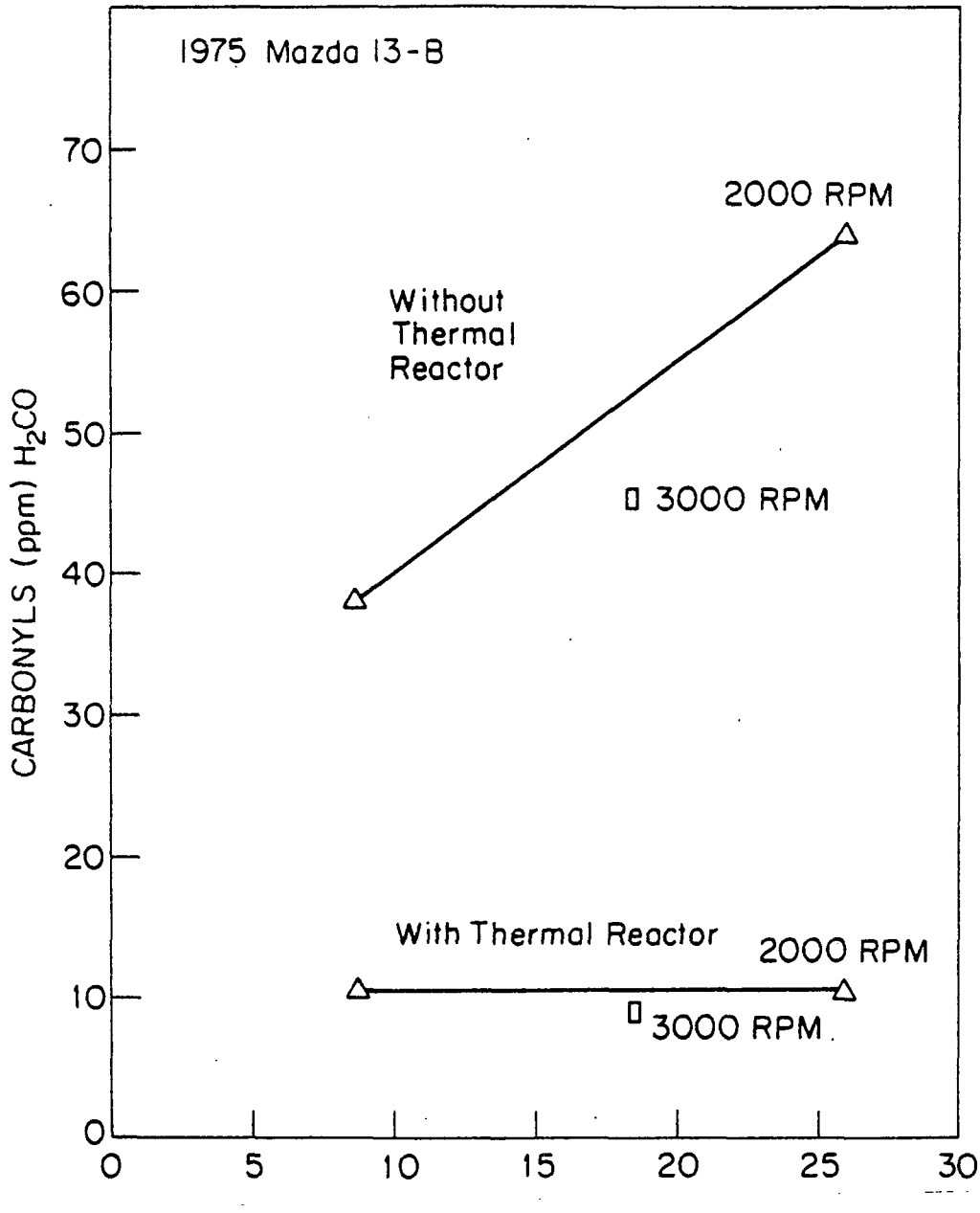

Figure 45. Aldehyde emissions as a function of brake horsepower at selected conditions, Mazda 13-B engine with and without thermal reactor.

conducted, the one with MBT ignition timing and the other with stock ignition timing. The trends observed were in general similar to those observed for conventional reciprocating spark-ignited engines (12,13). For each series the individual dependent variables of brake specific fuel consumption and emissions are plotted as a function of equivalence ratio* for the three test conditions.

1. MBT Timing

Brake specific fuel consumption as a function of equivalence ratio is plotted in Fig. 46. The minimum occurs slightly lean of stoichiometric and is significantly lower for the 2000 rpm, 26.3 bhp test point. The result at 26.3 bhp can be attributed to a higher load factor as well as more efficient combustion resulting from lower exhaust residual dilution and faster burning, because of reduced heat transfer per unit mass of the working fluid. At 8.7 bhp, 2000 rpm the residual dilution is probably the most significant factor in the higher BSFC results.

Brake specific hydrocarbon emissions are plotted in Fig. 47. In general the curve shapes are similar to one another and to the BSFC curves. However, several interesting points are evident. At 2000 rpm, 8.7 bhp the minimum occurs at approximately .95 equivalence ratio and the upturn in BSHC at leaner mixtures is gradual. At 2000 rpm, 26.3 hp, the minimum occurs near an equivalence ratio of .85, however, the data is not definitive in this region. The 3000 rpm, 18.7 bhp curve was the most erratic. It demonstrated a significant dip in hydrocarbon emissions at the leanest mixtures, and no minimum point was evident in the range tested. The significantly lower emissions at lean mixtures compared to the 2000 rpm conditions may have been due to some exhaust reaction in the exhaust system without the thermal reactor. This reaction was observed in earlier work on a Curtiss-Wright rotary engine (10).

The BSCO emissions, shown in Fig. 48, were similar to one another at the three speed and load conditions and exhibited behavior similar to that expected for reciprocating spark-ignited engines. Air-fuel ratio is well recognized as the dominant factor in CO emission levels.

Figure 49 is a plot os $BSNO_x$ emissions. The NO_x emissions are maximum slightly on the lean side of stoichiometric. The important effect of engine load on this constituent is shown by the comparison between the 26.3 and 8.7 bhp data at 2000 rpm. The maximum at the heavier load setting is approximately five times

*Equivalence ratio or relative fuel-air ratio is the ratio of the actual fuel-air ratio to the stoichiometric fuel-air ratio or the ratio of the stoichiometric air-fuel ratio to the actual air-fuel ratio.

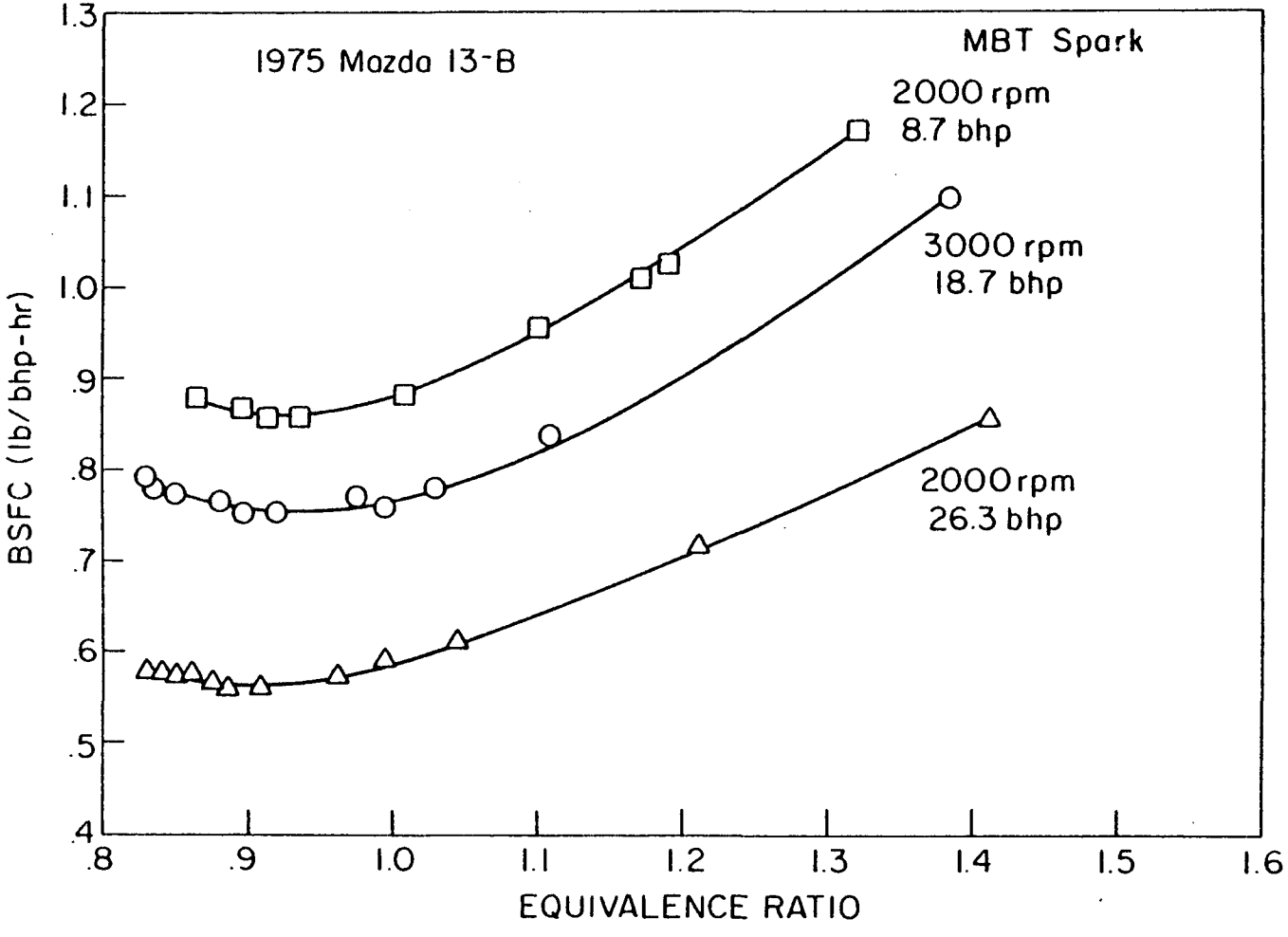

Figure 46. Brake specific fuel consumption as a function of equivalence ratio, Mazda 13-B engine, MBT spark.

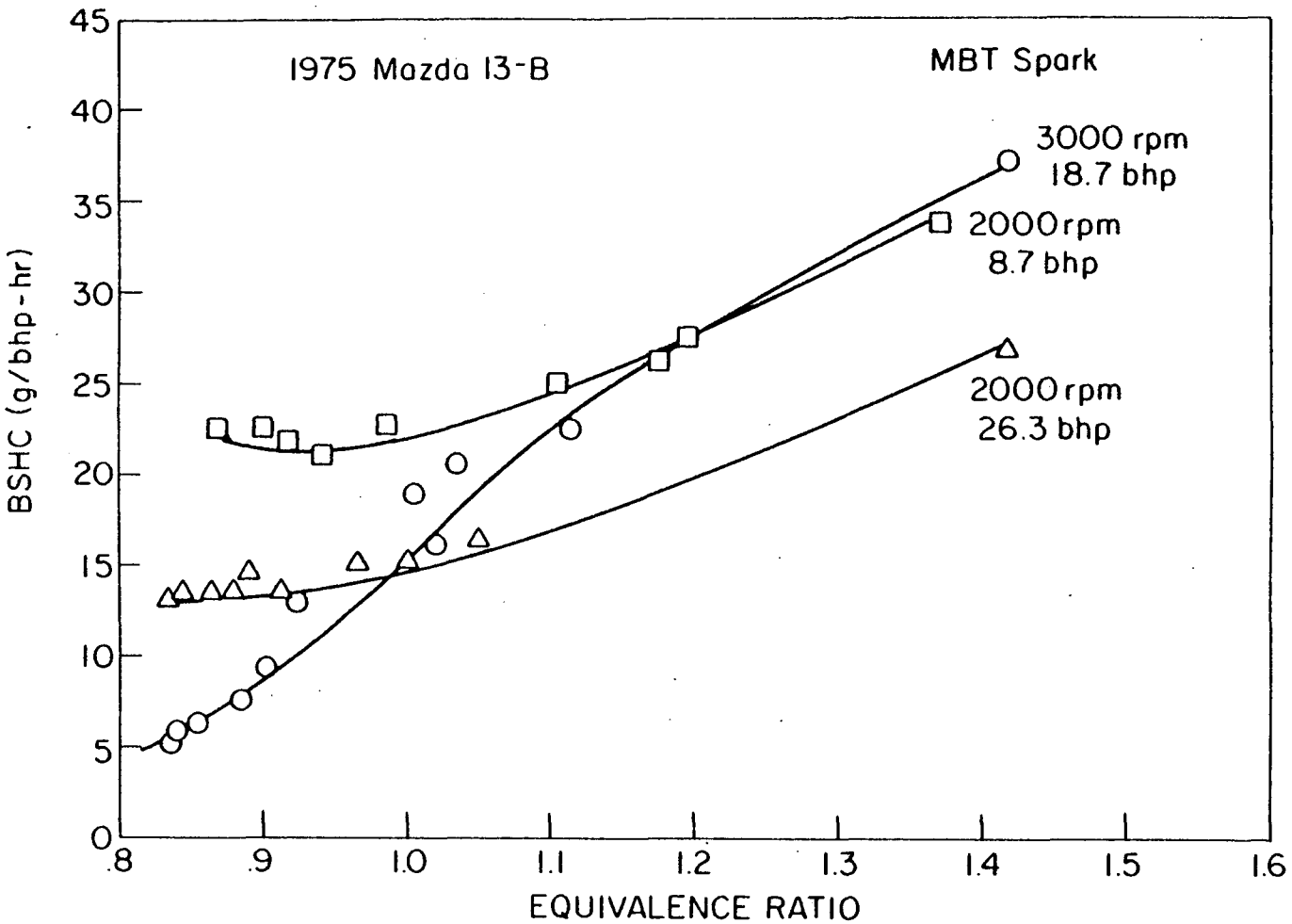

Figure 47. Brake specific hydrocarbon emissions as a function of equivalence ratio, Mazda 13-B engine, MBT spark.

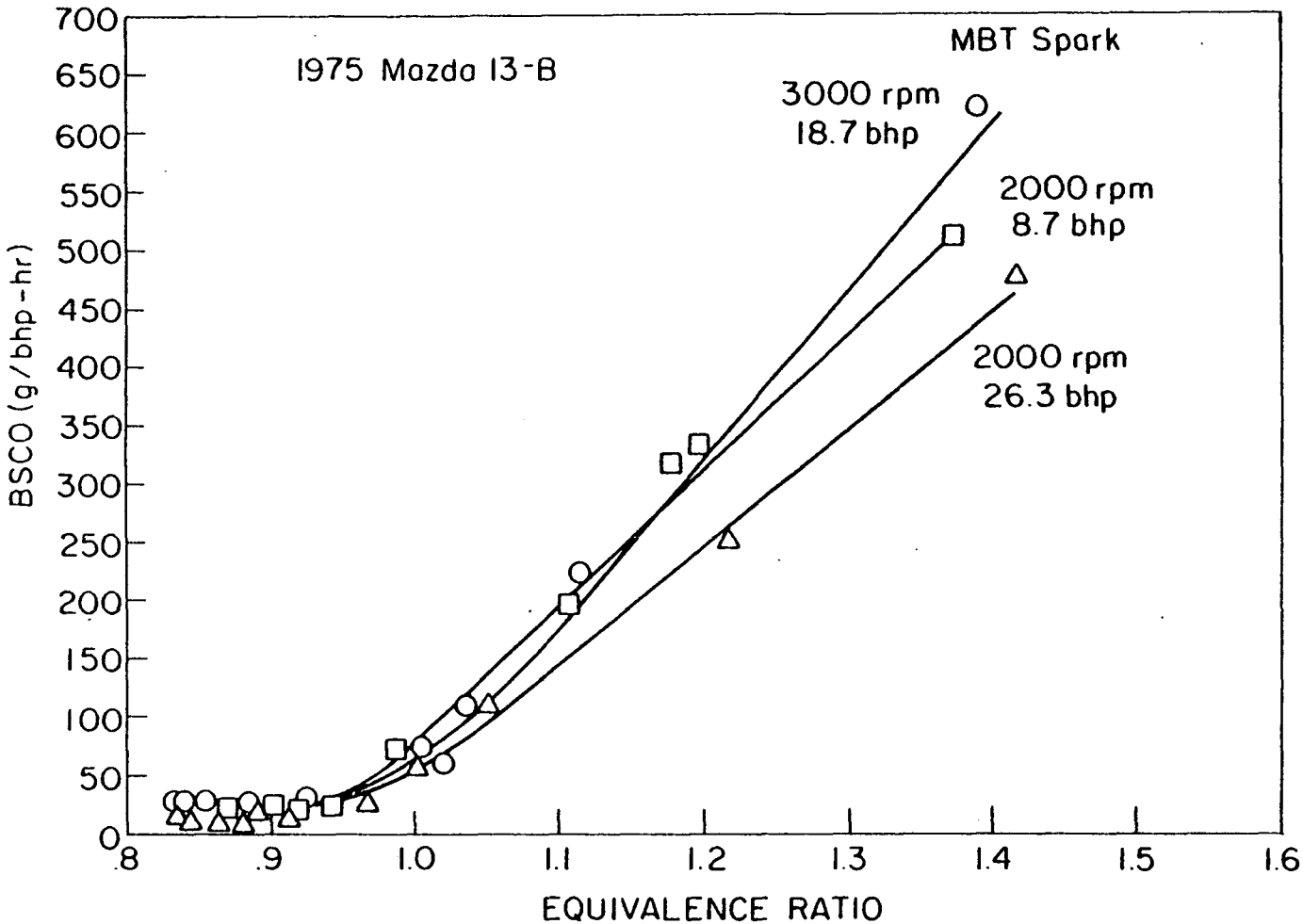

Figure 48. Brake specific carbon monoxide emissions as a function of equivalence ratio, Mazda 13-B engine, MBT spark.

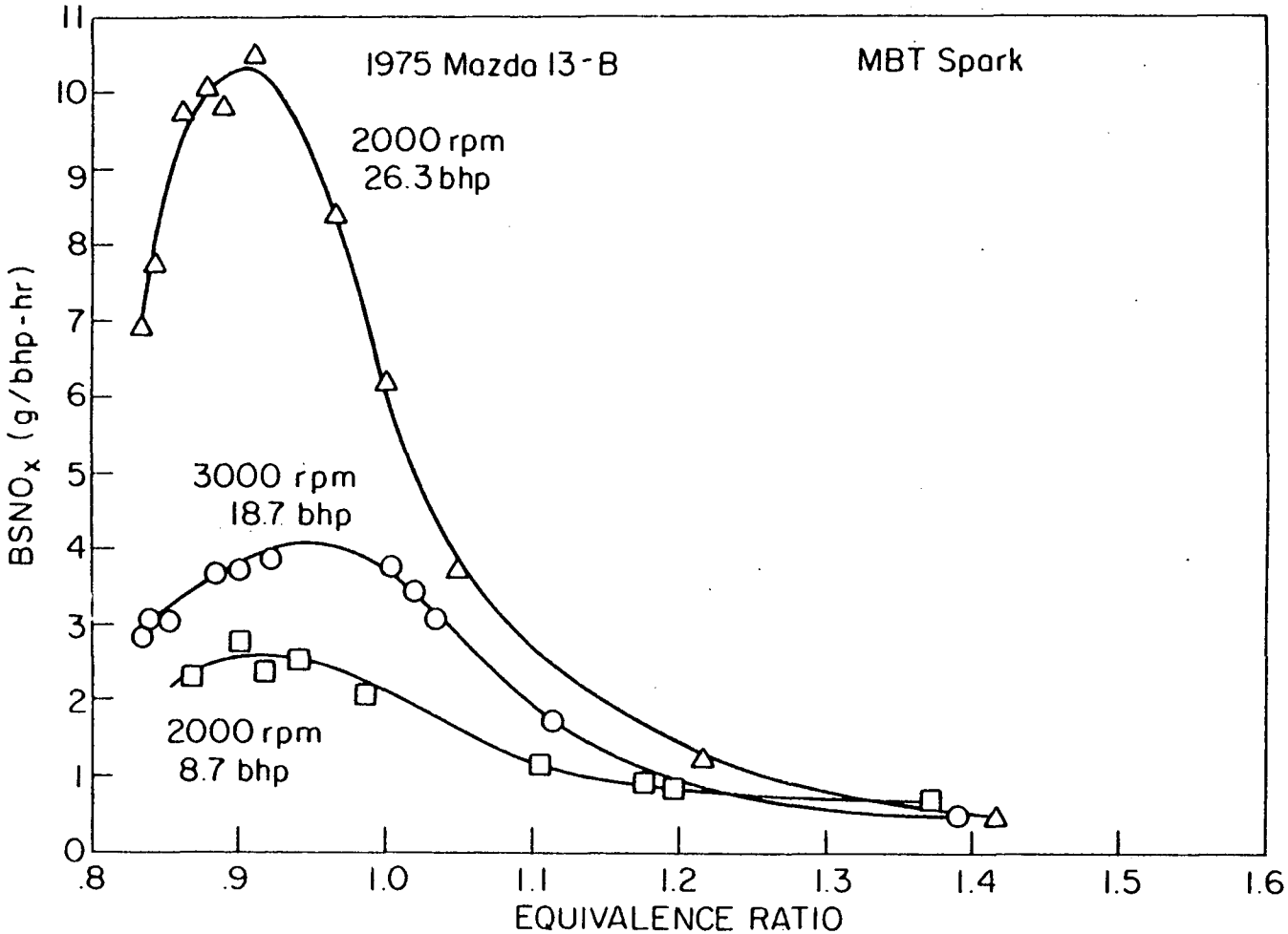

Figure 49. Brake specific nitrogen oxide emissions as a function of equivalence ratio, Mazda 13-B engine, MBT spark.

that at the lower load. This difference, however, essentially disappears at mixture ratios greater than 1.1. The 3000 rpm NO_x emissions near stoichiometric mixture ratio are greater than the light load 2000 rpm emissions probably because of higher combustion temperatures. Decreased residence time at these higher temperatures is less significant than the temperature effect.

2. Stock Ignition Timing

The effects of air-fuel ratio on specific fuel consumption and exhaust emissions for the stock ignition timing are shown in Figs. 50 through 53. In this test series the effective ignition timing was retarded with respect to the stock setting at both leaner and richer mixtures than those furnished by the stock carburetor. The data trends are similar to the results with MBT timing. The BSFC data, Fig. 50, are almost identical in shape but are universally displaced to higher values as expected.

The BSHC emissions shown in Fig. 51, also follow a similar trend to those with MBT spark. However at richer mixtures the BSHC was generally slightly higher than at MBT. In addition, at leaner mixtures (equivalence ratio of approximately .9) the emissions appeared to decrease significantly. The primary factor in this attentuation was the effective spark retard from MBT due to slower burning coupled with increased thermal reaction.

The BSCO emissions are shown in Fig. 52 with stock timing. The results are essentially identical to those with MBT timing and show the very clear relationship between CO and the equivalence ratio. No evidence is present indicating a CO thermal reaction with lean mixtures as the CO emissions at this condition are already low. In addition, CO does not react as readily as unburned hydrocarbons in the thermal reactor. Brake specific NO_x emissions are shown in Fig. 53. Both the trend and magnitude of the data are similar to that observed with MBT timing. It was anticipated that the effective retard would result in a moderate reduction in NO_x from the data at MBT but this did not occur.

In summary, it is evident that the air-fuel ratio influence on emissions and fuel consumption of the rotary engine is similar to that expected for reciprocating gasoline engines. One exception may be the apparent significant thermal reaction of hydrocarbons at lean mixtures at some conditions, particularly with slight retardation of the timing from MBT. This can be attributed to the normally higher exhaust temperatures (at similar operating conditions) in the rotary engine in comparison to those observed in a reciprocating engine.

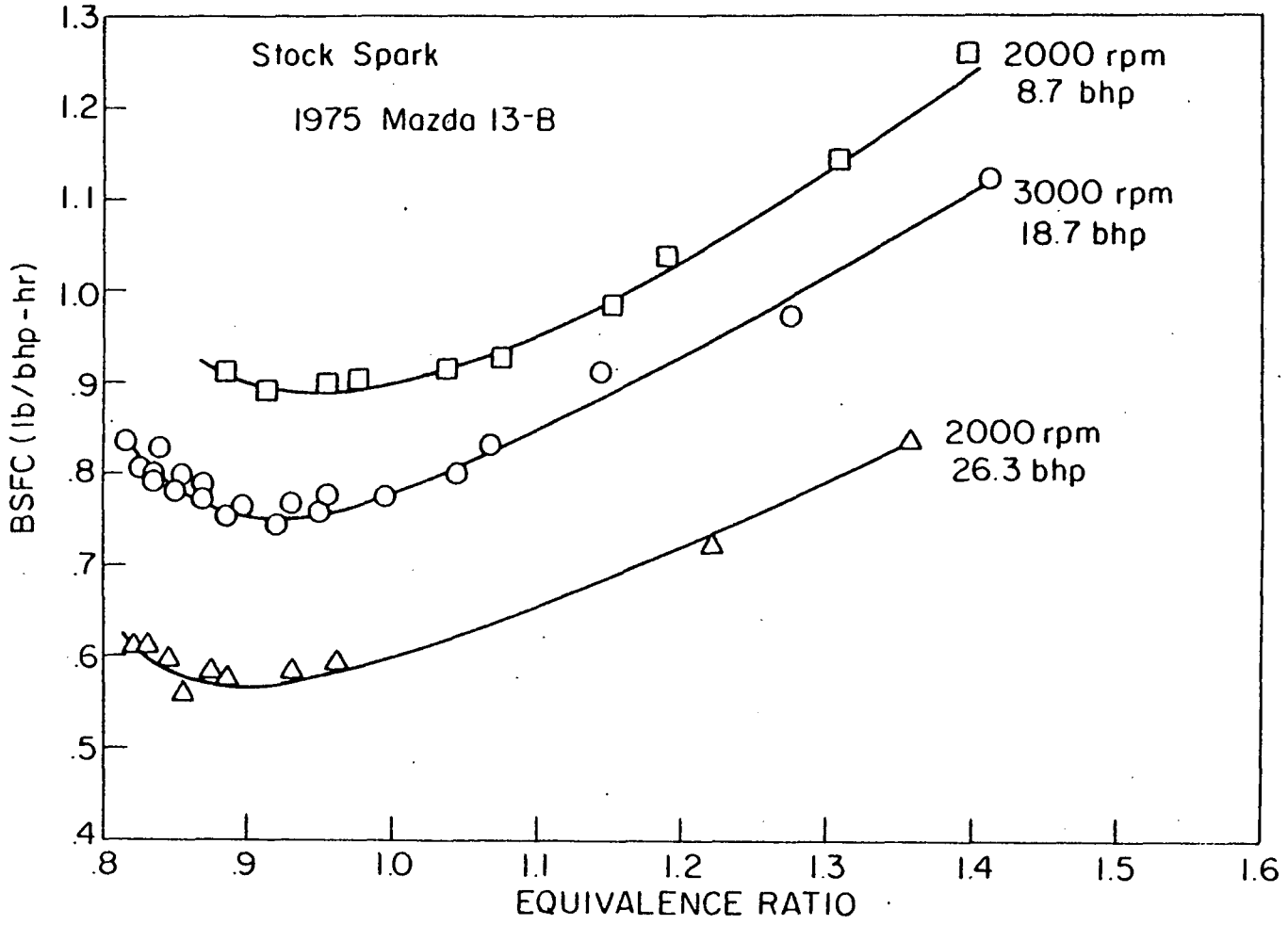

Figure 50. Brake specific fuel consumption as a function of equivalence ratio, Mazda 13-B engine, stock spark timing.

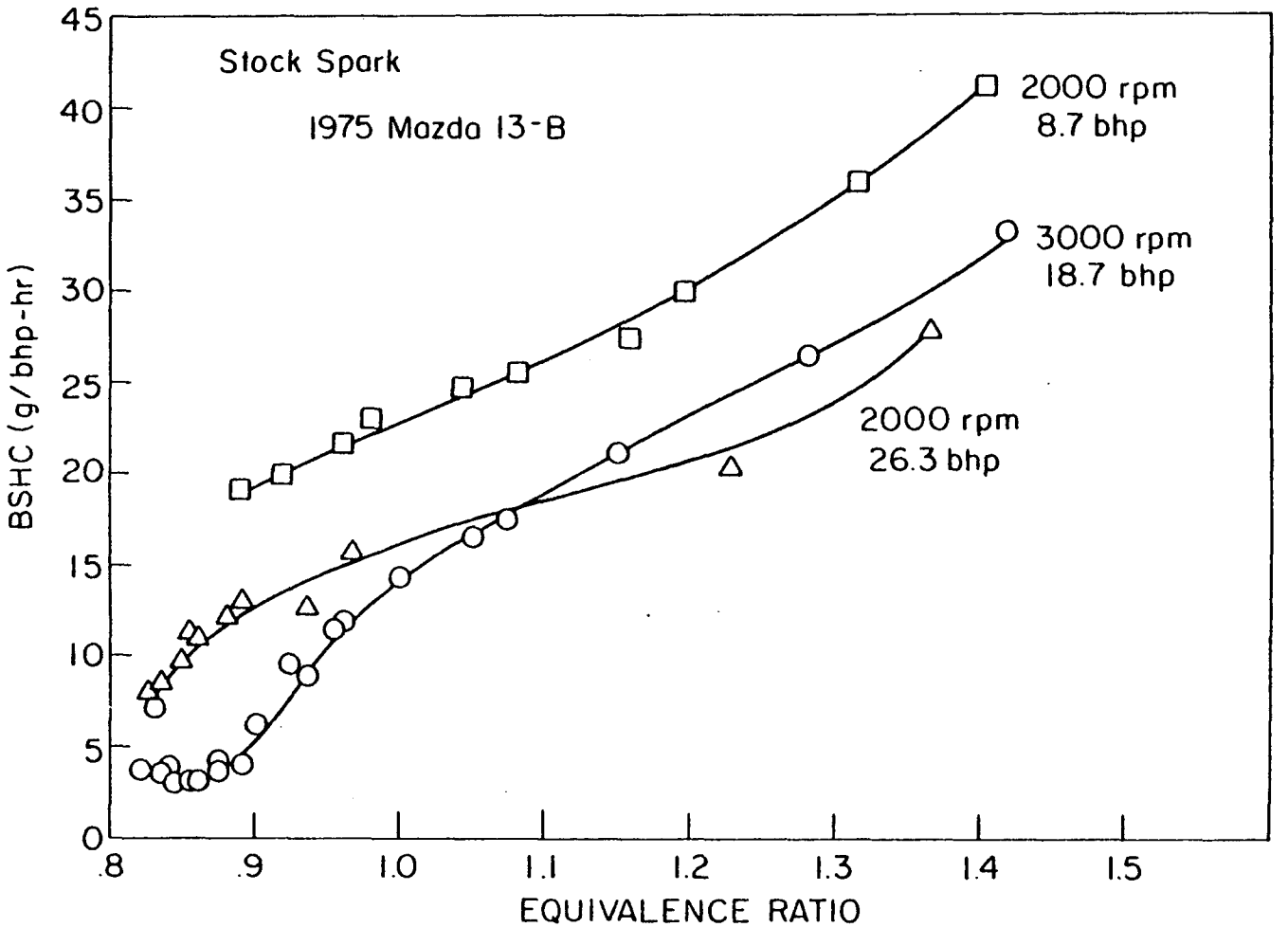

Figure 51. Brake specific hydrocarbon emissions as a function of equivalence ratio, Mazda 13-B engine, stock spark timing.

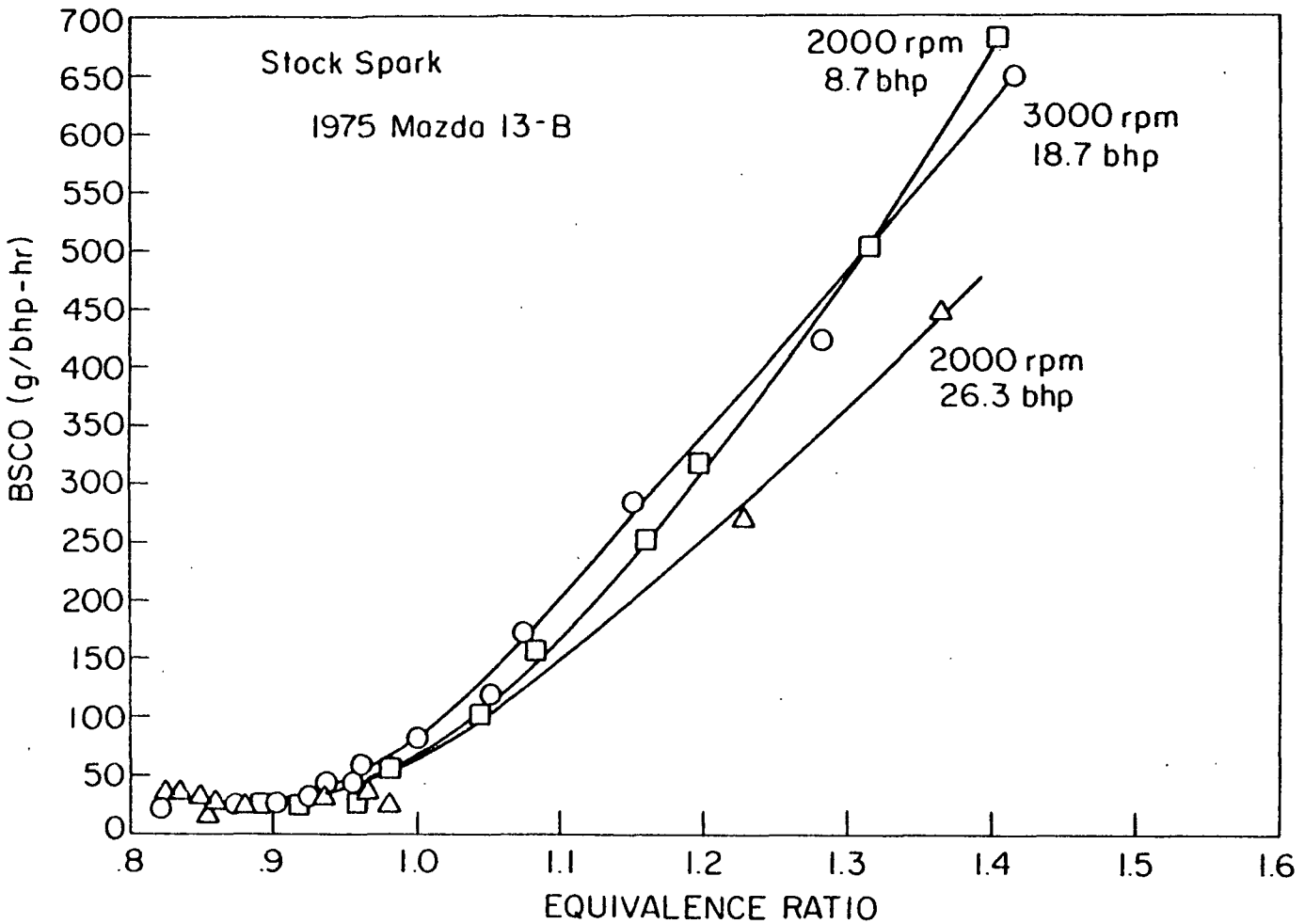

Figure 52. Brake specific carbon monoxide emissions as a function of equivalence ratio, Mazda 13-B engine, stock spark timing.

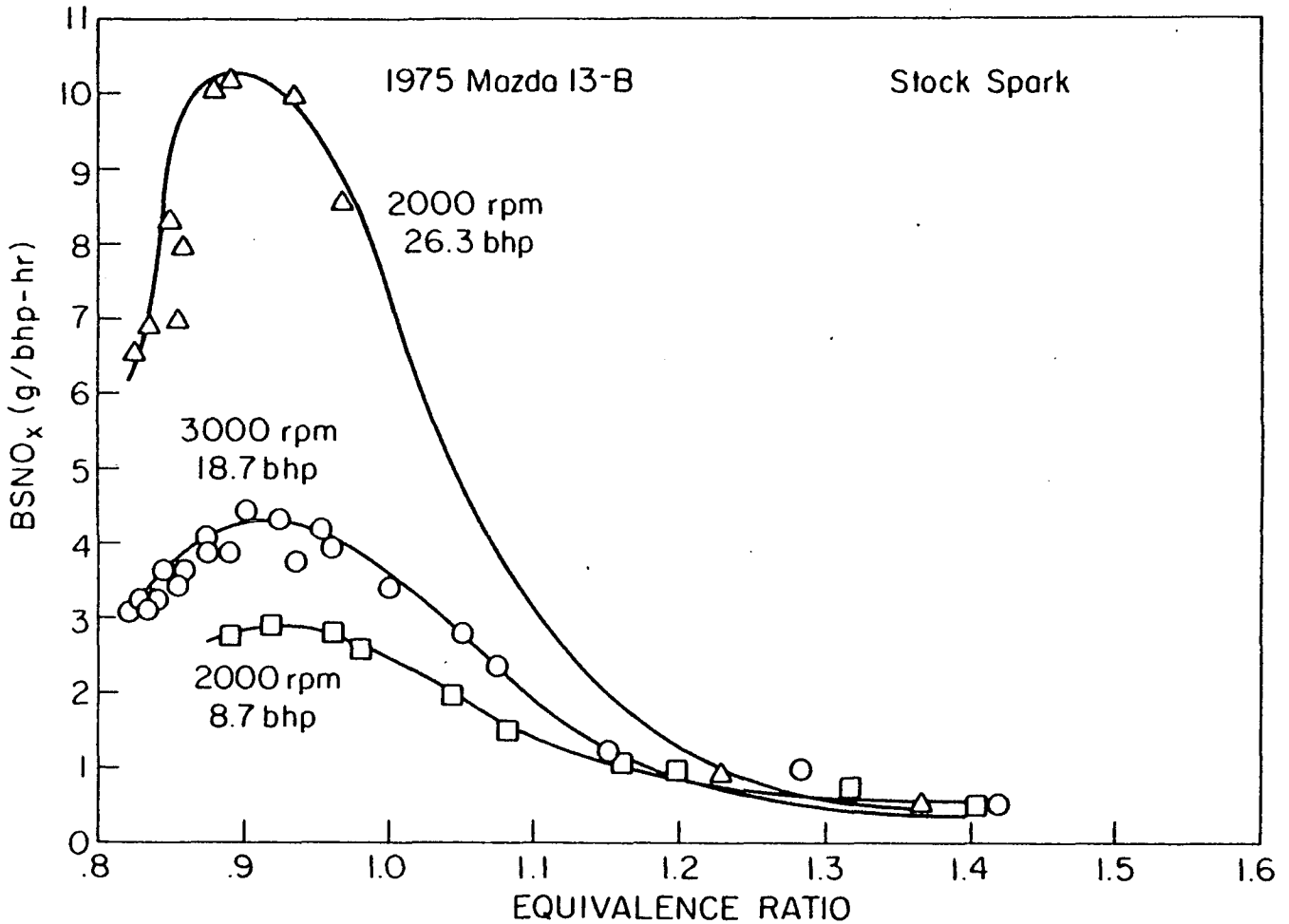

Figure 53. Brake specific nitrogen oxide emissions as a function of equivalence ratio, Mazda 13-B engine, stock spark timing.

F. EFFECT OF IGNITION TIMING ON FUEL CONSUMPTION AND EXHAUST EMISSIONS - MAZDA 13-B ENGINE

Two series of tests were conducted to ascertain the effect of ignition timing on fuel consumption and emission characteristics. The first series was conducted with a fixed air-fuel ratio, 16:1, which was relatively close to the LBT* setting for the Mazda engine. The second series was conducted with the stock mixture ratio as delivered by the production carburetor. Three test conditions were selected (identical to those used for the air-fuel ratio parametric tests), 2000 rpm with 8.7 and 26.3 bhp and 3000 rpm, 18.7 bhp.

1. Air-Fuel Ratio of 16:1

The data for the first series of tests at 16:1 air-fuel ratio are shown in Figs. 54-57. These illustrate brake specific fuel consumption, hydrocarbon, carbon monoxide and nitrogen oxides emissions as a function of ignition timing. The BSFC data, Fig. 54, shows that the thermal efficiency was relatively insensitive to ignition timing near the MBT spark timing. At the 2000 rpm, light load and 3000 rpm condition the BSFC increased greatly with significant spark retardation. In general the trend of the results is consistent with similar data for reciprocating engines although the Mazda appears to be less sensitive to ignition advance.

The BSHC emissions, Fig. 55, decreased with spark retard at all conditions. The major hydrocarbon reduction observed at 3000 rpm with spark retard was probably caused by enhanced thermal reaction both within the engine and in the exhaust collector due to an increase in gas temperature caused by spark retard. A slight increase in misfiring with spark advance may also have been present. To a limited extent these factors appear to be present at other conditions. Additional factors probably include changes in instantaneous combustion chamber surface/volume ratio which influence wall quenching and changes in combustion chamber pressure which affect the leakage contribution to total hydrocarbon emissions.

Brake specific CO emissions in Fig. 56 indicate little variation with ignition timing. The lean air/fuel ratio used produced the generally low level.

The BSNO$_x$ emissions in Fig. 57 are interesting in comparison to typical data observed in a spark-ignited reciprocating engine which generally exhibits decreased NO$_x$ emission with spark retard. The rotary engine data showed that there was relatively little influence of spark timing on NO$_x$ emissions. However a small increase was observed with spark retard. This behavior is probably caused by factors that increase maximum cycle temperature or reduce the effectiveness of the NO decomposition reaction rather than residence time factors. Slightly delayed (from optimum for best

*Leanest mixture for best torque.

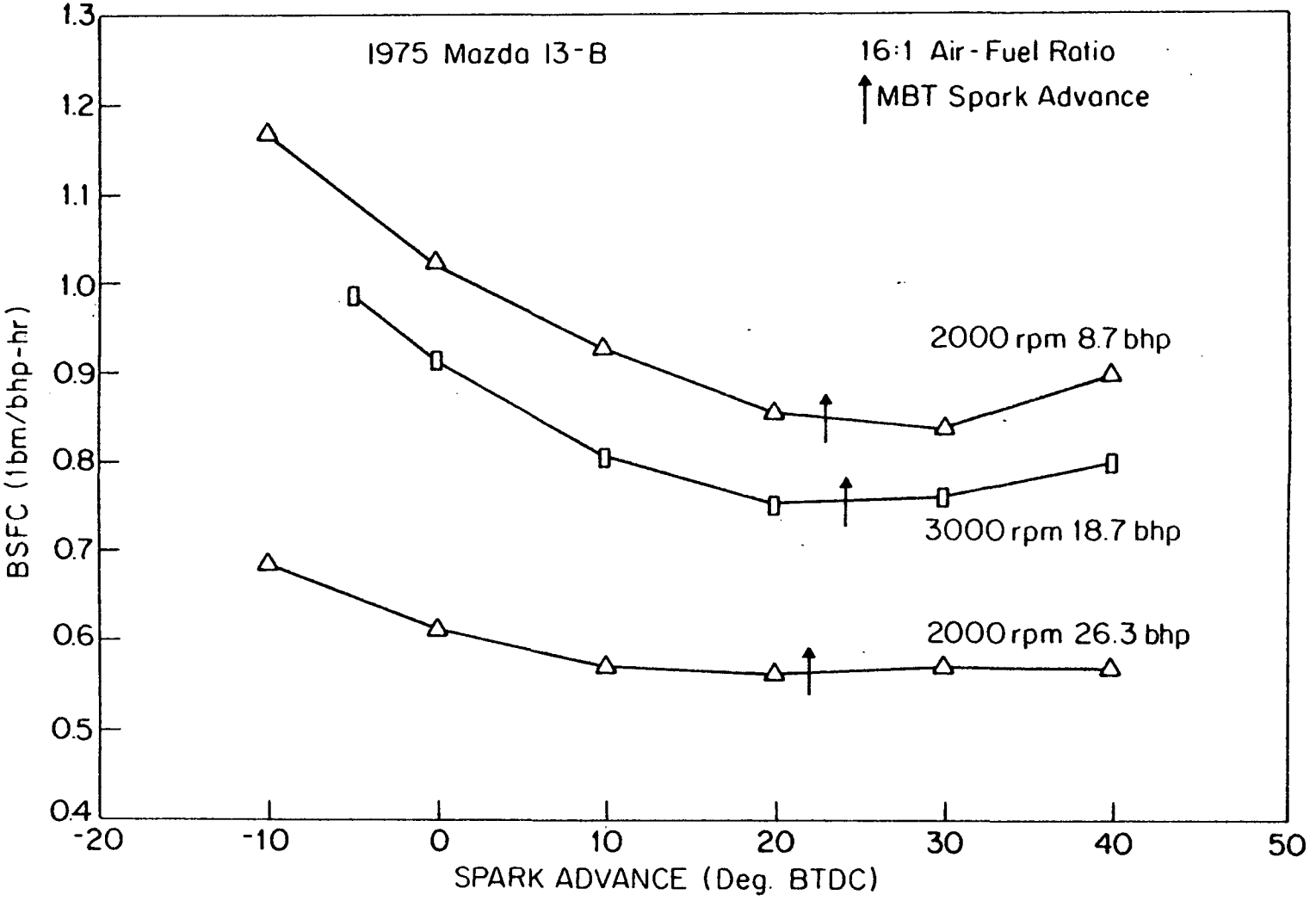

Figure 54. Brake specific fuel consumption as a function of spark advance, Mazda 13-B engine, 16:1 air-fuel ratio.

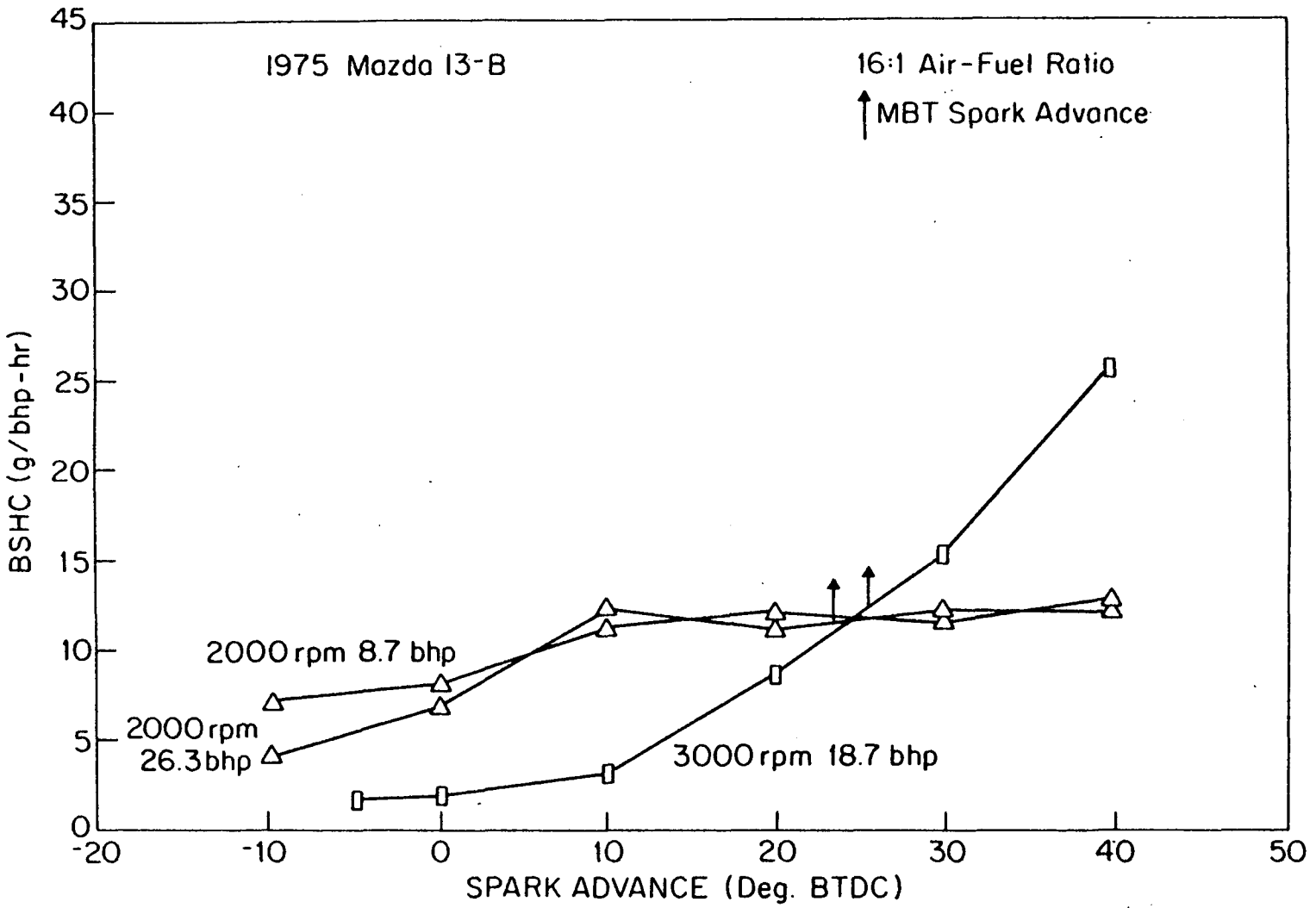

Figure 55. Brake specific hydrocarbon emissions as a function of spark advance, Mazda 13-B engine, 16:1 air-fuel ratio.

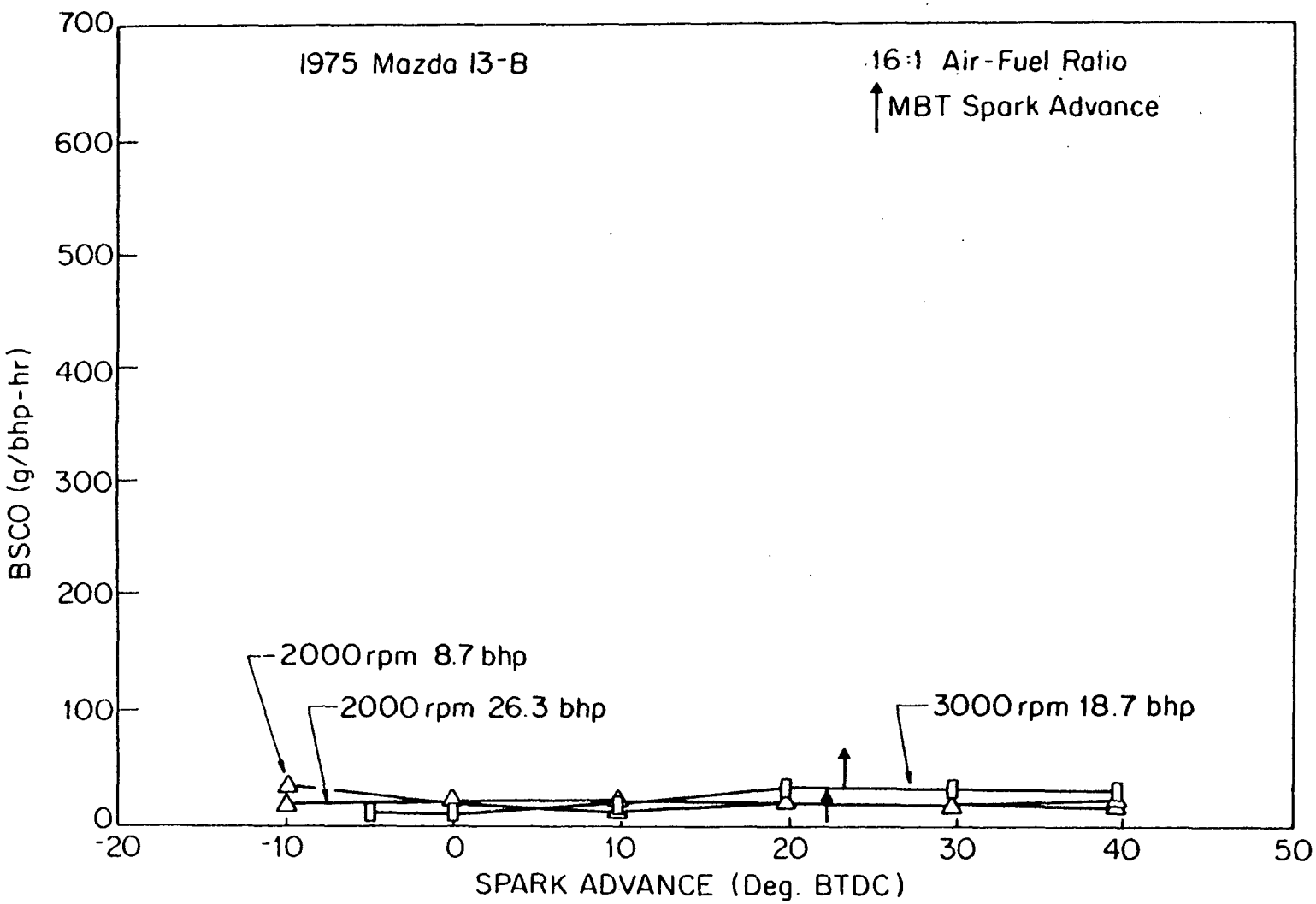

Figure 56. Brake specific carbon monoxide emissions as a function of spark advance, Mazda 13-B engine, 16:1 air-fuel ratio.

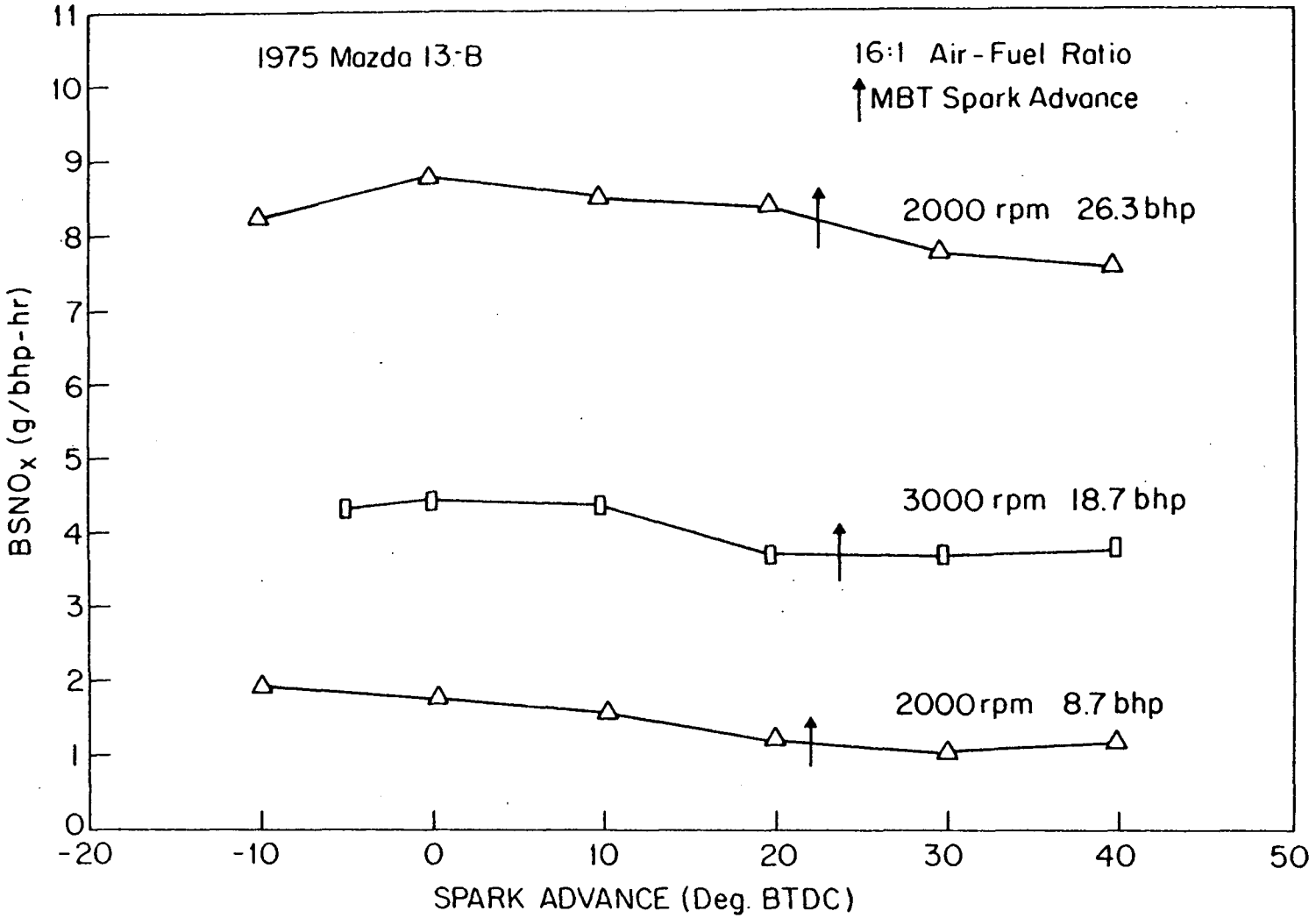

Figure 57. Brake specific nitrogen oxide emissions as a function of spark advance, Mazda 13-B engine, 16:1 air-fuel ratio.

BSFC) high temperature burning is suggested rather than additional burning late in the expansion or exhaust processes. An additional factor in the slight NO_x increase is the increase in engine air and fuel flow required to maintain a constant horsepower with spark retard. However, without a detailed study this analysis is speculative. The relative position of the curves follow the expected trend based on the BSFC results. The relatively poor combustion at 2000 rpm light load is characterized by a reasonably low overall level of NO_x emissions whereas the higher load 2000 rpm point is considerably more efficient resulting in higher levels of NO_x emissions. It was anticipated that spark retardation would significantly reduce the NO_x emissions and these observations to the contrary suggest spark retard to be an ineffective control strategy for NO_x.

2. Stock Air-Fuel Ratio

The second series of tests was conducted at the same speeds and loads but with the stock carburetion. The BSFC results are shown in Fig. 58, and are similar to those of the leaner mixture studies. However, as expected the curves were displaced to a greater BSFC level because of the richer mixtures.

The hydrocarbon emission data in Fig. 59 was also displaced vertically from the data at a leaner mixture. In addition there was an apparent diminished after-reaction of hydrocarbons with spark retard that was particularly evident at the 3000 rpm test condition with 16:1 air-fuel ratio. This arose because the mixture was too rich to permit reaction in the exhausting chamber and exhaust collector (limited O_2 availability). Hence spark retardation exhibited relatively little influence on the hydrocarbon emission level.

Brake specific CO emissions are shown in Fig. 60 for the stock carburetion. These data clearly demonstrate that there is essentially no influence of spark timing on this pollutant. The major factor was the higher CO arising from richer combustion as is evidence by the vertical displacement of the curves in comparison to the data at 16:1 air-fuel ratio.

The brake specific NO_x emissions are shown in Fig. 61. The results appear to be consistent with established theory in that they are generally displaced lower than for the data with 16:1 air-fuel ratio. The 2000 rpm, 8.7 hp data were not included because they were in error and were impossible to recheck. The general increase of the NO_x emissions with spark retardation is generally unexpected as noted earlier. In any event the influence of spark retardation appears to be far less signification than observed in a reciprocating engine in which spark retard effectively reduces NO_x.

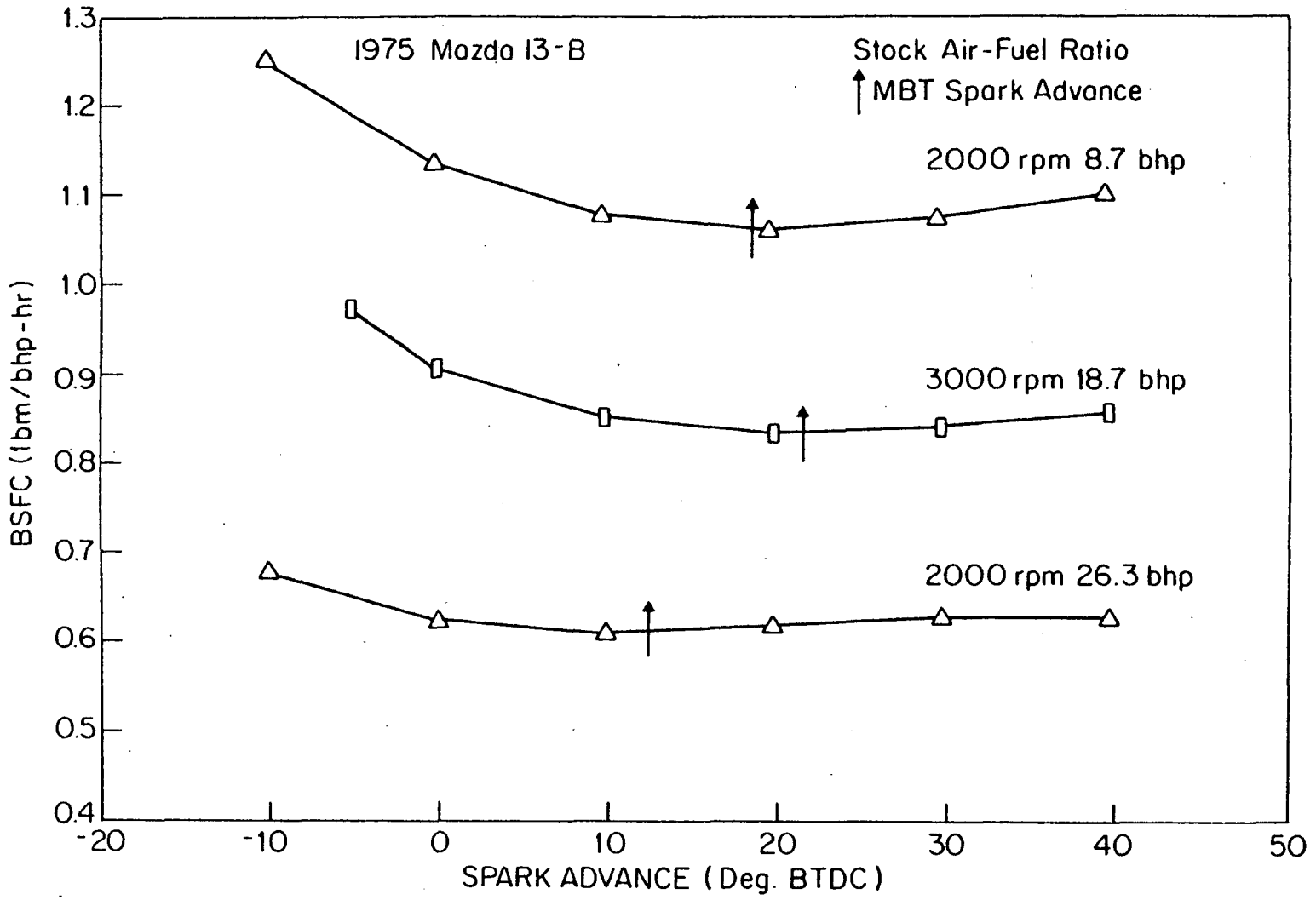

Figure 58. Brake specific fuel consumption as a function of spark advance, Mazda 13-B engine, stock air-fuel ratio.

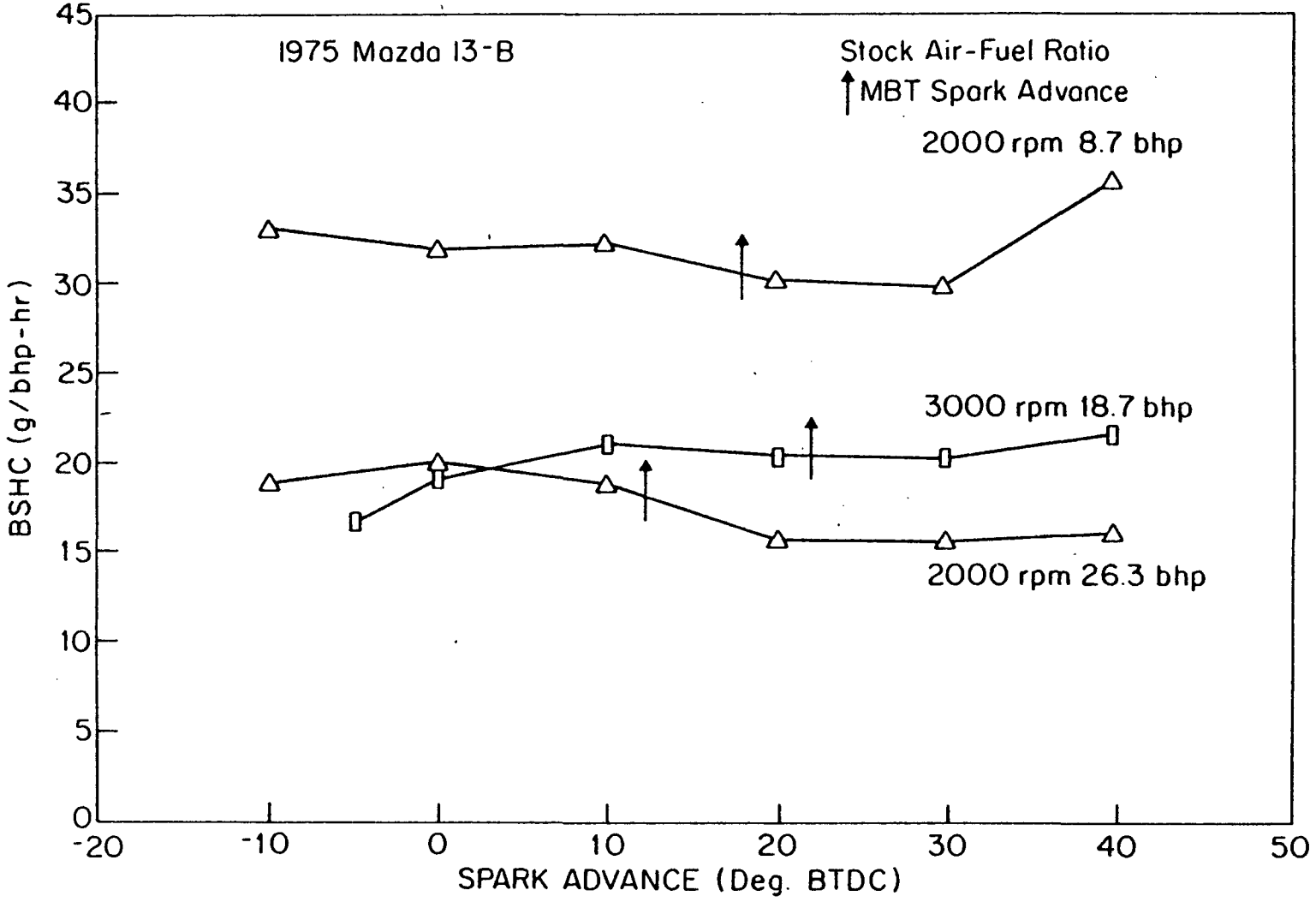

Figure 59. Brake specific hydrocarbon emissions as a function of spark advance, Mazda 13-B engine, stock air-fuel ratio.

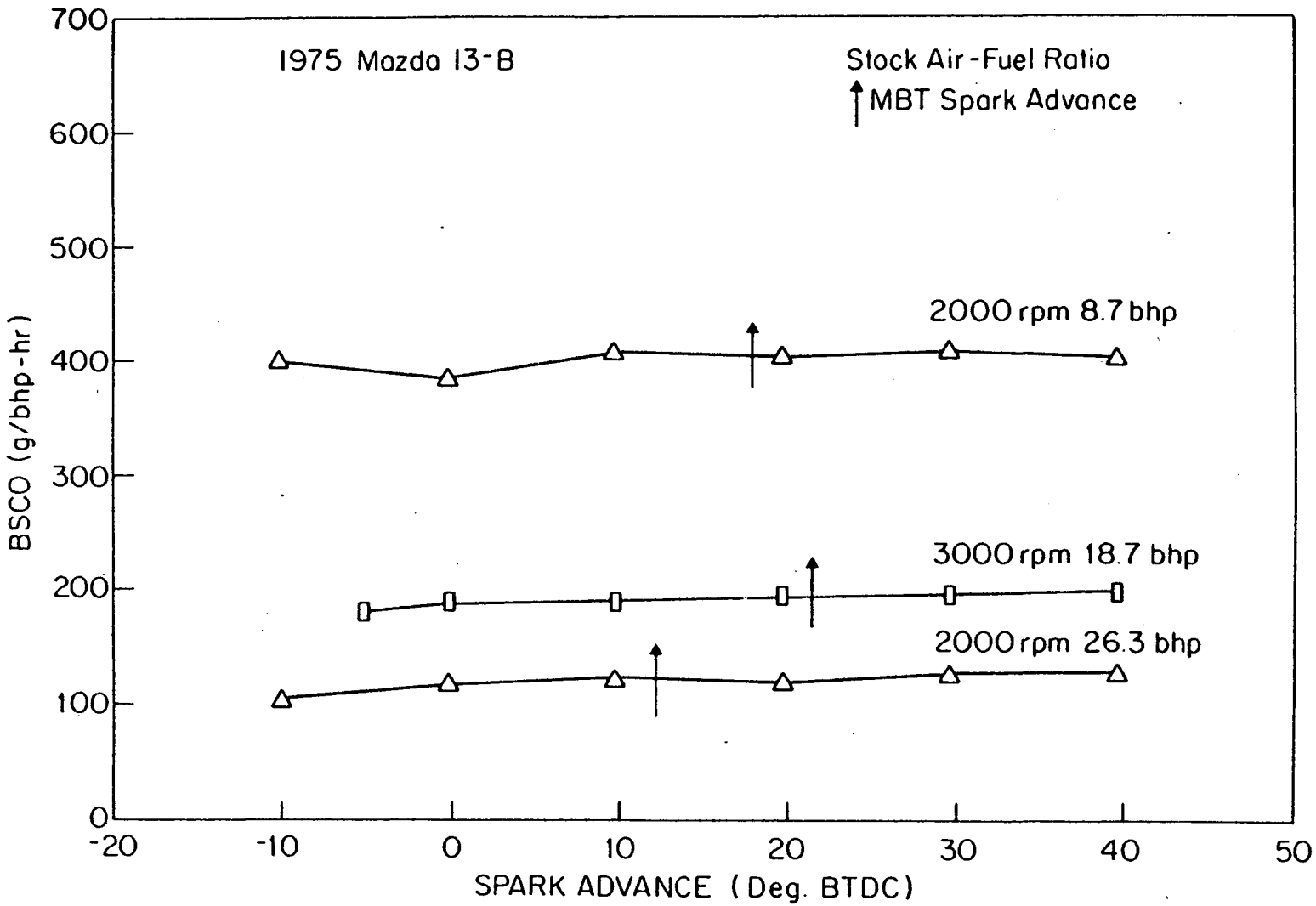

Figure 60. Brake specific carbon monoxide emissions as a function of spark advance, Mazda 13-B engine, stock air-fuel ratio.

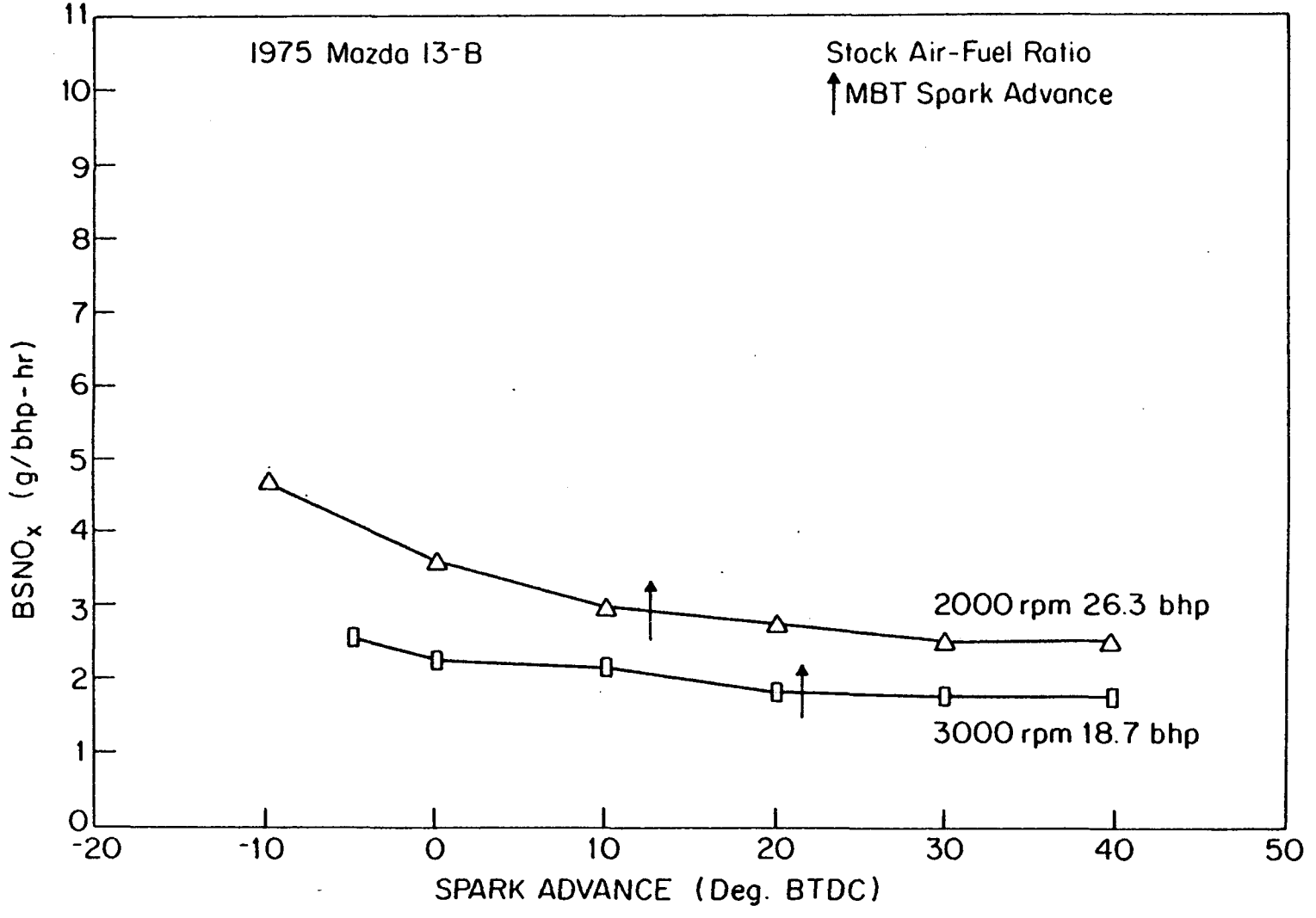

Figure 61. Brake specific nitrogen oxide emissions as a function of spark advance, Mazda 13-B engine, stock air-fuel ratio.

It is perhaps appropriate here to make several general observations related to the effect of ignition timing on combustion and therefore fuel consumption and emission performance of the Mazda engine. The measured performance parameters were generally found to be far less sensitive to variation in timing than in reciprocating engines. The major reason behind this behavior is the shape of chamber volume during the combustion phase of the cycle. The mixture burns relatively slow (low turbulence) until the combustion chamber approaches its minimum volume, TDC, position. At this point the volume of the leading portion of the chamber begins to increase rapidly and a commensurate shrinkage occurs in the trailing to leading section. This increased mixture motion greatly accelerates the burn rate. A relatively wide variation in ignition timing during the "slow burn or low turbulence" portion of the combustion cycle, (before TDC) would therefore be expected to have little influence on the total combustion process and consequently a limited effect on fuel consumption and emissions.

G. SPATIAL DISTRIBUTION STUDIES OF THE HYDROCARBON AND CARBON MONOXIDE EMISSIONS FROM THE MAZDA ENGINE

These tests were conducted to gain some inference as to the internal engine sources of hydrocarbon emission in the rotary engine. The unburned hydrocarbons were the focus of this fundamental emission source study because they have been the most difficult emission to control from this engine.

The exhaust hydrocarbon emissions of the rotary engine are a result of several processes which are also important in the conventional 4-stroke engine(14,15). These common processes, and how they apply particularly to this engine are outlined below:

Wall Quenching - An important emission source results from the well known but little understood wall quenching phenomena. As the propagating flame front approaches the relatively cool chamber wall, it is extinguished or quenched a finite distance from the wall. This so-called "quench zone" retains raw fuel-air mixture, partially burned and/or cracked fuel, carbon monoxide, and other less noxious products. During the exhaust process some of these "quench zone" products are scavenged from the chamber walls and released to the atmosphere, and some remain to be partially burned on the succeeding cycle.

This emission source is particularly significant in the rotary engine for two basic reasons.

- This engine has a relatively high surface/volume ratio in the combustion chamber and thus, a large quench zone volume. This contribution may be partially compensated by higher wall temperatures resulting from the localization of combustion in one housing quadrant. The schematic of the engine combustion cycle shown in Fig. 62 illustrates the geometric factors involved.

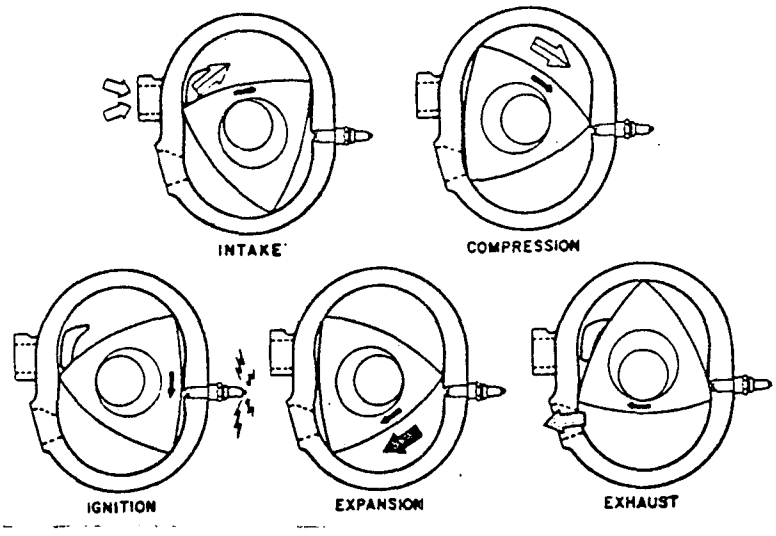

Figure 62. Schematic diagram of rotary engine operating cycle.

.The trailing apex seal of a given rotating combustion chamber "scrapes" the quench layer off the rotor housing and into the peripheral exhaust port.

Crevice Effect or Gap Quenching - The second source arises from another "quench" process. In this case, if two relatively cool surfaces enclosing a fuel-air mixture are brought progressively closer together, a certain separation distance (quench distance) will be reached beyond which a flame will not propagate. The mass contained in this quench region or "dead volume" consists of a high-percentage of fuel-air mixture and, therefore, has an extremely high concentration of unburned hydrocarbons. Where significant crevices exist unburned hydrocarbon emissions are large.

The present configuration of the rotary engine has substantial "dead volume" including:

.The volume radially beyond the side gas seal between the rotor and side housing.

.The leading and trailing portions of the rotor surface at those phases of the cycle where they approach close to the rotor housing.

Blowby of Unburned Charge - Leakage of unburned mixture to the atmosphere can also affect the emissions significantly. Even a small percentage loss of unburned mixture can have a large effect on the overall concentration of hydrocarbons in the exhaust.

A conventional four-stroke cycle automotive engine blowby loss is to the crankcase and only a very small portion of unburned mixture if any, is lost past the closed exhaust valve and during the valve overlap period. The rotary engine blowby leakage loss to the crankcase is zero with side intake ports since all side gas seal leakage is automatically vented to the intake ports. The leakage of raw

mixture past the leading apex seal, however, passes directly through the exhaust port into the exhaust system. Further, if a peripheral inlet port configuration were to be used, unburned mixture could be lost during the unavoidably higher port overlap period. Mixture leakage is probably the single most significant source of hydrocarbon emissions in the rotary engine depending on the design and conditions of the sealing system. High exhaust oxygen concentration even with rich mixture combustion and no air injection is evidence of a leakage problem.

Incomplete Combustion - Incomplete combustion may be a source of hydrocarbon emissions, particulary with very rich or lean fuel-air mixtures and/or poor mixing of the fuel and air. This problem is intensified where exhaust residual is high as it is at light-load conditions. This factor may not be of primary importance because the rotary engine operates reasonably well on lean mixtures and has intense combustion chamber turbulence in the leading portion of the chamber. Turbulence promotes complete combustion. However, some evidence of incomplete combustion in the more quiescent trailing section of the chamber has been provided by high-speed movies.

Unfortunately it is impossible to "ride" with engine rotor and quantify the true source of the hydrocarbon emissions. Instrumentation and other hardware complexities have prevented use of a timed sampling valve in the engine combustion chamber to obtain spatially resolved emission data. However, evidence of the hydrocarbon formation in the combustion chamber can be obtained from the exhaust since it was believed that relatively little mixing occurs in the engine after combustion and during expansion and exhaust. The spatial distribution present during the hydrocarbon formation processes may be qualitatively present in the exhaust as it leaves the engine. Hence a program was developed to determine the spatially resolved hydrocarbon content in the exhaust. For this a specially constructed exhaust pipe was built. Two different methods were tried.

.Cox timed sampling valve
.Series of steady-state sampling probes

Unfortunately neither of these techniques permit an exact evaluation of the hydrocarbon sources since several of the sources can affect the same region of the engine chamber. For example it is impossible to discriminate between hydrocarbons leaking past the leading apex seal of one chamber into the trailing portion from incomplete flame propagation in this region. However, knowledge of the region of the chamber most responsible for the high emissions could assist the engine designer.

1. Sampling Valve Study

In this series of tests the Cox sampling valve, discussed in the Instrumentation section, was used to withdraw a small fraction

of the exhaust sample in a specially constructed exhaust system near the exhaust port. Similar studies have been reported on reciprocating engines (16). The sample was withdrawn at known times with respect to the crankshaft position and thus the position of the rotor. The data are presented as a function of crank angle relative to the start of exhaust the process. Zero degrees is the point where a given engine chamber begins the exhaust process. The fluid mechanics in the engine exhaust system are substantially different from a 4-stroke reciprocating engine. In the rotary engine the exhaust flow never ceases for a substantial crank interval as it does in a reciprocating engine. In fact, exhaust flow is occurring from two engine chambers to (or back flow) the exhaust system during the period the apex seal is traversing the port. The total exhaust process for a given chamber occupies 360 crankshaft degrees in the rotary engine. The hydrocarbon concentration emissions are plotted as parts per million (ppm) of n-hexane as a function crank angle. Carbon monoxide emissions were also measured and plotted as a function of crank angle. Numerous test conditions were evaluated, 2000 rpm, 8.8 and 14.2 bhp, 2500 rpm, 13 and 22.4 bhp and 3000 rpm, 18.7 and 34.3 bhp. Both hydrocarbon and CO data corresponding to these test conditions are plotted in Figs. 63-74. In several cases multiple sets of data were collected to assess repeatability. Since it has been hypothesized that the principal sources of unburned hydrocarbon emissions from the rotary engine are: (a) exhaust of the quench layer volume associated with the large surface/volume ratio, (b) leakage of unburned fuel past the leading apex seal of a given combustion chamber to the preceding chamber which is in the exhaust mode, and (c) incomplete flame propagation both in the trailing and leading regions of a given chamber and since they may affect the same region of the chamber, it was not possible to discriminate as to the distribution of sources. The CO emissions are not significantly affected by these factors other than that with the reduced combustion of the fuel, a lower CO concentration should be evident. The local CO is essentially a function of the local mixture ratio in the engine chamber. A significant variation in CO data as a function of sample position in the exhaust would have been indicative of mixture stratification in the engine. This did not occur however.

The results of the study generally followed similar trends for the various test conditions, with one exception at 2000 rpm, 8.8 bhp. All results were characterized by hydrocarbon peaks at the beginning and/or end of a given "slug" of exhaust.

The hydrocarbon emissions while initially high rapidly decreased to a level less than 1000 ppm which in turn was followed by a relatively rapid increase to the original level. Several anomalies were observed in the data. At 2000 rpm, 14.2 bhp, the hydrocarbon increase near the tail of the exhaust sample began near the center of the exhaust process (180 crankangle degrees), and increased almost linearly to the maximum reading at 360°. At 2500 rpm, 13 bhp, the decrease in hydrocarbons occurred later and

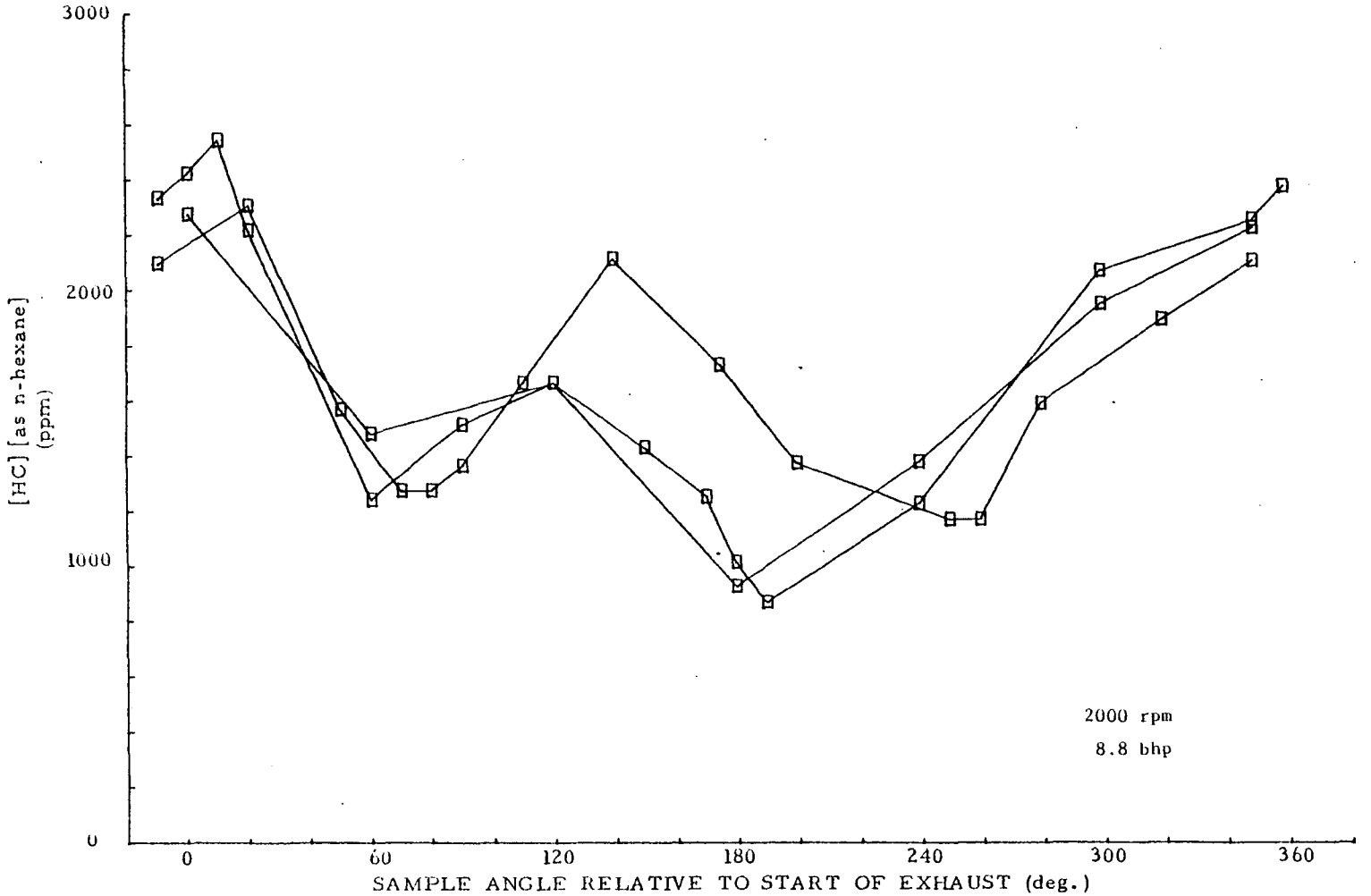

Figure 63. Exhaust hydrocarbon concentration as a function of crank angle relative to the start of the exhaust process, Mazda 13-B engine, 2000 rpm, 8.8 bhp. Data obtained with a Cox timed sampling valve.

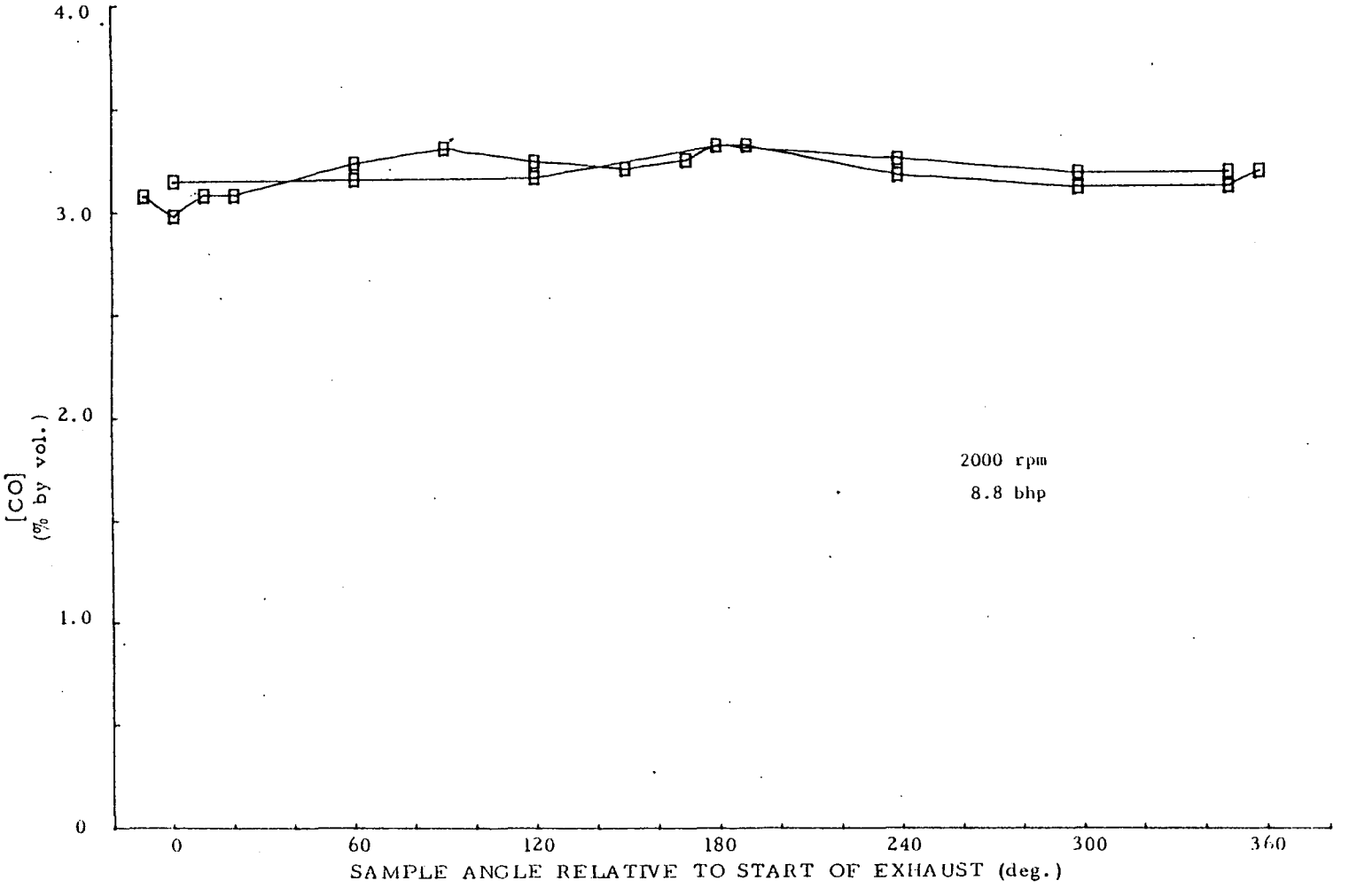

Figure 64. Carbon monoxide concentration as a function of crank angle relative to the start of the exhaust process, Mazda 13-B engine, 2000 rpm, 8.8 bhp. Data obtained with a Cox timed sampling valve.

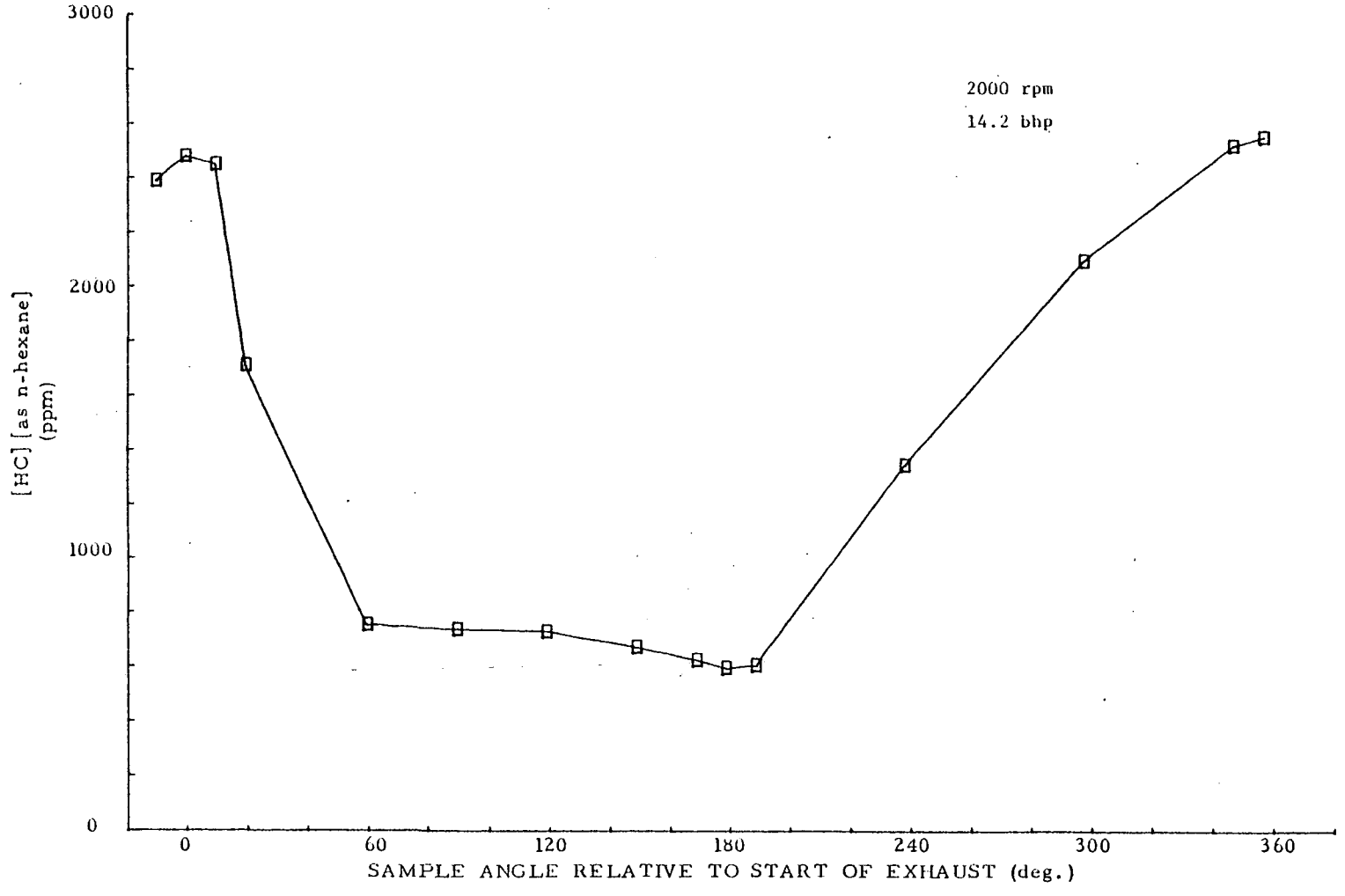

Figure 65. Exhaust hydrocarbon concentration as a function of crank angle relative to the start of the exhaust process, Mazda 13-B engine, 2000 rpm, 14.2 bhp. Data obtained with a Cox timed sampling valve.

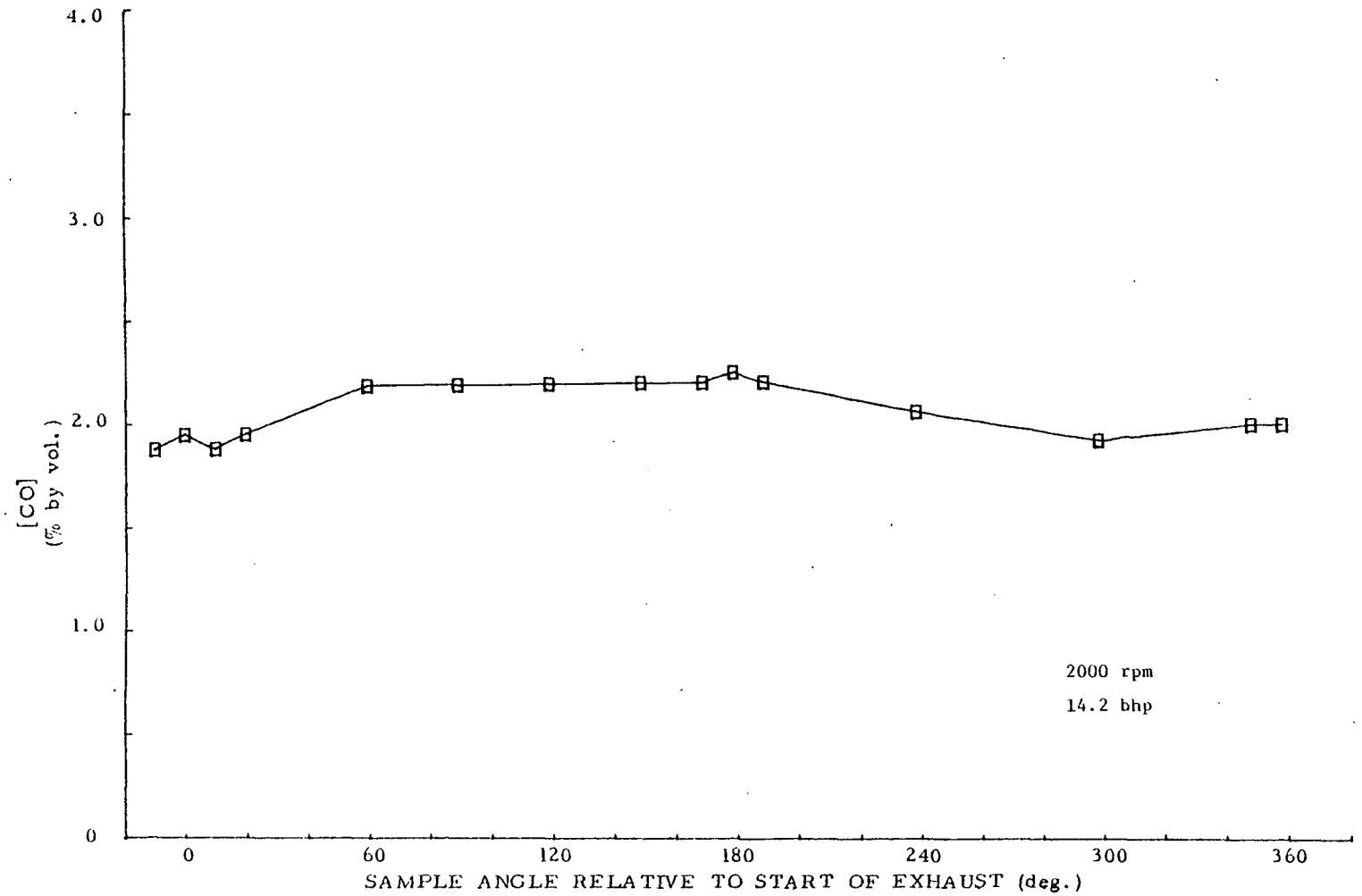

Figure 66. Carbon monoxide concentration as a function of crank angle relative to the start of the exhaust process, Mazda 13-B engine, 2000 rpm, 14.2 bhp. Data obtained with a Cox timed sampling valve.

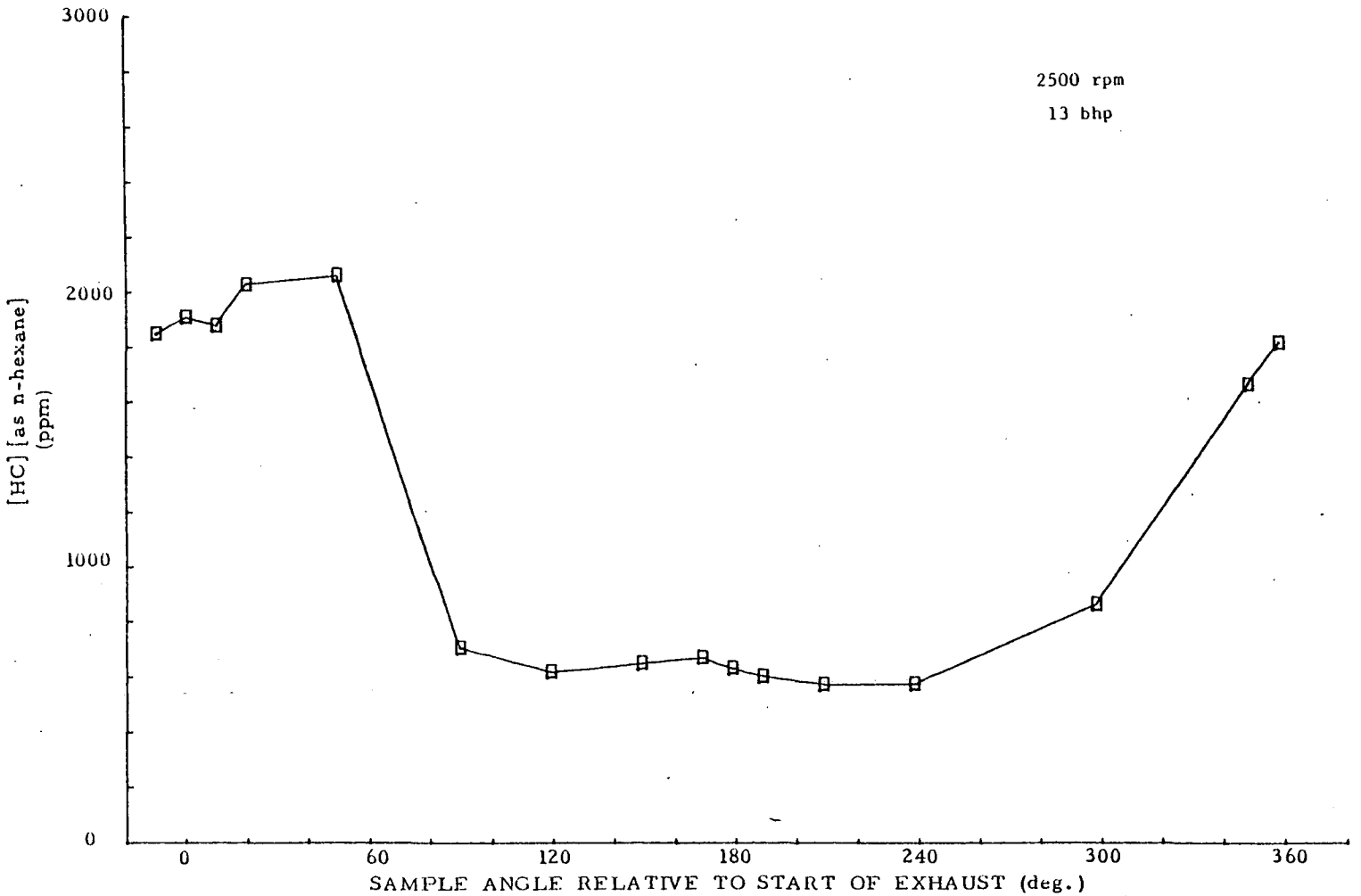

Figure 67. Exhaust hydrocarbon concentration as a function of crank angle relative to the start of the exhaust process, Mazda 13-B engine, 2500 rpm, 13 bhp. Data obtained with a Cox timed sampling valve.

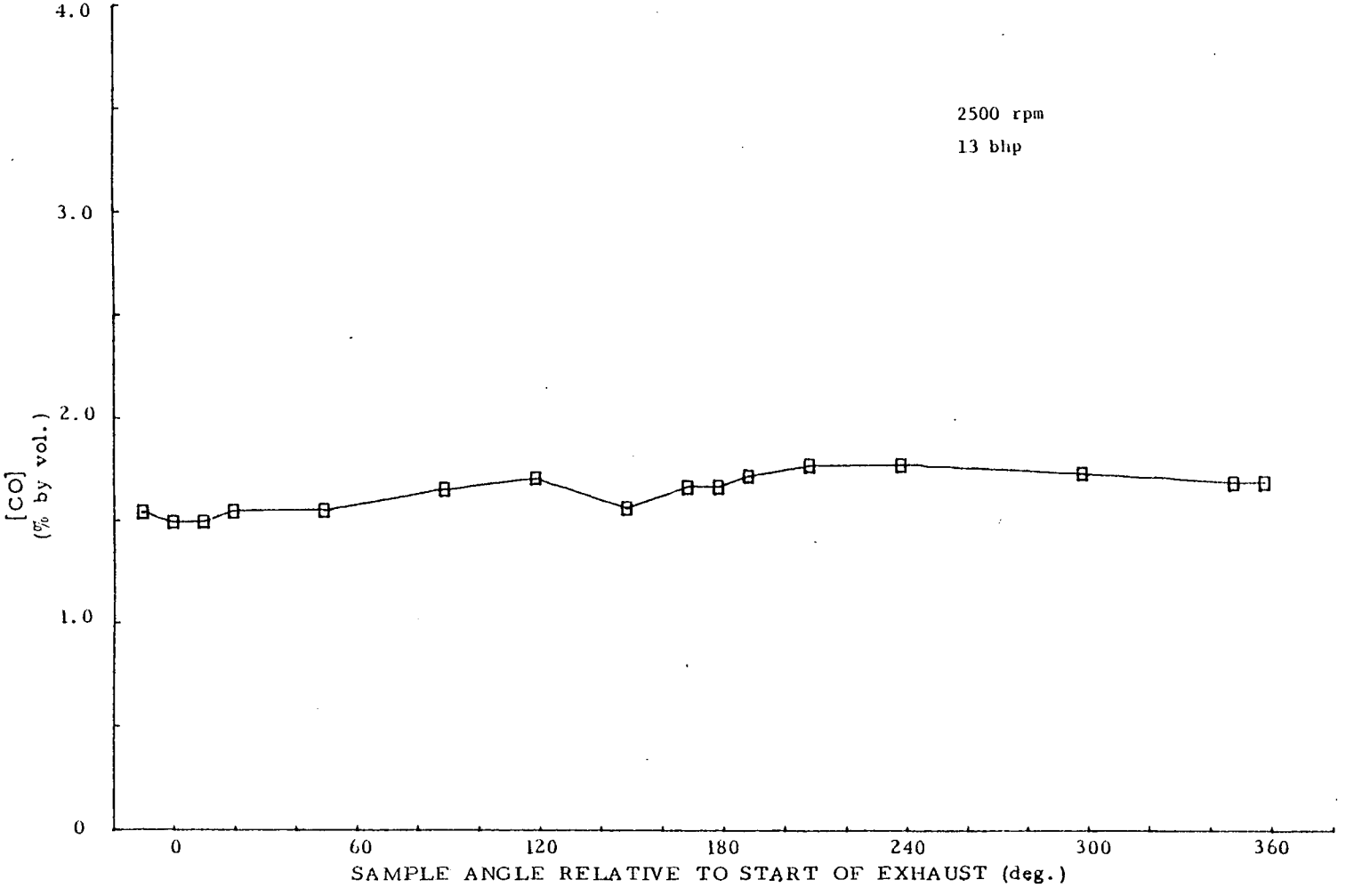

Figure 68. Carbon monoxide concentration as a function of crank angle relative to the start of the exhaust process, Mazda 13-B engine, 2500 rpm, 13 bhp. Data obtained with a Cox timed sampling valve.

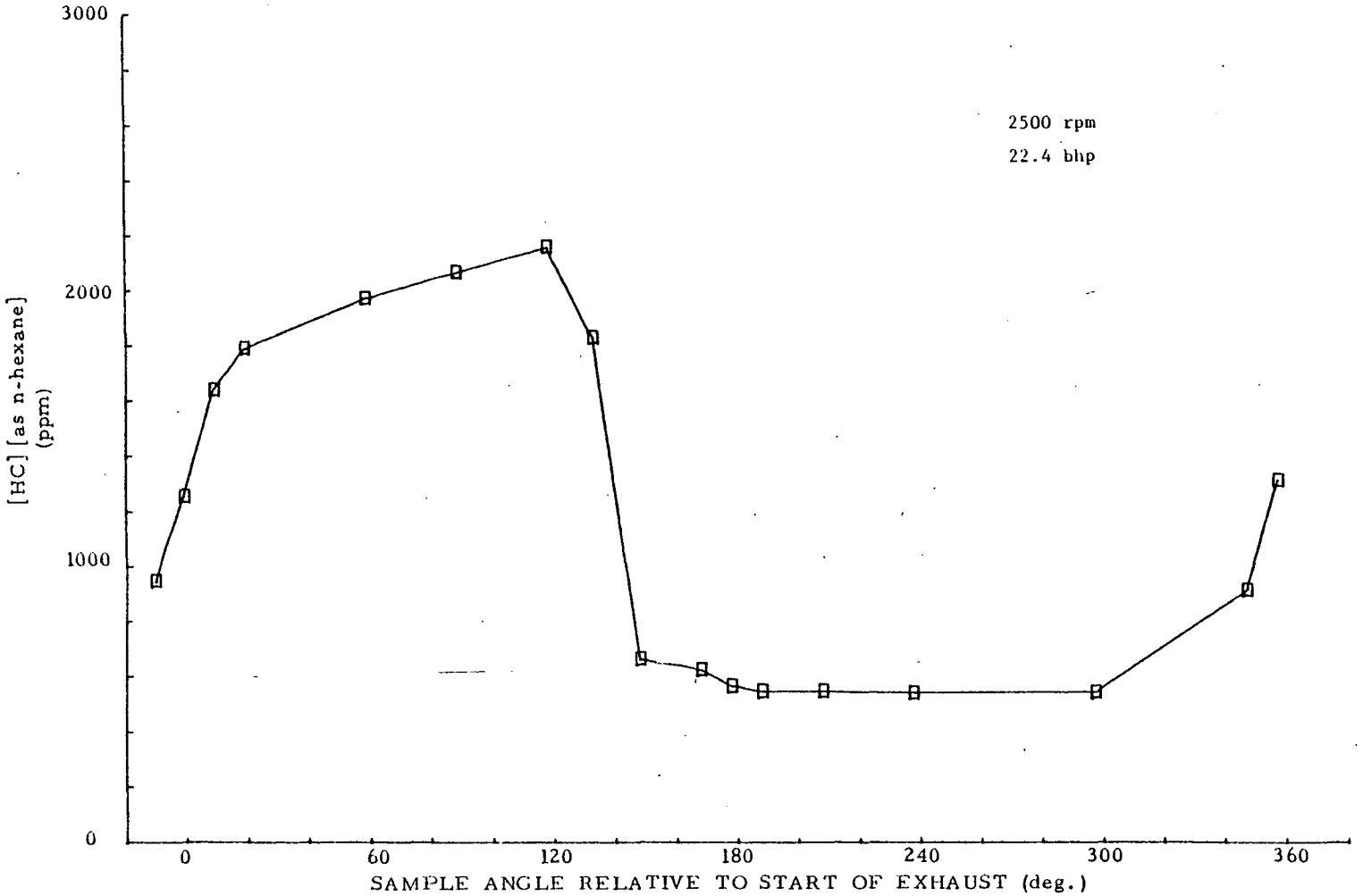

Figure 69. Exhaust hydrocarbon concentration as a function of crank angle relative to the start of the exhaust process, Mazda 13-B engine, 2500 rpm, 22.4 bhp. Data obtained with a Cox timed sampling valve.

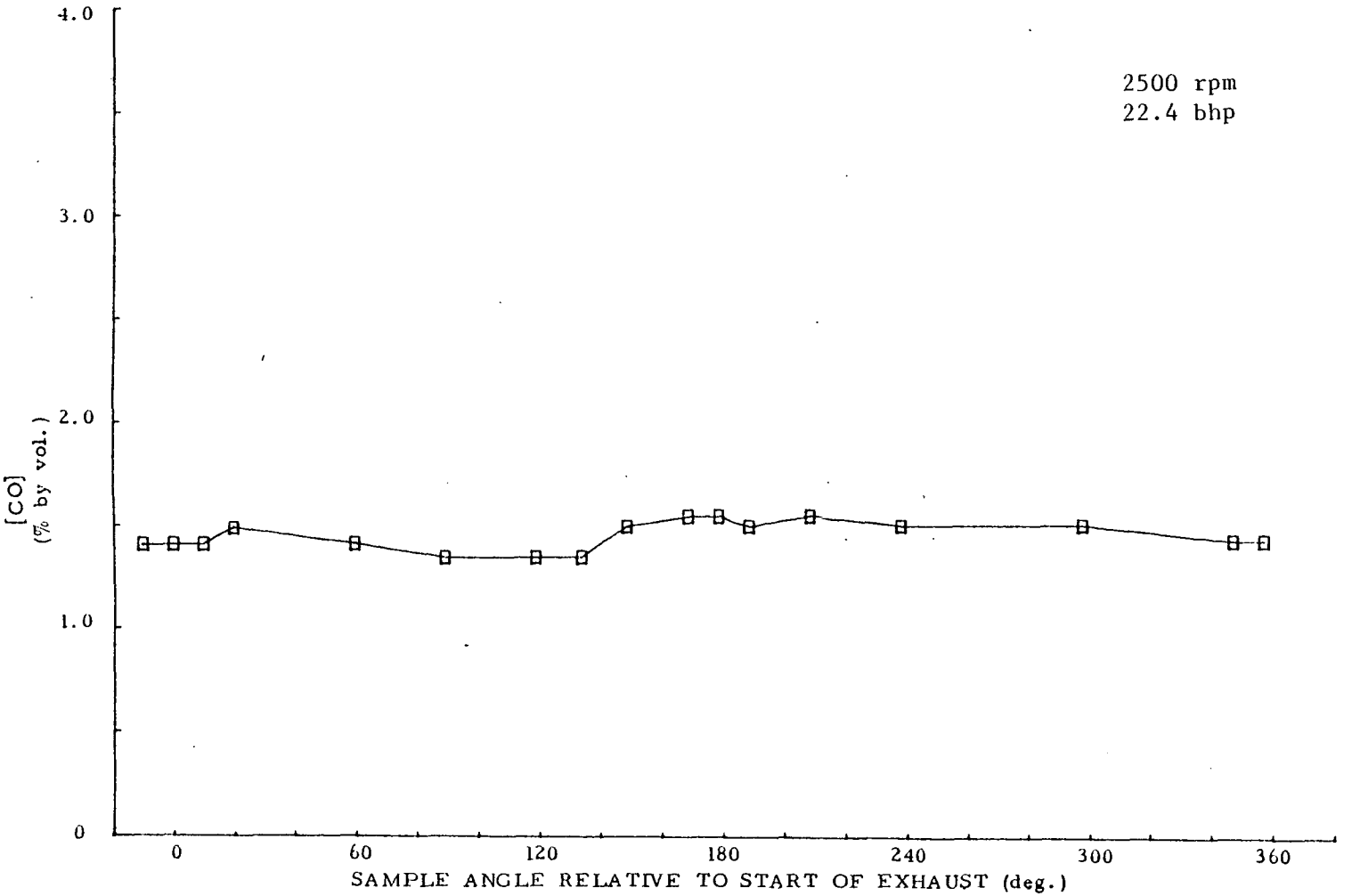

Figure 70. Carbon monoxide concentration as a function of crank angle relative to the start of the exhaust process, Mazda 13-B engine, 2500 rpm, 22.4 bhp. Data obtained with a Cox timed sampling valve.

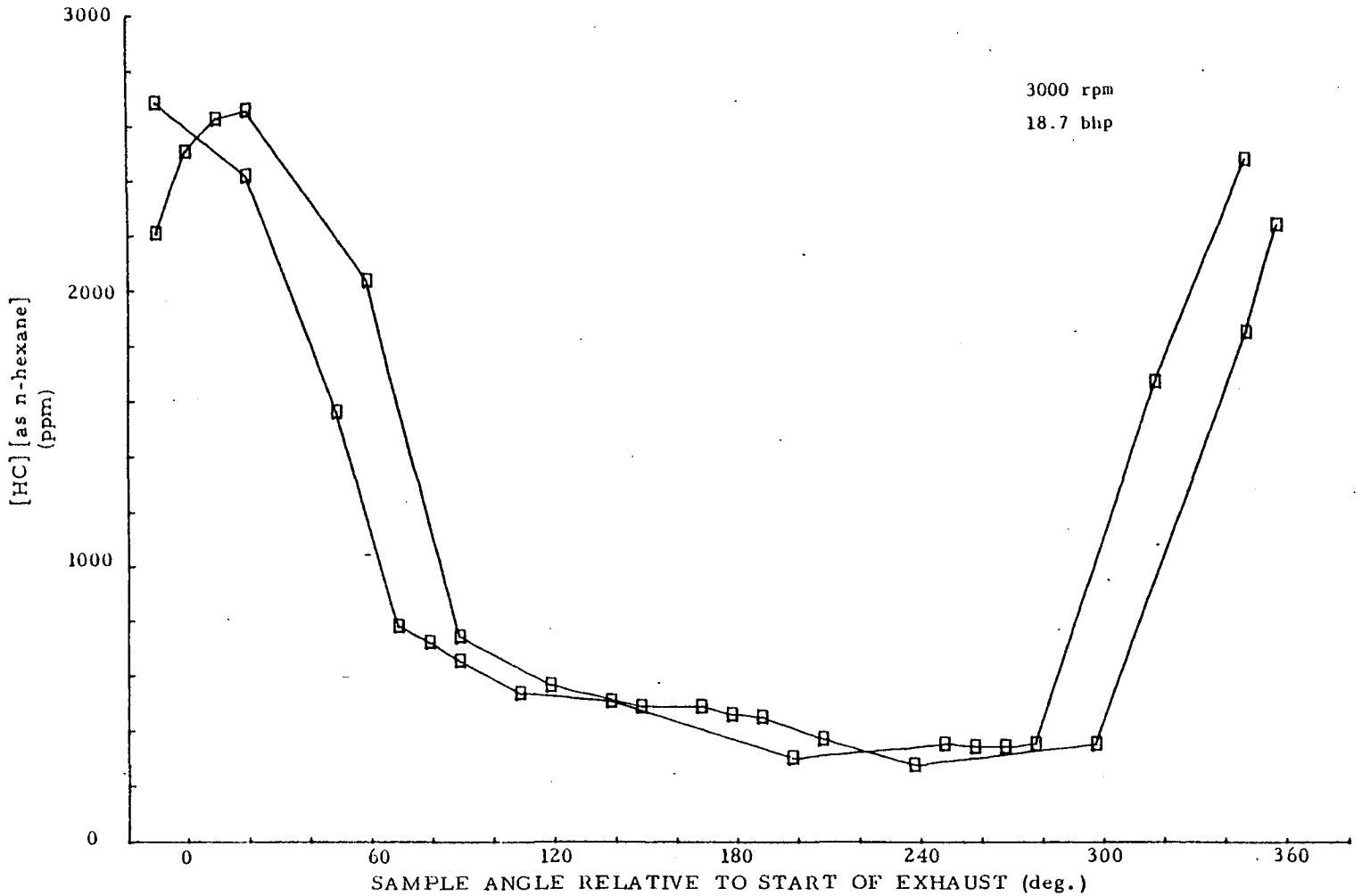

Figure 71. Exhaust hydrocarbon concentration as a function of crank angle relative to the start of the exhaust process, Mazda 13-B engine, 3000 rpm, 18.7 bhp. Data obtained with a Cox timed sampling valve.

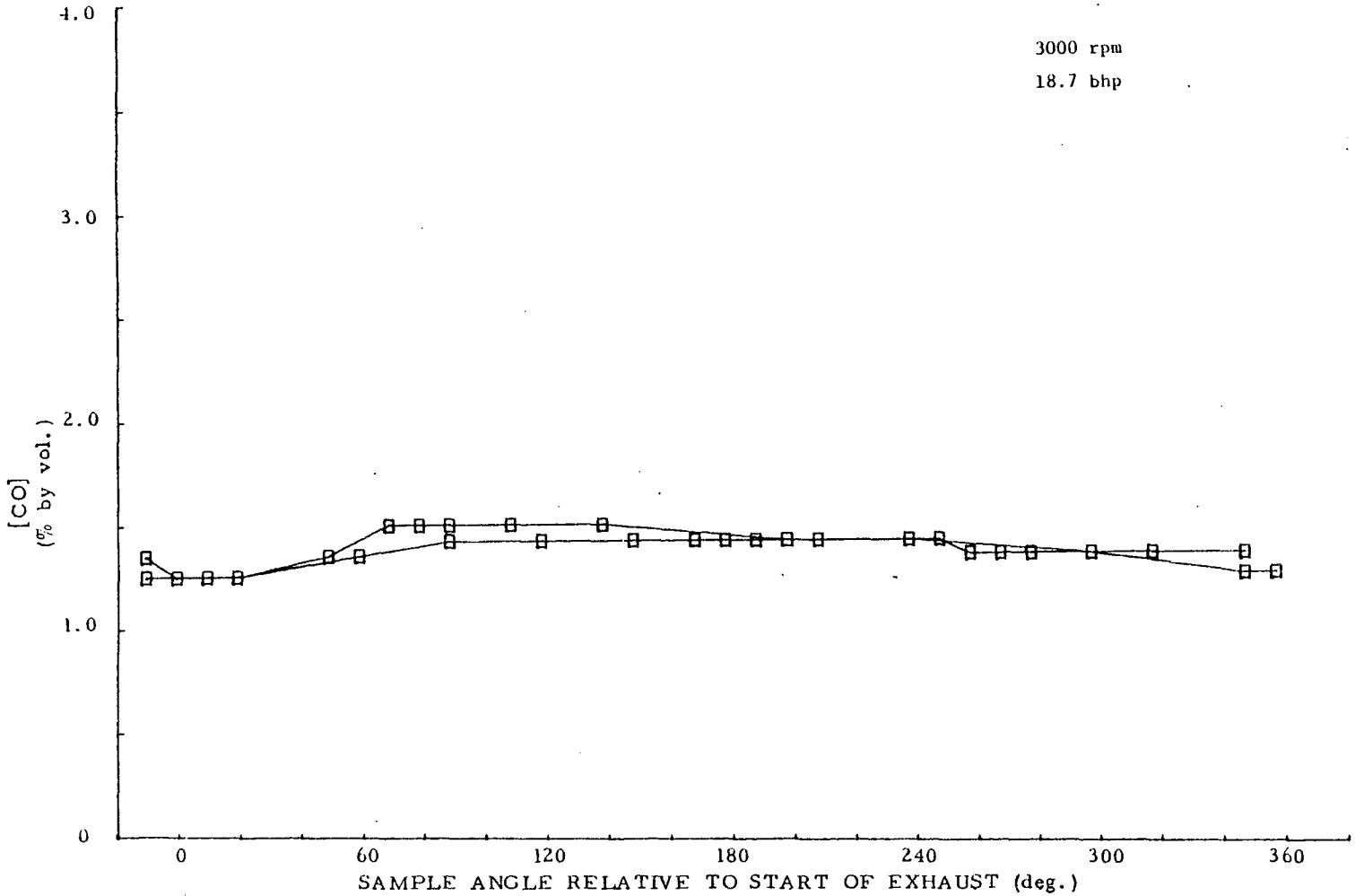

Figure 72. Carbon monoxide concentration as a function of crank angle relative to the start of the exhaust process, Mazda 13-B engine, 3000 rpm, 18.7 bhp. Data obtained with a Cox timed sampling valve.

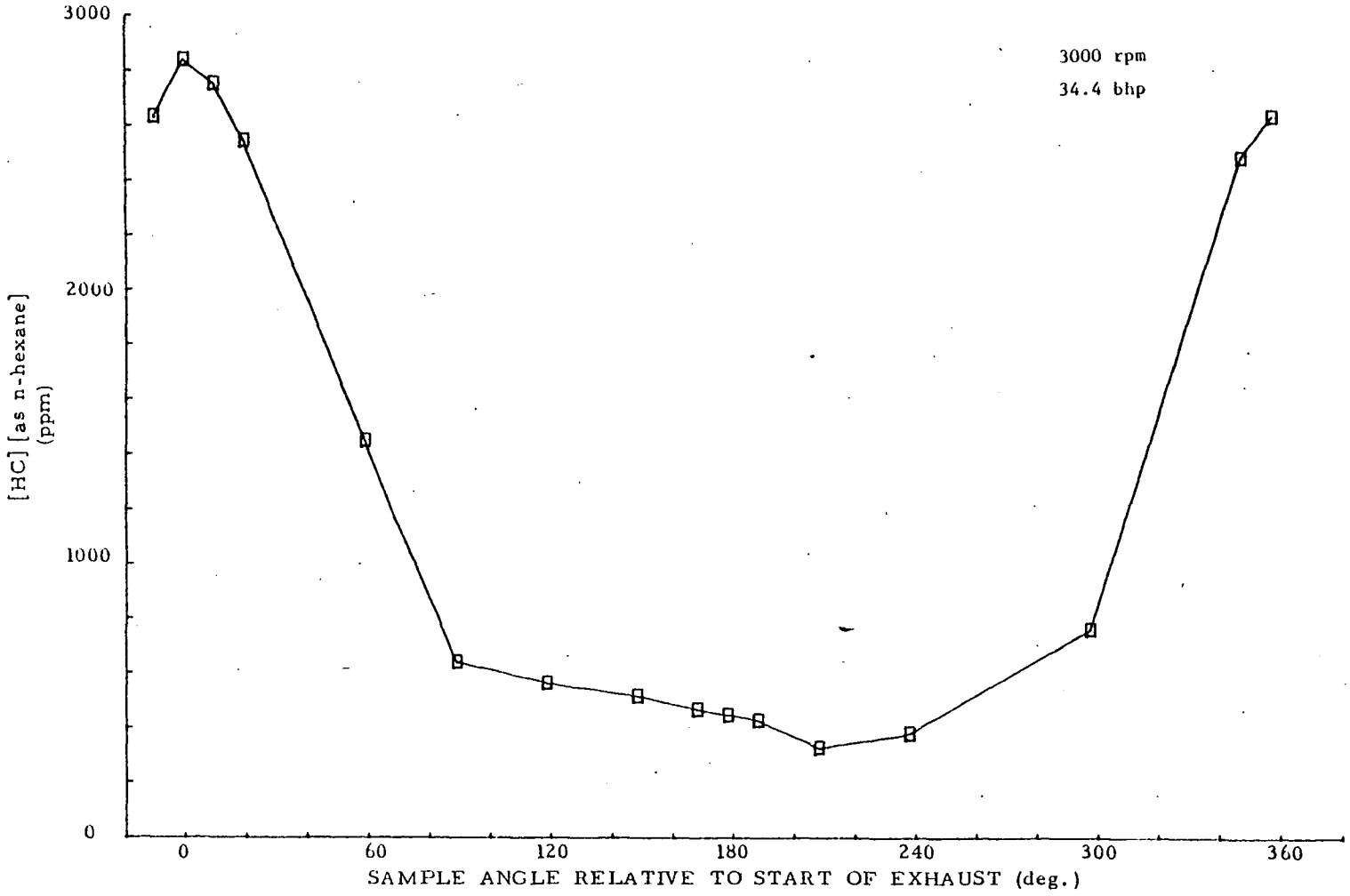

Figure 73. Exhaust hydrocarbon concentration as a function of crank angle relative to the start of the exhaust process, Mazda 13-B engine, 3000 rpm, 34.3 bhp. Data obtained with a Cox timed sampling valve.

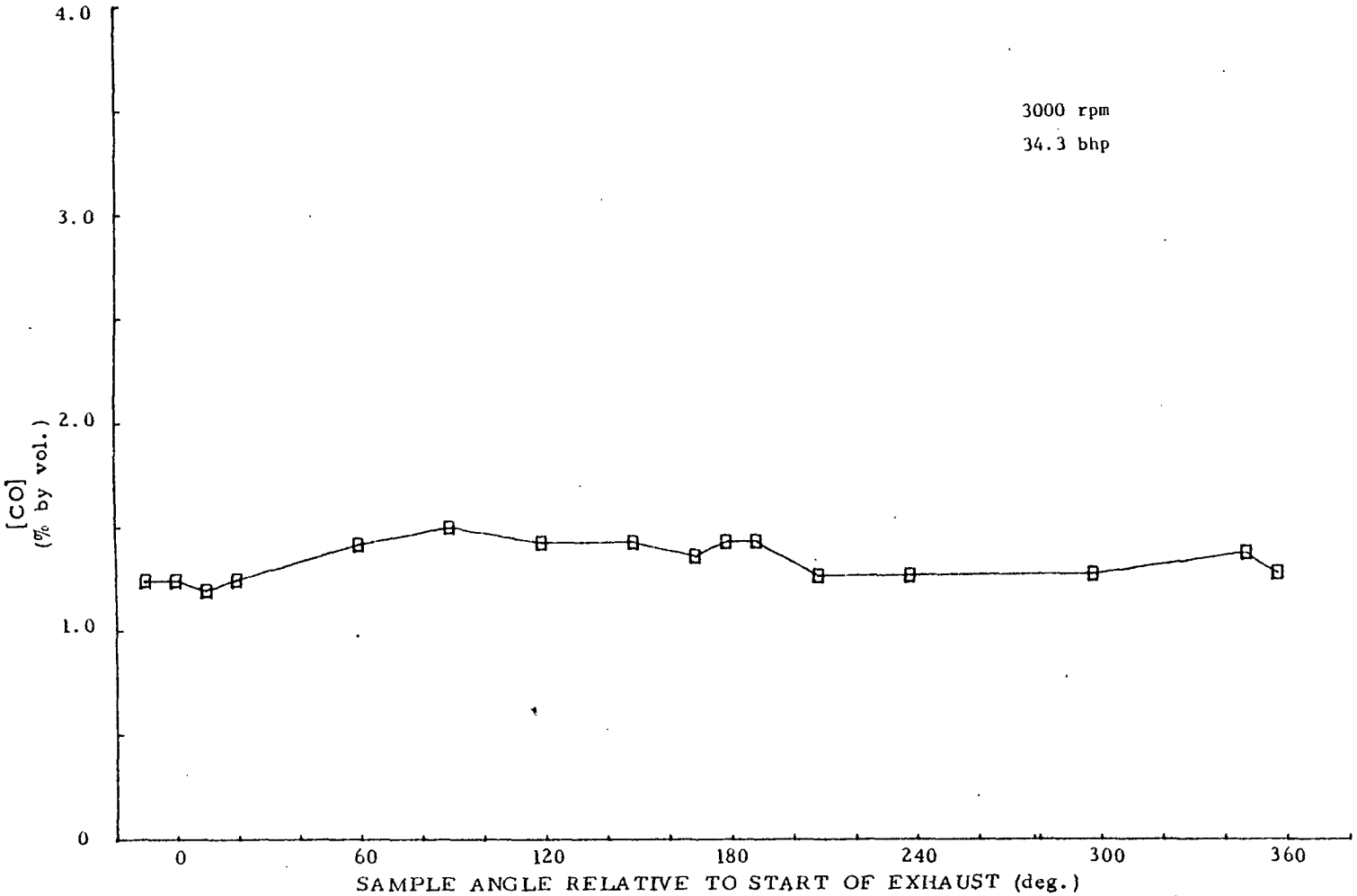

Figure 74. Carbon monoxide concentration as a function of crank angle relative to the start of the exhaust process, Mazda 13-B engine, 3000 rpm, 34.4 bhp. Data obtained with a Cox timed sampling valve.

the increase near the end of the exhaust process also occurred later. This same trend was even more pronounced at 2500 rpm, 22.4 bhp. However, it is evident that because the exhaust sample was taken about 2 inches from the exhaust port opening the curves may have been displaced because of changes in position of the Cox valve opening with respect to the front end of a given column of exhaust gas. Hence the curves may be nearly identical but displaced in time with the peaks still corresponding to the point of exhaust port opening for a given chamber. The data at 3000 rpm, at both 18.7, 34.4 bhp tended to contradict this "shift" theory because the peaks occurred close to the zero position.

At 2000 rpm, 8.8 bhp, the hydrocarbons in the leading portion of the exhaust sample (which cannot be totally separated from the trailing portion of the prior chamber's exhaust sample) were approximately 2300 ppm. This decreased rapidly to approximately 1300 ppm, then increased during the middle of the exhaust process followed by another decrease and subsequently increased back to the level corresponding to the leading position. It is evident from these data that the hydrocarbon emissions are significant at both the leading and/or trailing section of the chamber, and at the light load condition there is some evidence of incomplete burning in the central region of the chamber. This region corresponds to the position of the cycle where the exhaust flow rate is relatively rapid, i.e. the rotor chamber volume is changing at the highest rate near 180° crank angle from the opening position of the exhaust port for a given chamber. A slight increase in CO was observed in the region where the hydrocarbon emissions were generally lower as expected because of the more complete burning of the hydrocarbons in this region and consequently greater potential for the formation of CO.

From the majority of the hydrocarbon data it is evident that the gases that initially leave the chamber and/or those that leave last are rich in hydrocarbons. This appears to confirm the hypothesis that important sources of hydrocarbon emissions are due to leakage and incomplete burning mixture near the leading or trailing portions of the chamber. In addition these trailing/leading section results may be influenced by the physical scrapping of the quench layer off the outer housing surface by the trailing apex seal with the subsequent concentration of these gases in the latter portion that leaves the chamber. Thus all three hypothesized factors may give rise to the high concentrations in the leading and/or trailing portions of the exhaust sample. Of course, it must be recognized that because of the length of exhaust system from chamber to the sample valves, some integration of sample or mixing has undoubtedly occurred.

2. Manifold Sampling System Study

As an adjunct to the investigation of exhaust emission profile in the exhaust system using the Cox fast response sampling valve, a separate study was conducted using a more qualitative technique.

In this investigation, a special exhaust pipe was constructed which contained steady-state sampling probes located at measured intervals along the pipe. An exhaust sample was withdrawn and analyzed from each sample probe. The hydrocarbon emission results from the various probes were then plotted on a concentration basis as a function of probe position. From these data it was possible to infer whether the hydrocarbons produced in the chamber were coming from local regions within the engine or were basically related to a homogeneous process. If the hydrocarbon emissions were related to some form of homogeneous reaction, one would anticipate that the exhaust hydrocarbon profile would not vary as a function of probe location. A variation from probe to probe would infer that the hydrocarbon emission at least partially resulted from local processes in the chamber. Similar studies have been performed in reciprocating engines with good results (16). In the rotary engine, however, the dynamics of the exhaust process are considerably different. In a reciprocating engine the exhaust slug is periodically stationary during the time when the exhaust valve is closed whereas in the rotary engine the exhaust flow is always dynamic (an exhaust process is always occurring). At a constant sample rate a given probe will take in a greater proportion of the sampled gas from a part of the exhaust "slug" that is moving more slowly than from a fast moving segment. By placing probes at intervals along the exhaust pipe as indicated above, it may be possible to determine a qualitative measure of the distribution of hydrocarbons in the exhaust. The reader is referred to Ref. 18 which is a rather complete study performed by John White at the University of Michigan. The referenced report contains an analysis of the data and in addition develops a computer simulation by which the profile of the exhaust can be determined as if the probes were moving in phase with the exhaust gas (equivalent to use of fast response sample valve). One value of this technique is that the equipment requirements are considerably less sophisticated than utilization of the sampling valve.

Sample data are plotted in Figs. 75-77. In Figure 75 hydrocarbon concentration is plotted as a function of exhaust probe position at 2000 rpm for both road load and 100% road load horsepower. Similar data is plotted in Fig. 76 at 2500 rpm road load and 170% road load. Clearly these data suggest that there is a considerable variation in concentration as a function of position in the exhaust "slug" and confirms the behavior, at least qualitatively, observed with the Cox sampling valve. The curves at the different loads are shifted considerably horizontally because of the different exhaust "slug" volumes at different loads. Figure 77 shows a similar plot for three different engine speeds at road load conditions. Again the significant variation in concentration within the exhaust slug is evident. The data presented here are a relatively small sample from the study that was performed, however, all of the data in both raw and reduced form, show clearly that the exhaust composition varies considerably along the exhaust "slug". These results confirm the suspicion that the hydrocarbons

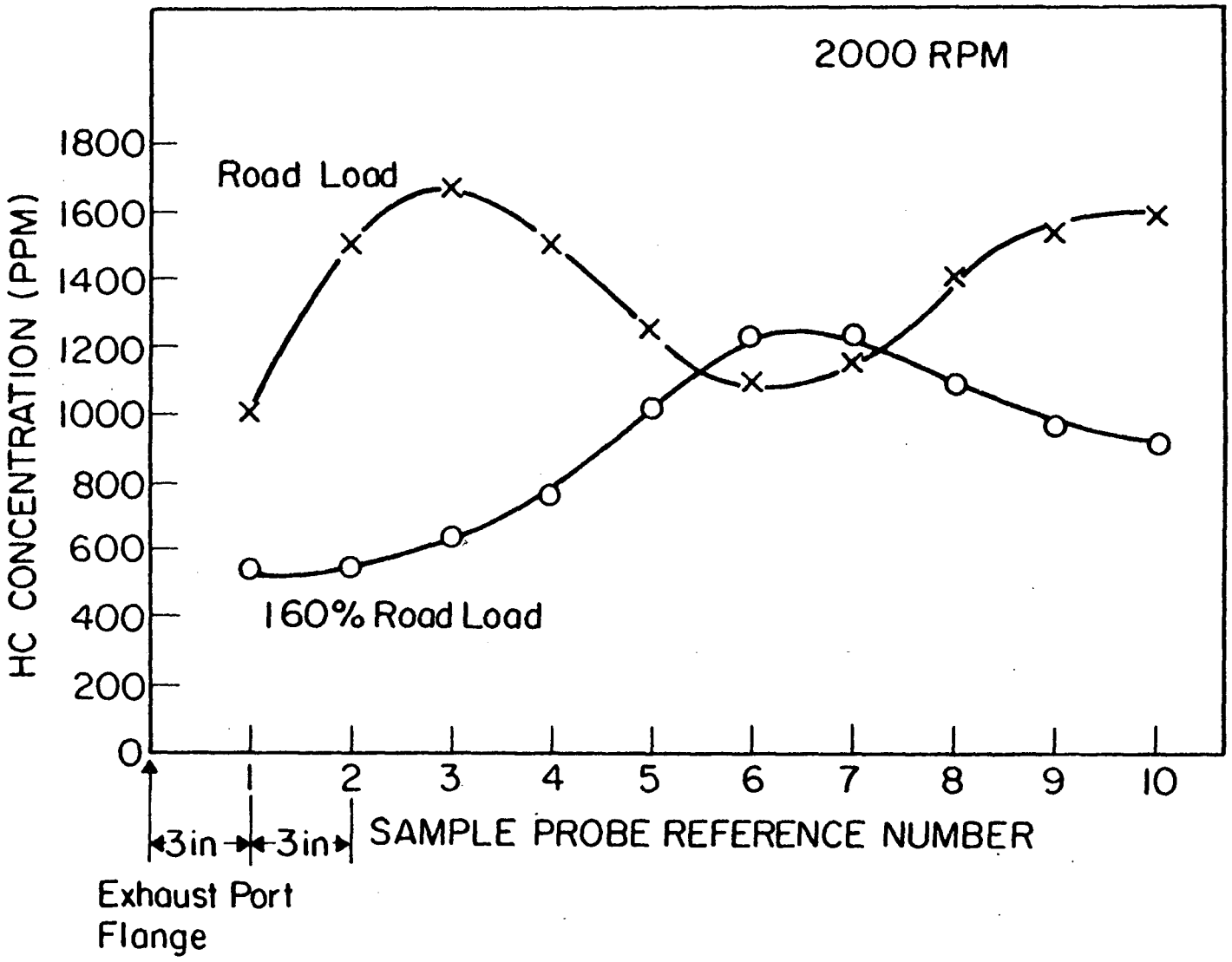

Figure 75. Hydrocarbon concentration as a function of exhaust sample probe position in the exhaust pipe, Mazda 13-B engine, 2000 rpm, manifold sampling system.

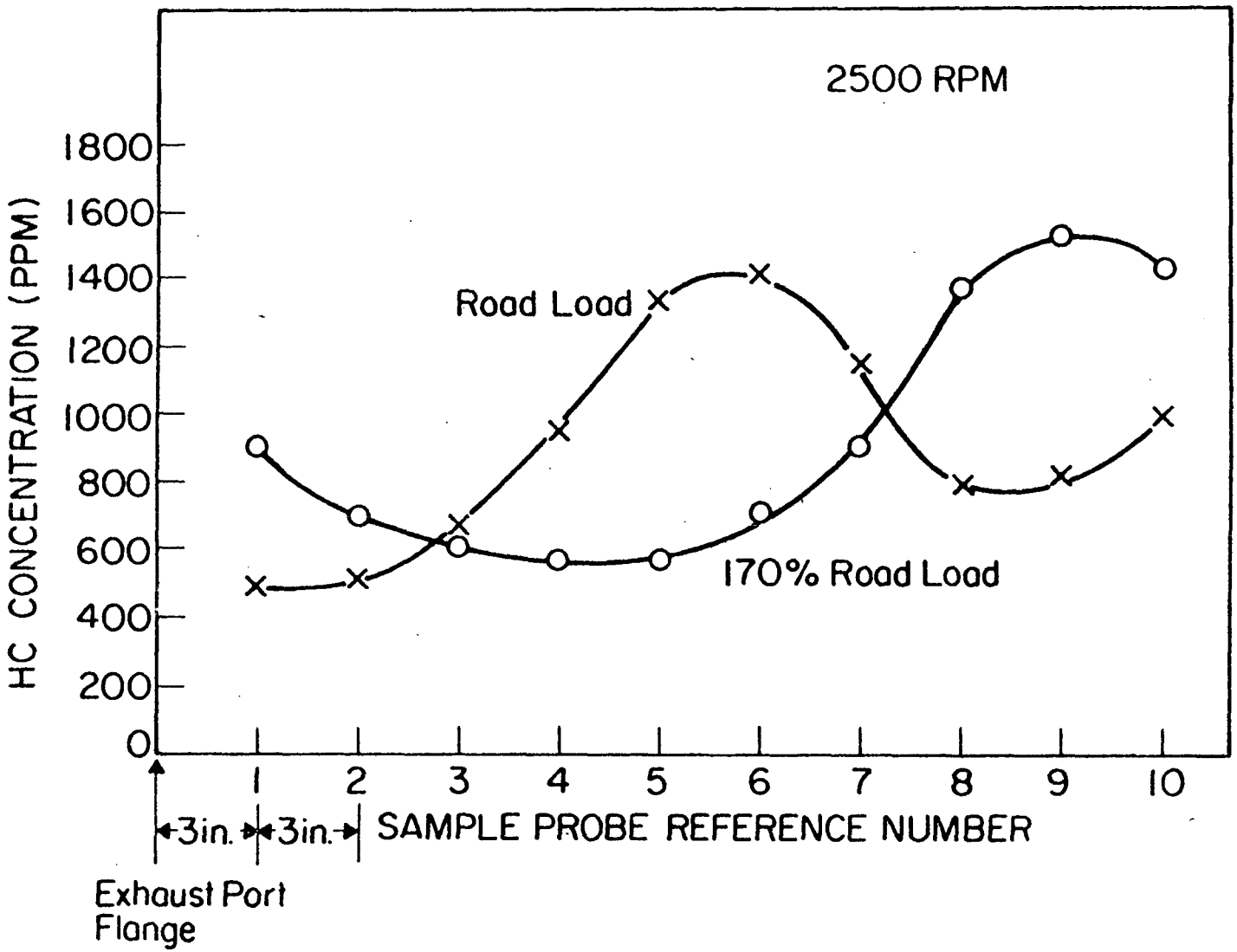

Figure 76. Hydrocarbon concentration as a function of exhaust sample probe position in the exhaust pipe, Mazda 13-B engine, 2500 rpm, manifold sampling system.

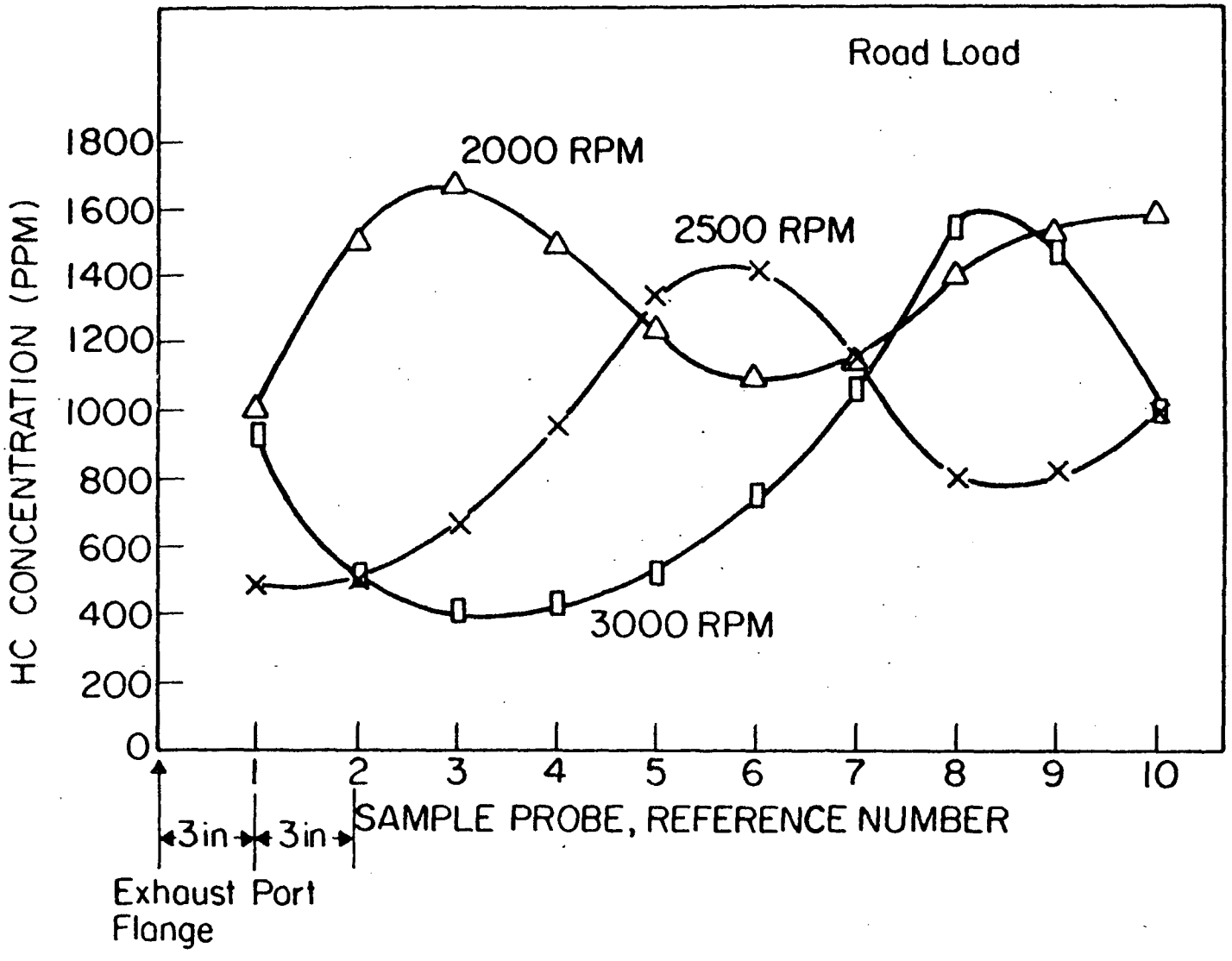

Figure 77. Exhaust hydrocarbon concentration as a function of sample probe location in the exhaust system, Mazda 13-B engine, manifold sampling system.

are formed non-uniformly within the engine chamber. The apex seal region is probably the most significant contributor either because of gas leakage to the exhausting chamber, "pile-up" of the quench layer due to physical scraping of the seal on the chamber and/or incomplete flame propagation.

H. CHAMBER PRESSURE STUDY - MAZDA ENGINE

Cylinder pressure records were taken in the Mazda engine at both motoring and firing conditions. The purpose was to compare the polytropic exponents with values for piston engines and other rotary engines reported in the literature. From such a comparison it was hoped differences in combustion and heat transfer might be inferred.

A study of Fig. 11 in Section III reveals that with a single transducer the pressure can only be measured for 360 deg. of crank rotation. The pressure for most of the compression and about half of the expansion stroke may be obtained in this manner. The important portion of combustion is thus covered. It should be noted that the pressure observed near the end of the expansion trace is grossly distorted, for the recorded value is at a changing level between the relatively high pressure at 120° atc and the low pressure early in the compression stroke.

Pressure records were obtained under the following conditions:

Firing Engine: Production carburetion and ignition timing

RPM	Brake Horsepower
2500	22.4
2500	13.1
2000	14.0
2000	8.8

Motoring

RPM	Throttle
2000	closed
2000	part
2000	WOT
2500	closed
2500	part
2500	WOT

Results - Firing

Figures 78,79,80 show pressure-crank angle, pressure-volume and log pressure versus log volume respectively for the engine at 2500 rpm, 22.4 bhp. The pressure crank-angle diagram clearly shows the 360° degree "window" in which pressures were measured as well as the rapid drop in cylinder pressure near the end of the measurement as the apex seal moves across the transducer sampling hole. Similar information is seen in Fig. 79. Obviously insufficient

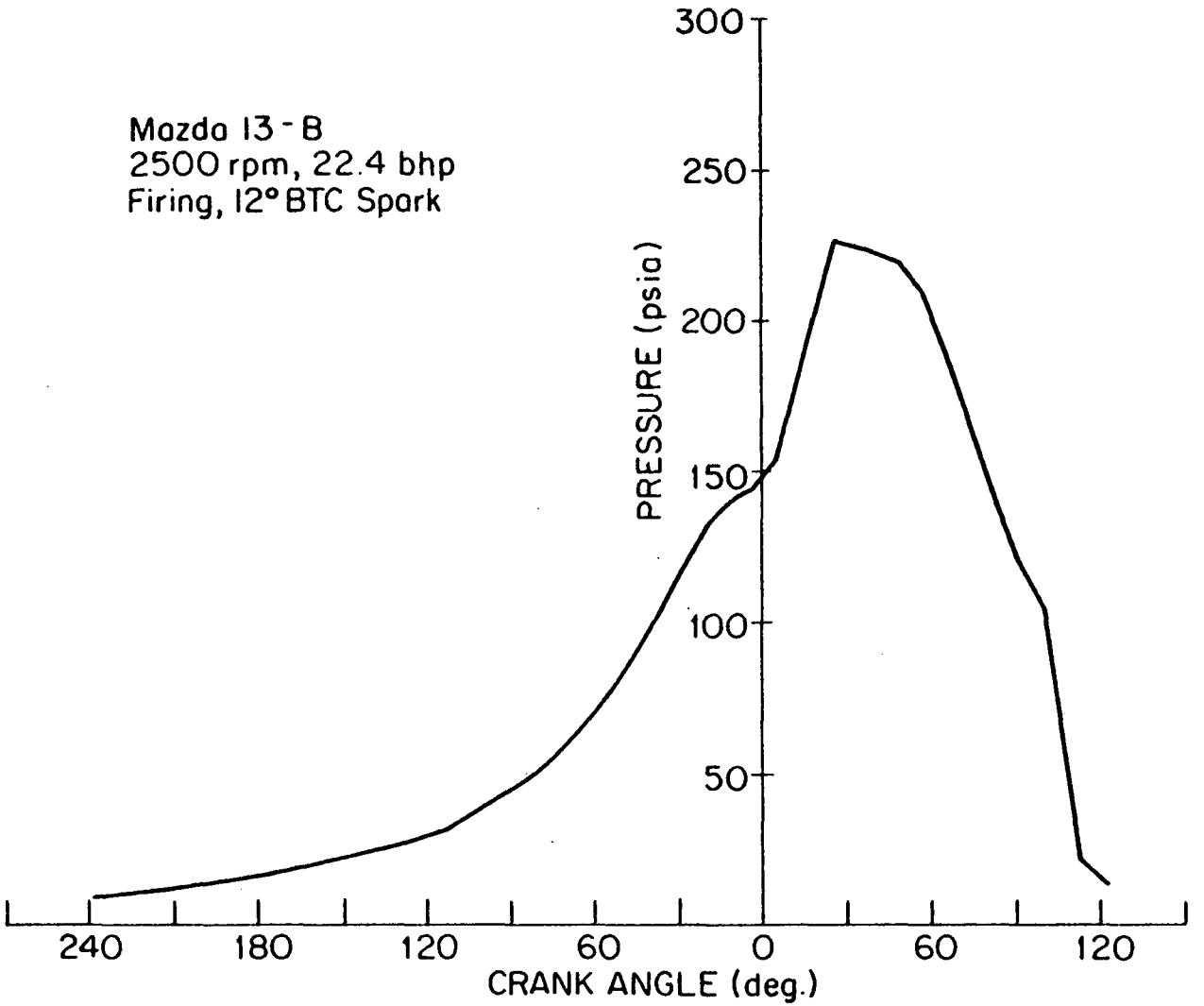

Figure 78. Cylinder pressure as a function of crankangle, Mazda 13-B, at 2500 rpm, 22.4 bhp.

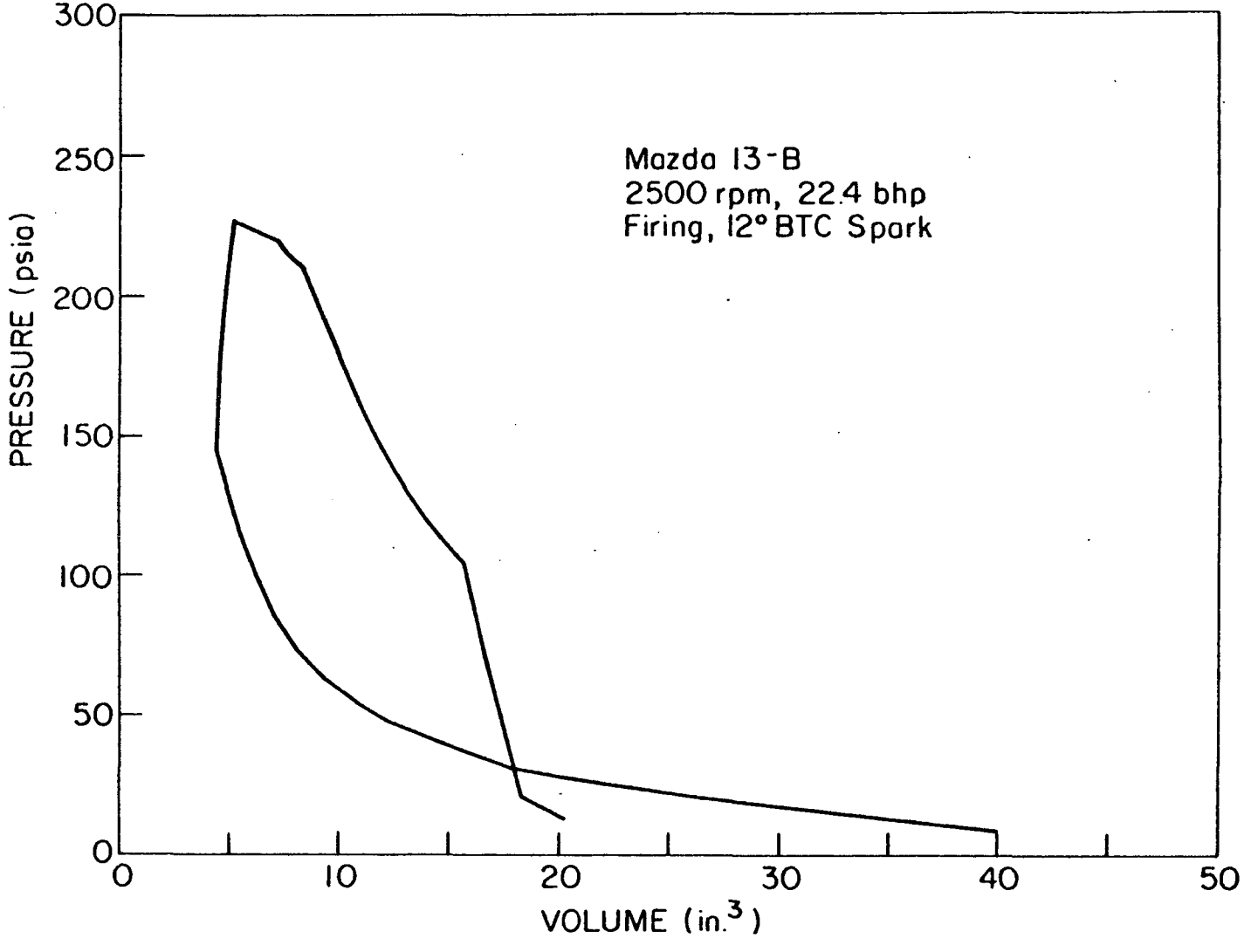

Figure 79. Cylinder pressure as a function of volume, Mazda 13-B, at 2500 rpm, 22.4 bhp.

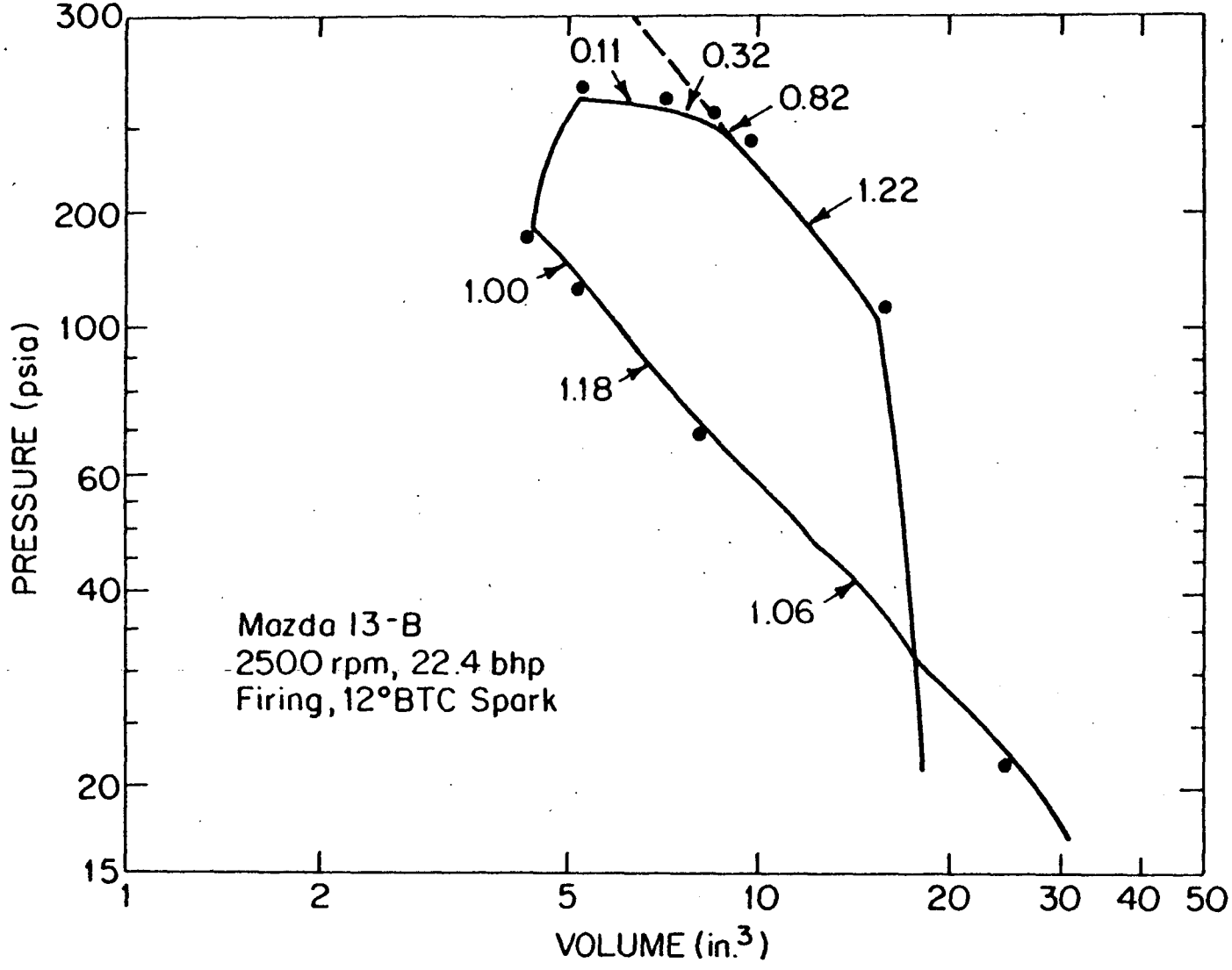

Figure 80. Cylinder pressure as a function of volume, logarithmic plot, Mazda 13-B, at 2500 rpm, 22.4 bhp.

information exists to determine cycle work. Figure 80 shows the pressure-volume record on logarithmic coordinates. The varying nature of the signal suggests the need to ascribe several polytropic exponents over the cycle. The beginning and end of the trace were not analyzed for reasons discussed previously.

Figure 81 shows all four of the logarithmic pressure-volume plots for the fired engine data. In each case, multiple exponents appear warranted. Similar results were reported by Froede in Ref. (18) for a KKM-250-5 engine.

In comparing data from Froede with our results some similarities and differences are evident. A considerable amount of after-burning is seen to exist. In the Mazda engine, an expansion exponent of less than 0.63 persists until about 10 in^3 (164 cc) cylinder volume or 2.22 x the minimum volume. In the KKM-250-5 a similar after-burning period exists. In the absence of such after-burning, the expansion line at the start of expansion would be an extension of the line later in expansion whose slope for the Mazda was 1.22-1.23. Such an extended line is shown with dashes in Fig. 81. Of course all engines whether reciprocating or rotating have some degree of afterburn due to the finite progression of combustion and the re-association of dissociated species during expansion. However this afterburning appears somewhat more extensive than that reported by Nelson for an 8.7:1 compression ratio experimental piston engine at part load in Fig. 14 of Ref. (19). In that case after-burning ceased at an expansion volume equalling 1.8 x the minimum volume. Moreover the after-burning in the Mazda was clearly greater than that reported by Lancaster in Ref. (20) for a single cylinder piston engine. In comparing with Froede's results on the KKM-250-5, it is noted that the polytropic expansion exponent for the Mazda, (ave. 1.22) is slightly lower than Froede's result (ave. 1.27) if his one value of 1.7 is ignored. It is also lower than Nelson's average value of 1.29 and Lancaster's 1.30 for reciprocating engines. No firm conclusions can be drawn from these small differences in expansion exponents in light of the probable differences in mixture ratio, load and measurement technique between the various researchers. In general, a lower expansion exponent suggests more after-burning whereas a higher value suggests greater heat transfer and leakage.

The compression exponents of this study ranged from 0.89 to 1.12. These values are quite low compared to the values of Froede which were 1.2 or greater and those of Nelson and Lancaster which were about 1.3. The characteristic of a lower exponent late in compression is similar to the finding of Froede and suggests excessive leakage and heat loss near top center piston position. However the problems appeared more extensive in the Mazda engine than the KKM-250-5 engine. Typically the piston engine compression line is well represented by a single polytropic exponent. Consequently, the low and multiple valued compression exponent of this study is distinctly different from that of the piston engine. Leakage of unburned mixture past the leading apex seal is thought to be a

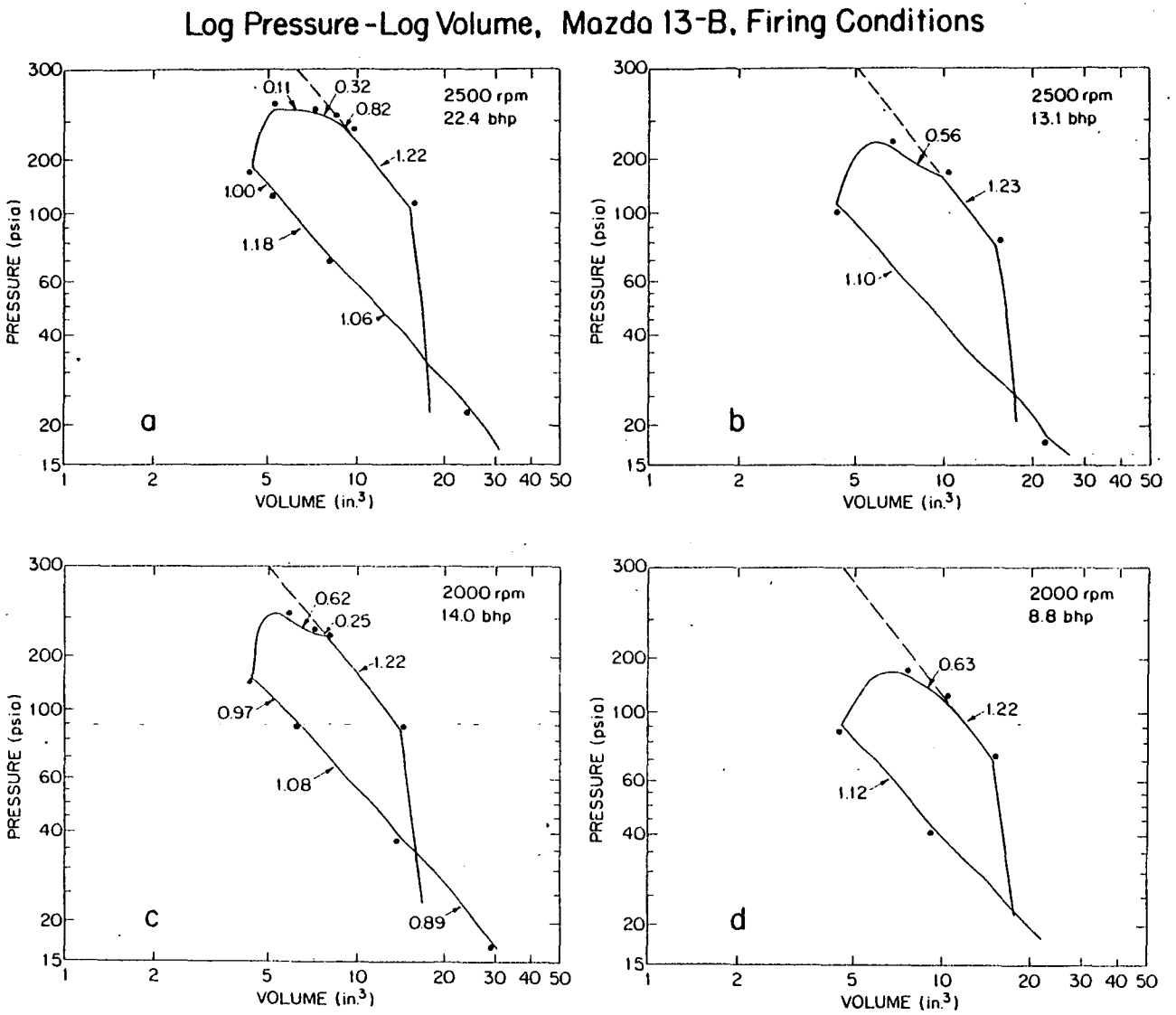

Figure 81. Logarithmic plots of pressure as a function of volume, fired Mazda 13-B engine.

major source of unburned hydrocarbons in the rotary engine and the low observed compression exponent especially near top center probably indicate such leakage.

Results - Motoring

Six pressure records were obtained under motoring engine conditions without fuel at 2000 and 2500 rpm, various throttle openings. These are shown in Fig. 82. In viewing these curves it is well to keep in mind that the expansion lines are lower than the compression lines. This is a common observance in engines of all types without combustion and is due to heat transfer and leakage. As in the fired case, multiple exponents may be assigned. Lower exponents near top center on compression reflect leakage and heat transfer in that portion of the cycle. The larger exponents during expansion reflect the same phenomena. In general the motoring exponents are higher than the firing exponents. This results from the absence of fuel since the polytropic exponent of a fuel-air mixture is lower than that of pure air. Lancaster's results scale to a compression exponent of 1.3 and an expansion exponent of 1.43 in a reciprocating engine. In general it is concluded that the motoring exponents are lower on compression and higher on expansion than a piston engine and this suggests greater leakage and heat losses in the rotary engine. However because of the unique sealing system of the rotary engine, one must be careful about drawing conclusions on sealing in a non-fired test.

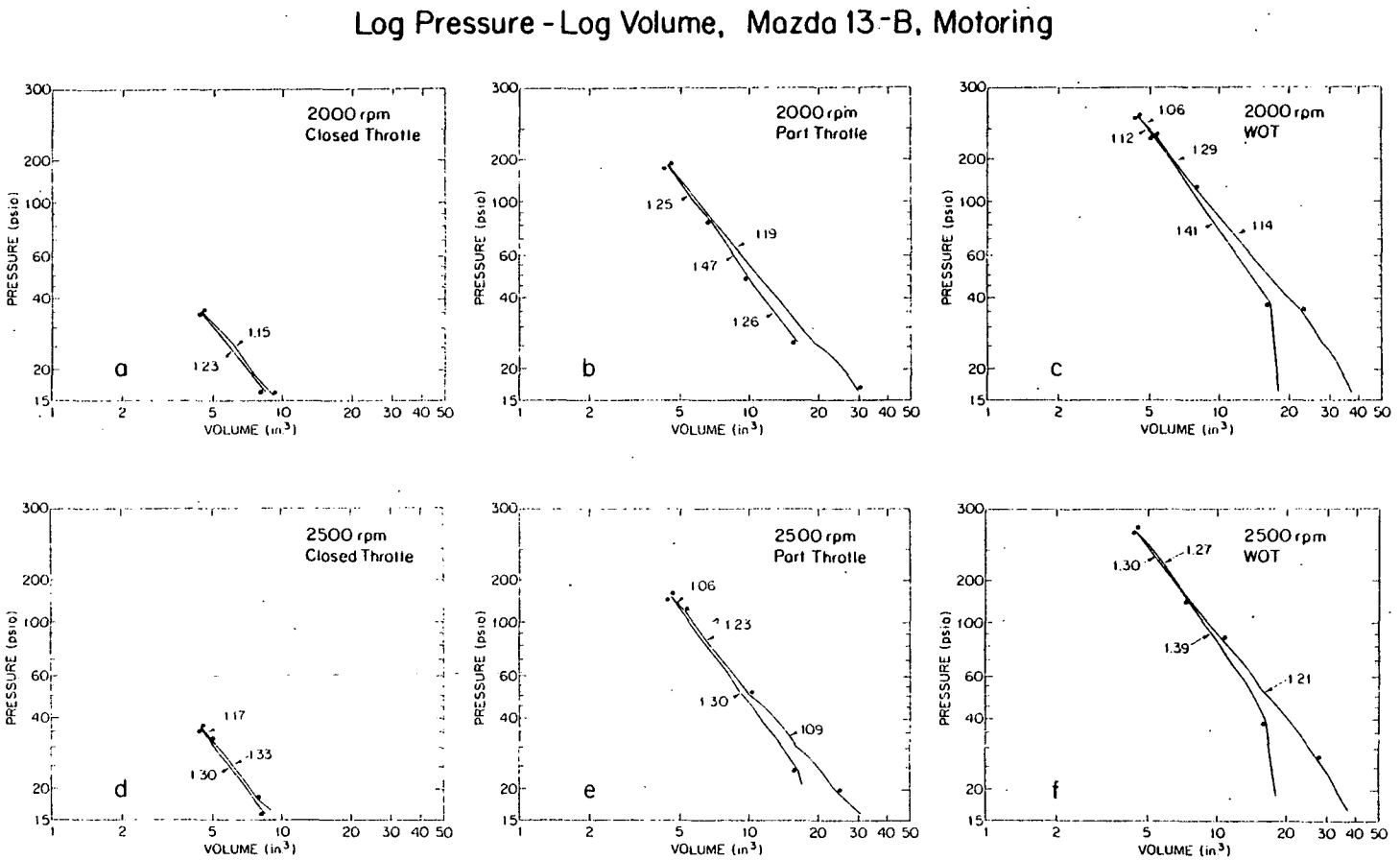

Figure 82. Logarithmic plots of pressure as a function of volume, motored Mazda 13-B engine.

REFERENCES

1. Jones, C., The Curtiss-Wright Rotating Combustion Engines Today, SAE Trans., v. 73, 1965
2. Personal communications with representative of the General Motors Corporation.
3. 1975 Gas Mileage Guidefor New Car Buyers, U.S. Environmental Protection Agency and Federal Energy Admin., 1974-75.
4. 1975 Mazda shop manual.
5. Papa, L. J., Gas Chromatography - Measuring Exhaust Hydrocarbons Down to Parts Per Billion, SAE paper 670494, SAE Progress in Technology, v. 14, 1971.
6. Oberdorfer, P. E., The Determination of Aldehydes in Automobile Exhaust Gas, SAE paper 670123, SAE Progress in Technology Series, v. 14, 1971.
7. Sampling Procedure for Determining Exhaust Aldehyde Emissions, Internal Report, University of Michigan, W. E. Lay Automotive Laboratory
8. Obert, E. F., Internal Combustion Engines, Intext Co., Scranton, Pa., 1968, pg. 481.
9. Taylor, C. F., Taylor, E. S., The Internal Combustion Engine, Intext Co., Scranton, Pa., 1970, pg. 411-342.
10. Cole, D. E., Jones, C., Reduction of Emissions from the Curtiss-Wright Rotating Combustion Engine with an Exhaust Reactor, SAE paper 700074, SAE Progress inTechnology Series, v. 14, 1971.
11. Patterson, D. J., Kadlec, R. H., Kinetics of Oxidization and Quenching of Combustibles in Exhaust Systems of Gasoline Engine, Final report No. 310830-3-F, University of Michigan, 1972.
12. Jackson, M. W., Wiese W. M. and Wentworth, J. T., The Influence of Air-Fuel Ratio, Spark Timing and Combustion Chamber Deposits on Exhaust Hydrocarbon Emissions, SAE paper 486A, SAE Technical Progress Series, v. 6, 1964.
13. Hagen, D. F., Holiday, G. W., The Effects of Engine Operating and Design Variables on Exhaust Emissions, SAE paper 486C, SAE Technical Progress Series, v. 6, 1964.
14. Daniel, W. A., Why Engine Variables Affect Exhaust Hydrocarbon Emission? SAE paper 700108, SAE Progress in Technology Series, v. 14, 1971.

15. Cole, D. E., Emission Characteristics of the Wankel Rotary Engine, SME paper MM73-654, 1973.

16. Daniel, W. A., Wentworth, J. T., Exhaust Gas Hydrocarbons - Genesis and Exodus, SAE 486B, SAE Progress in Technology Series, v. 6, 1964.

17. White, J. H., Investigation and Analysis of the Exhaust Chamber Hydrocarbon Stratification in an Existing Mazda 13-B Rotary Engine masters thesis, University of Michigan, Ann Arbor, Mich., 1976.

18. Froede, Walter G., The NSU-Wankel Rotating Combustion Engine, SAE paper 288A, January 1961.

19. Caris, D. F., Nelson, E. E., A New Look at High Compression Engines, SAE paper 61A, June 1968.

20. Lancaster, D. R.,et al, Measurement and Analysis of Engine Pressure Data, SAE paper 750026, February 1975.